THE ERUPTIVE HISTORY OF THE TEQUILA VOLCANIC FIELD, WESTERN MEXICO: AGES, VOLUMES, AND RELATIVE PROPORTIONS OF LAVA TYPES

BY

CATHERINE B. LEWIS-KENEDI

Author

Catherine B. Lewis-Kenedi

Title

The eruptive history of the Tequila volcanic field, western Mexico: ages, volumes, and relative proportions of lava types

Submitted for Publication in:

Bulletin of Volcanology

in lieu of thesis in partial fulfillment
of the requirements for the degree of
Master of Science in Geology
Department of Geological Sciences
The University of Michigan

Accepted by:

Rebecca Lange Signature	Rebecca A. Lange Name	7/9/03 Date
S E Kesler Signature	Stephen E. Kesler Name	7/9/03 Date
Joel D Blum Department Chair	Joel D. Blum Name	8/1/03 Date

I hereby grant the University of Michigan, its heirs and assigns, the non-exclusive right to reproduce and distribute single copies of my thesis, in whole or in part, in any format. I represent and warrant to the University of Michigan that the thesis is an original work, does not infringe or violate any rights of others, and that I make these grants as the sole owner of the rights to my thesis. I understand that I will not receive royalties for any reproduction of this thesis.

☑ Permission granted.

☐ Permission granted to copy after: _____
Date

☐ Permission declined.

C. B. L. K.
Author Signature

The eruptive history of the Tequila volcanic field, western Mexico: ages, volumes, and relative proportions of lava types

Catherine B. Lewis-Kenedi, Rebecca A. Lange, Chris M. Hall, Hugo Delgado-Granados

C.B. Lewis-Kenedi, R.A. Lange (corresponding author), C.M. Hall
Department of Geological Sciences
University of Michigan, Ann Arbor, MI 48109-1063 USA
E-mail: becky@umich.edu
Phone: +1-734-7647421
Fax: +1-734-7634690

H. Delgado-Granados
Instituto de Geofísica, UNAM
Coyoacan, Mexico 04510 DF

Submitted to: Bulletin of Volcanology, June 2003

Abstract

The eruptive history of the Tequila volcanic field (1600 km^2) in the western Mexican arc is obtained from $^{40}Ar/^{39}Ar$ chronology and volume estimates for eruptive units $\leq$ 1 Ma. Ages are reported for 49 volcanic units, including Volcán Tequila (an andesitic stratocone) and peripheral domes, flows, and cinder cones. Volumes were obtained with the aid of field mapping, aerial photographs, digital elevation models (DEMs), and ArcGIS software. Between 1120 Ma and 200 ka, a bimodal distribution of rhyolite (~34 km^3) and high-Ti basalt (~39 km^3) dominated the volcanic field. Between 685 and 225 ka, less than 5 km^3 of andesite and dacite erupted from > 15 isolated vents; these lavas are crystal-poor and show little evidence of storage in an upper crustal magma chamber. Approximately 200 ka, ~31 km^3 of andesite erupted within $\leq$ 24 kyrs to form the stratocone of Volcán Tequila, indicating a cone-building eruption rate of $\geq$ 1.3 km^3/kyr. The phenocryst assemblage of these lavas suggests storage within a chamber at ~2-3 km depth. After a hiatus of ~110 kyrs, ~14 km^3 of andesite erupted along the NW and SE flanks of Volcán Tequila at ~90 ka, most likely from a second, discrete magma chamber located at ~5-6.5 km depth. The youngest volcanic feature (~60 ka) around Volcán Tequila is the small andesite stratocone, Cerro Tomasillo (~2 km^3). Over the last 1 Myr, a total of 127 ± 16 km^3 of lava erupted in the Tequila volcanic field, leading to an average eruption rate of ~79 m^3/km^2 per year or an accumulation rate of ~8 cm/kyr. The relative proportions of lava types are ~24-40 % basalt, ~0.6 % basaltic andesite, ~32-50 % andesite, ~2 % dacite, and ~19-36 % rhyolite. On the basis of eruptive sequence, proportions of lava types, phenocryst assemblages, textures, and geochemistry, the lavas do not reflect the differentiation of a single (or only a few) parental liquid in a long-lived magma chamber. The rhyolites are geochemically diverse and likely were formed by episodic partial melting of sialic crust in response to emplacement of basalts into the upper crust. There are no examples of mingled rhyolite and basalt magmas. Any process invoked to explain the origin of the andesite and dacite at the Tequila volcanic field must account for a persistent background leakage of geochemically diverse, small-volume batches of crystal-poor magma ranging from basaltic andesite through dacite punctuated by voluminous bursts of andesitic magmatism.

Keywords $^{40}Ar/^{39}Ar$ geochronology; GIS; Eruption rates; Aphyric andesites; Mexican volcanoes; Trans-Mexican Volcanic Belt

Introduction

The Quaternary Tequila volcanic field, in the western Mexican arc, includes a large andesitic stratocone (Volcán Tequila), cinder cones and flows of basaltic through dacitic composition, and rhyolitic domes. Thus a complete compositional spectrum from basalt through rhyolite is present, and an accurate assessment of possible petrogenetic links among them requires a detailed eruptive history that includes the ages, volumes, and relative proportions of lava types. In this study, an intensive $^{40}Ar/^{39}Ar$ dating program is coupled to quantitative estimates of erupted volumes based on field mapping, aerial photographs, digital elevation models, and ArcGIS software. Such detailed information on the chronology and volume of erupted lavas can reveal whether a time-progressive pattern in composition is present, which can be used to test various models of magma differentiation. These data also constrain the length of time required to build a large composite volcano, which bears on the longevity of the underlying upper-crustal magma chamber feeding the cone-building eruptions. When eruption rates are combined with a detailed study of the textures and phenocryst assemblages of the lavas erupted from large, central volcanoes vs. small, peripheral vents, additional constraints on the time-scale for upper crustal storage of these arc magmas are obtained.

The applicability of the $^{40}Ar/^{39}Ar$ dating technique to Pleistocene lavas and comparisons with conventional K-Ar dating was first documented by Hall and York (1978, 1984) and later revisited by Lanphere (2000). Previous work by Hildreth and Lanphere (1994), Singer et al. (1997), Druitt et al. (1999) and Hildreth et al. (2003) have demonstrated the success of both K-Ar and $^{40}Ar/^{39}Ar$ methods in dating large suites of arc volcanic rocks $\leq$ 1 Ma. In this study, our strategy was to date as many different lavas as possible with an accuracy and precision of at least $\pm$ 50 kyrs; in most cases the results are far better. Our primary goal was to identify and date all lavas erupted within the last 1 Myr, so that their individual and combined volumes could be evaluated.

The difficulty in quantifying eruptive volumes at arc volcanic fields has long been recognized; factors include severe glacial erosion (e.g., Singer et al. 1997; Hildreth et al. 2003) and/or extensive pyroclastic activity (e.g., Druitt et al. 1999). The Tequila volcanic field is ideal for a quantitative assessment of the volumes and proportions of different lava types owing to its mild climate (no glacial activity) and the minor role of explosive

volcanism. The rural, agricultural nature of the Tequila volcanic field provides numerous roads and trails that allow excellent access to all volcanic units. Moreover, many of them have been previously mapped and characterized (Demant 1979; Harris 1986; Nixon et al. 1987; Wopat 1990; Wallace and Carmichael 1994), and topographic maps, aerial photographs, and digital elevation models (DEMs) are available for the entire area.

This study of the Tequila volcanic field is the second in a series designed to obtain a high-resolution record of the chronology and volume of erupted magma ($\leq$ 1 Ma) along the western Mexican arc. The results of this work can be compared with a similar study of the Ceboruco-San Pedro volcanic field (Frey et al. 2003) located 75 km to the northwest. These two adjacent volcanic fields have similar subduction parameters such as crustal thickness, age of the subducting slab, and rate of subduction. Thus a comparison of the eruptive history between the two volcanic fields within the last 1 Myr can be used to test the relationship between subduction parameters and the average composition of erupted magma. These studies are further strengthened by a comparison with the chronological studies and volume estimates on the Mt. Adams and Mt. Baker volcanic fields in the Cascade arc (Hildreth and Lanphere 1994; Hildreth et al. 2003, respectively).

Tectonic setting

Volcán Tequila is one of eight major volcanic centers in the western Trans-Mexican Volcanic Belt (TMVB) (Figure 1). The crustal thickness in this region is estimated at 35-40 km from the gravity model of Urrutia-Fucugauchi and Flores-Ruis (1996). The TMVB is associated with subduction of two plates under North America: the ~9 Ma Rivera plate in the west (Klitgord and Mammerickx 1982), and the 12-18 Ma Cocos plate in the east. Seismic evidence suggests that the Rivera plate descends at an angle of 10° from the Middle America trench to a depth of 20 km, after which the angle steepens to 50° at 40 km; the subduction angle is unconfirmed below ~50 km owing to a lack of seismicity (Pardo and Suárez 1993). If the dip of 50° continues as the slab descends, then Volcán Tequila lies more than 200 km above the Wadati-Benioff zone, significantly further than the globally observed median distance of 125 ± 38 km to the volcanic front (Gill 1981). The rate of subduction of the Rivera plate is estimated at 1.9

± 0.3 cm/yr along the western portion and 3.8 ± 0.4 cm/yr in the east, at the Rivera-Cocos boundary (DeMets and Wilson 1997). Of special interest to this study is the evidence given by DeMets and Traylen (2000) that subduction of the Rivera plate ceased ~2.6 Ma and then resumed normal convergence ~1 Ma at a rate of ~3.2 cm/yr.

Volcán Tequila is located within the Tepic-Zacoalco graben of western Mexico (Figure 1), one of three grabens that intersect 50 km south-southwest of Guadalajara. Five andesitic stratovolcanoes, V. San Juan, V. Sangangüey, V. Tepetiltic, V. Ceboruco, and V. Tequila, as well as two silicic centers, Las Navajas and Sierra La Primavera, are confined to the Tepic-Zacoalco graben. Northwest-trending fractures and normal faults are common in the graben, and cinder cones frequently align along these northwest-trending lineaments (Allan et al. 1991).

The Tequila Volcanic Field

As illustrated in the aerial photograph in Figure 2, the andesitic stratocone of Volcán Tequila forms the center of the 1600 km^2 Tequila volcanic field and is surrounded by rhyolite domes, flanking andesite flows, several cinder cones, and to the north, the Santa Rosa basalt plateau. Volcán Tequila rises to a summit of 2920 m, 1800 m above the surrounding plains, and is constructed of andesite flows that are described in Wallace and Carmichael (1994). An erosional gully (300 m deep) cuts from the summit of the volcano to the northeast and has produced an alluvial fan that spreads over most of the northeastern flank. At the summit, there is a 300 m spine of high-silica andesite (63 wt % SiO_2; Harris 1986). Whereas Volcán Tequila is primarily an effusive volcano, minor ash deposits are found at the summit and remnants of a small, dacitic air-fall deposit are located on the northern (TQ23) and southwestern flanks (Figure 2).

A small andesitic stratocone, Cerro Tomasillo, rests on the southeast flank of Volcán Tequila. A line of four, small dacite domes and associated flows are found immediately southeast of C. Tomasillo. Fissure-fed flows of andesite blanket the northwest and southeast flanks of Volcán Tequila and were likely erupted along the same NW-SE lineament that includes the central vents of V. Tequila, Cerro Tomasillo, and the line of four dacite domes (Figure 2). Nine small cinder cones of andesite and dacite occur along the southern and western margins of V. Tequila, and five cinder cones of

basalt and basaltic andesite (and one of andesite) occur to the west, north, and east of the stratocone. Twelve rhyolite domes surround V. Tequila and are partly covered by younger andesite flows; nine of these domes are concentrated along the northwest margin of V. Tequila. The rhyolites of the Tequila volcanic field have been described in detail, and seven of them dated with the K-Ar method, by Harris (1986).

Immediately north of V. Tequila, fissure-fed flows of basalt (and minor basaltic andesite) comprise the Santa Rosa plateau, which slopes ~1 ° to the N-NE and spans an area of ~190 km^2. Wopat (1990) described the plateau lavas and dated seven with the K-Ar method. The Santa Rosa plateau underlies the agricultural lands between the northern base of Volcán Tequila and the southern rim of the Rio de Santiago canyon. This southern rim has an average elevation of ~1100 m, whereas the northern rim is ~700 m higher. As found elsewhere along the Rio de Santiago (Nieto et al. 1985; Wopat 1990), basaltic lavas appear to have periodically filled and flooded the canyon, causing the river to re-incise through the flows. It is likely that most, though not all, of the capping basalt lavas that form the primary cover to the Santa Rosa plateau were sourced by fissure eruptions located within the canyon, along the same NW-SE lineament that the Rio de Santiago follows. The capping basalts show no evidence of individual flow margins and/or pressure ridges, which suggests that they flooded from the canyon and were deposited on flat-lying lacustrine deposits (exposed beneath the basalts on the southern wall of the Santiago canyon). Owing to the difference in elevation between the northern and southern rims, canyon-filling flows will tend to flood toward the south. The current shallow dip of the Santa Rosa plateau toward the north is likely the result of continued normal faulting since the emplacement of the basalts. Normal faulting along this segment of the Santiago canyon has offset a 5.5 Ma ashflow on the northern wall by ~450 m (Nieto et al. 1985), and it likely accounts for the higher elevation of the northern rim of the canyon.

Several additional studies have contributed information on the Tequila volcanic field. Demant (1979) provided the first detailed geological study of the area, including the petrography and chemistry of several lavas from the area. Nieto et al. (1985) describe the stratigraphy and structure of this region and report both new K-Ar dates and those of others, including Damon et al. (1979). Nixon et al. (1987) revised the geologic map and

report new chemical analyses and K-Ar ages on three samples: an andesite from the upper part of V. Tequila, a basalt from the Santa Rosa plateau, and a dacite flow north of the town of Tequila.

Composition and Mineralogy of Lava Types

Fifty-one samples were analyzed for major element chemistry by inductively coupled plasma (ICP) analysis and for trace and rare earth element chemistry by ICP mass spectrometry (ICP-MS) at Activation Laboratories in Ancaster, Ontario (Table 1). The lavas are classified on the basis of silica content as follows: basalt (< 52 wt % SiO_2), basaltic andesite (52-56 wt % SiO_2), andesite (58-63 wt % SiO_2), dacite (64-69 wt % SiO_2), and rhyolite (≥ 70 wt % SiO_2). Modal abundances were determined by point counts with > 1400 points (Table 1). Crystals > 0.3 mm are classified as phenocrysts, microphenocrysts are 0.03-0.3 mm, and groundmass is < 0.03 mm. Whole-rock analyses and/or thin sections of collected samples were used to create the geologic map shown in Figure 3.

Basalts and Basaltic Andesites

Basalt and minor basaltic andesite comprise the fissure-fed Santa Rosa plateau as well as cinder cones and associated flows on top of the plateau. Both the basalts (49-51 wt. % SiO_2) and basaltic andesites (52-56 wt % SiO_2) are enriched in TiO_2 (2.0-2.6 and 1.3-2.1 wt. %, respectively) (Table 1). These mafic lavas contain phenocrysts of olivine + plagioclase ± augite. One basaltic andesite (TEQ33) from a small cinder cone contains phenocrysts of hornblende in addition to plagioclase, olivine, and augite. The olivine basalts that filled and flooded the canyon (e.g., TEQ10, TEQ12) have a coarsely crystalline groundmass combined with abundant plagioclase microphenocrysts (~20-30 vol %) and many fewer (< 5 vol %) plagioclase phenocrysts, in marked contrast to similar olivine basalts erupted as cinder cones or flows on top of the Santa Rosa plateau (e.g., ETZ1, TEQ39). These samples have a fine groundmass with few microphenocrysts and more abundant phenocrysts.

Andesites

Andesites in the Tequila volcanic field are divided into four categories: (1) the main edifice of Volcán Tequila, (2) younger flows along the southeast and northwest flanks of V. Tequila, (3) the small stratocone of Cerro Tomasillo, and (4) peripheral cinder cones and flows. The lavas from V. Tequila span a range in silica (59-63.5 wt %; Table 1) similar to that of the younger flank lavas (59.1-63.7 wt %; Table 1), and both groups have TiO_2 concentrations that range from 0.9-0.6 wt %. Both groups of andesites display a mineralogy and texture typical of that seen in large, andesitic stratovolcanoes; they are phenocryst-rich (10-25 %), with plagioclase and two pyroxene assemblages. Plagioclase is the most abundant phenocryst and often displays complex zoning, as well as inner cores (sometimes bands) that are riddled with melt inclusions (Wallace and Carmichael 1994). Most of the younger flank lavas contain hornblende phenocrysts as well. The flows from Cerro Tomasillo dated in this study are described in Wallace and Carmichael (1994); they are similar in most respects to those from V. Tequila.

Peripheral flows and cinder cones of andesite are not associated with the central vent or flank flows of V. Tequila and are texturally and compositionally distinct. Although their range in silica (58-62 wt %) is similar to that for the lavas from V. Tequila and its flanks, the peripheral andesites contain higher concentrations of both TiO_2 (1.2-1.4 wt %) and total iron (Table 1). These flows are remarkably crystal-poor (3-10 vol %) and include sparse euhedral prisms of plagioclase with inner cores that often contain abundant melt inclusions. Orthopyroxene and augite are always present, and hornblende is found in all peripheral lavas with $\geq$ 59.5 wt % SiO_2. The hornblende is often completely surrounded by an opaque reaction rim (opacite). Rare xenocrysts of sieve-textured plagioclase with no rims are found in one sample (TAL 13).

Dacites

The most prominent occurrence of dacite is the line of four domes and associated flows immediately southeast of Cerro Tomasillo. A wet chemical analysis for one of these domes (Q-39) is reported in Harris (1986); the sample has 69 wt % SiO_2 and 0.4 wt % TiO_2. It contains 10 % phenocrysts of plagioclase, hornblende, and minor orthopyroxene (Wallace and Carmichael 1994). Pumice of dacitic composition (TEQ23)

from an airfall deposit contains phenocrysts of hornblende, plagioclase, and trace amounts of orthopyroxene. There are five additional occurrences of dacite: all occur as glassy cinder cones and are peripheral to V. Tequila and its flank flows. These cinder cones range from 64.6-68.4 wt % SiO_2 and, like the peripheral andesitic cinder cones, are notably crystal-poor (3-8 vol %) and relatively enriched in TiO_2 (0.9-0.5 wt %). The phenocrysts include clear euhedral prisms of plagioclase, in addition to orthopyroxene, sparse augite, and opacitic hornblende.

Rhyolites

The rhyolitic domes and flows in the Tequila volcanic field include peraluminous, metaluminous, and peralkaline varieties that range from 70-76.5 wt. % SiO_2 (Harris 1986). Domes consist of light-colored, porphyritic flows that contain 0-5 vol. % phenocrysts of plagioclase ± sanidine ± augite in fine-grained groundmass; no quartz phenocrysts were found in the samples collected by Harris (1986) or in the seven samples collected and examined in this study. For our samples, SiO_2 contents range from 75-76.5 wt. % (Table 1; after LOI correction for TEQ29 pumice). Four of the samples have no phenocrysts or microphenocrysts. The remaining three samples contain sparse phenocrysts of sanidine + plagioclase, and TEQ29 has additional hornblende.

$^{40}Ar/^{39}Ar$ Geochronology Methods

Forty-nine samples were dated by the $^{40}Ar/^{39}Ar$ laser ablation, step-heating method. Samples from lava and cinder cones, flows, and domes were selected to provide the broadest coverage of the field area. All analyses were run at the University of Michigan, and the procedures closely followed those described in Hall and Farrell (1995), Conway et al. (1997), and Frey et al. (2003). Groundmass was dated due to the lack of potassic minerals in the samples, except in two cases (TEQ9 and TEQ29) for which hornblende was dated.

Samples were taken from the interiors of lava flows or the inner cores of dense volcanic bombs from cinder cones, and each sample was checked for alteration using a petrographic microscope. Hand samples were crushed using a jaw crusher and ceramic mortar and pestle, and 1-2-mm sized grains of groundmass were hand picked under a

binocular microscope in order to exclude grains with phenocrysts and/or vesicles. Grains were washed ultrasonically with deionized water and were packaged in 99.5% aluminum foil. Fish Canyon Tuff-3 biotite, with a K-Ar age of 27.99 ± 0.04 Ma (2σ error) as calibrated against MMhb-1 (Hall and Farrell 1995; Samson and Alexander 1987) was used as the standard. This age is in agreement with the reported age of 27.95 ± 0.09 Ma by Renne et al. (1998) and the average age of 27.95 Ma reported by Baksi et al. (1996). One packet of standard for approximately every five packets of groundmass was arranged in quartz tubes that were evacuated and sealed. Samples were irradiated with fast neutrons for 6 hours at the Phoenix-Ford Nuclear Reactor at the University of Michigan. The measure of the neutron flux, *J*, was monitored at different heights of the quartz tube and interpolated to be applied to age calculations for individual sample positions.

Five grains of each irradiated sample (total weight of 5-20 mg) were loaded into individual wells of a copper tray and degassed (by heating overnight at 150-200°C) into the evacuated laser-line system to remove excess atmospheric argon. Samples were then step-heated at increasing levels of laser power from 100 to 4000 mW (13 steps for groundmass) using a defocused beam from a Coherent Innova 5-W continuous argon ion laser. The laser power was directed at individual sample grains for 30 seconds at each temperature while a liquid nitrogen-chilled cold finger and two SAES ST101 alloy getters operating at 0.45 amps cleaned the gas. Peaks over the mass range 40-36 were measured on a Daly detector. Fusion system blanks were subtracted from gas fractions at the five Ar mass positions, and blank levels were monitored after every fifth sample fraction. The data were corrected for interference reactions due to Ca, K, and Cl and for ^{37}Ar and ^{39}Ar decay. Ages were calculated using the decay constants in Steiger and Jäger (1977). Mass discrimination was monitored daily with an atmospheric Ar gas pipette and had a precision of 0.3-0.5% for the $^{40}Ar/^{36}Ar$ ratio.

$^{40}Ar/^{39}Ar$ results and assessment of accuracy

The $^{40}Ar/^{39}Ar$ data analyses for each sample, including gas spectra and inverse isochron diagrams, as well as a complete degassing history are given in the Data Repository (DR Figure 1 and DR Table 1). A summary of this information along with total gas, correlation, and plateau ages are reported for each sample in Table 2a. The error

analysis for each sample includes uncertainties in peak signals, system blanks, spectrometer mass discrimination, reactor corrections, and *J* values.

The criteria for determining whether the plateau and isochron ages from an incremental heating experiment are meaningful are as follows: 1) a plateau includes >50% of the ^{39}Ar gas released in at least three consecutive heating fractions, 2) the plateau passes a null hypothesis test such that for a heating experiment with 13 steps the MSWD is a maximum of 1.8, 3) the plateau and isochron ages are concordant at the 95% confidence level, and 4) the $^{40}Ar/^{36}Ar$ intercept of the isochron agrees with the atmospheric value of 295.5 at the 95% confidence level. If the isochron includes only the plateau points, the $^{40}Ar/^{36}Ar$ intercept will, by definition, be closely tied to the value of 295.5. Therefore we have done the regression as a subset of points that includes at least the plateau points but which may include all of the values resulting from the incremental heating experiment. The error on the plateau age is a standard weighted error for the individual steps by variance (Taylor 1982), i.e. release fractions with more precise results carry greater weight in the age calculation. Seven samples $\leq$ 1 Ma had disturbed spectra that did not result in a plateau; correlation and total gas ages are presented in Table 2b. For these samples, the isochron age is preferred in five cases; in all cases but one, the $^{40}Ar/^{36}Ar$ intercepts are within 2σ of 295.5 (atmospheric ratio). Four samples are > 1 Ma and are reported separately in Table 2c.

The accuracy of the $^{40}Ar/^{39}Ar$ dates reported in Table 2 were evaluated in three different ways: (1) a comparison with stratigraphic relations observed in the field, (2) a comparison with dates obtained on the same samples but from other laboratories, and (3) a replication of dates obtained in this study. Errors throughout the paper are given at the 1σ level. When comparisons are made at the 2σ level, it is stated explicitly in the text.

Stratigraphic relations

The $^{40}Ar/^{39}Ar$ geochronology is supported in all cases where a stratigraphic relation is observed in the field. We have documented eleven examples; locations are on Figure 2 and dates are on Figure 3a. (1) In the town of Santa Teresa, the basalt flow from cinder cone TEQ36 (261 ± 11 ka) overlies the rhyolite dome of TEQ45 (604 ± 3 ka). (2) This same flow (TEQ36, 261 ± 11 ka) overlies the capping basalt flow near the rim of the

Santiago canyon (dated at 848 ± 20 ka by Wopat 1990), and it also flowed around and abuts against the dacite flow of San Martin (dated at 630 ± 30 ka by Nixon et al. (1987)). (3) The basaltic andesite flow from cinder cone TEQ37 (427 ± 20 ka) overlies the rhyolitic dome of TEQ18/TEQ35 (642 ± 6 ka; 632 ± 8 ka). (4) Flows from Cerro Tomasillo, which have a mean age of 62 ± 11 ka (see below), overlie flows that form the main edifice of Volcán Tequila, which have a mean age of 196 ± 12 ka (see below). (5) Lavas from Cerro Tomasillo (62 ± 11 ka) flowed around the dacite domes immediately to the southeast. Nixon et al. (1987) report that these dacite domes are overlain by Tala Tuff airfall deposits (95 ± 10 ka; Mahood 1981); they are thus older than 75 ka at the 2σ level. (6) A lobe from the main edifice of V. Tequila (196 ± 12 ka) and a lobe from Cerro Tomasillo (62 ± 11 ka) each flowed around either side of cinder cone TAL13 (372 ± 18 ka). (7) The northernmost lobe of V. Tequila (TEQ60; 178 ± 8 ka) overlies the rhyolitic dome TEQ22 (416 ± 3 ka). (8) The basalt flow TEQ10 (671 ± 13 ka) from the southern wall of the Santiago canyon is underneath basalt flow TEQ12 (592 ± 20 ka). (9) The basaltic andesite flow TEQ40 (194 ± 15 ka) flowed around and abuts against the basaltic cinder cone TEQ39 (970 ± 34 ka). (10) The andesite flank flow of TEQ46/TEQ48 (mean age of 86 ± 47 ka) flowed around the basaltic andesite cinder cone TEQ33 (362 ± 13 ka). (11) The andesite flow of TEQ123 (87 ± 12 ka) overlies the northwest flank of V. Tequila (196 ± 12 ka).

Interlaboratory comparisons

Our $^{40}Ar/^{39}Ar$ results are in excellent agreement with previously published ages in all cases where the same lava flows or samples were dated. First, samples from two different rhyolite domes, TEQ22 and TEQ35, with $^{40}Ar/^{39}Ar$ ages from this study of 416 ± 3 ka and 632 ± 8 ka, correspond to samples 1075-46 and 1075-142, which have K-Ar ages of 456 ± 18 ka and 614 ± 20 ka, respectively (Harris 1986). Second, the spine of Volcán Tequila was sampled and dated at 206 ± 07 ka with the K-Ar method by Harris (1986), whereas the same sample (1075-Q9a) was dated in this study at 198 ± 11 ka with the $^{40}Ar/^{39}Ar$ method. Third, a basalt flow from the southern rim of the Santiago canyon that we collected and dated (TEQ12, 592 ± 20 ka) is the same as that collected and dated with the K-Ar method by Gilbert et al. (1985) (MW995-033, 530 ± 75 ka) and collected

and dated with the K-Ar method by Wopat (1990) (1081-011, 524 ± 36 ka). A sample from close to this same location and with a major element composition that is similar was collected and dated by Nixon et al. (1987) at 930 ± 30 ka. However, it is possible that this difference in dates may mark the boundary between a younger sequence of basalts that filled the canyon and lapped up against the erosional remnant of an earlier sequence of basalts that filled and flooded the river canyon. Finally, our date of 191 ± 13 ka for an andesitic lava from the main edifice of V. Tequila (TEQ17) is similar to the reported K-Ar age of 220 ± 30 ka by Nixon et al. (1987) for a Tequila lava located close to TEQ17 (Figure 2).

Replications

As a check on our $^{40}Ar/^{39}Ar$ method, different samples from the same volcanic edifice/flow were dated in order to evaluate the consistency between results. (1) Six samples were taken from different parts of the main edifice of V. Tequila (TEQ15, TEQ23C, TEQ60, TEQ17, TEQ6, 1075-Q9a; Figure 2) and resulted in a series of dates (196 ± 8, 196 ± 19, 178 ± 8, 191 ± 13, 216 ± 11, and 198 ± 11 ka; Figure 3a) that are all within 2 sigma error of each other. The mean eruption age for the main edifice of V. Tequila is thus 196 ± 12 ka. These results further suggest, within a 95 % confidence interval, that the bulk of the main edifice was erupted within ≤ 24 kyrs. (2) Two samples from Cerro Tomasillo (PW139 and PW143), collected and described by Wallace and Carmichael (1994), resulted in ages of 66 ± 20 and 58 ± 10 ka, respectively. Although Wallace and Carmichael (1994) label sample PW143 a flank andesite and do not assign it to Cerro Tomasillo, its location (field map of Paul Wallace, personal communication) is clearly a flow from Cerro Tomasillo as revealed by the newly available aerial photographs and digital elevation models with 2m vertical resolution (Figure 2). (3) Two peripheral andesite samples of nearly identical composition (Table 1) taken from a cinder cone (TEQ31) and the distal edge of its associated lava flow (TEQ38) were both dated and gave nearly identical results (691 ± 26 and 683 ± 32 ka, respectively). (4) Two rhyolite samples from the same dome (TEQ18 and TEQ35) with nearly identical major and trace element compositions also gave indistinguishable results (642 ± 6 ka, 632 ± 8 ka). (5) Two andesite samples from the same northwest flank flow (TEQ46/TEQ48) with

nearly identical compositions (Table 1) gave the same age within error. Their plateau ages are within 2σ of each other (53 ± 16 ka and 119 ± 18 ka), with a mean age of 86 ± 47 ka, whereas their isochron ages are within 1σ of each other (73 ± 24 ka and 108 ± 27 ka), with a mean age of 91 ± 25 ka. These flank andesite lavas were among the most difficult to date owing to their youthfulness and vesicularity.

Summary of results for samples ≤ 1 Ma

The eruption frequency of the different lava types (basalt/basaltic andesite, andesite, dacite and rhyolite) over the last 1 Myr is illustrated in Figure 4. The earliest eruptions of basalt occurred between 1 and 0.85 Ma within the Rio de Santiago canyon; the geographic distribution of ages, morphology of flows, and petrographic textures strongly suggest that this episode of basaltic volcanism led to the complete filling and ponding of this segment of the canyon, causing basalt to flood southward and create the primary surface of the Santa Rosa plateau. Flows that clearly post-date this primary surface include the TEQ31/TEQ38 andesite cone and flow near the town of Amatitan (691 ± 26; 683 ± 32 ka) and the 630 ka dacite flow, north of the town of Tequila, dated by Nixon et al. (1987). Basaltic eruptions continued to occur within the canyon; the next series of eruptions occurred between ~670 and 590 ka (TEQ10 and TEQ12) and appear to have filled the canyon locally and possibly caused the river to be re-routed several hundred meters northward. The most recent eruption of basalt within the canyon produced a lava cone (MW72) dated by Wopat (1990) at 364 ± 46 ka. Between 0.95 and 0.19 Ma, at least six different basalt and basaltic andesite eruptions occurred from isolated vents located on top of the Santa Rosa plateau. The youngest dated basalt (140 ± 12 ka) is from cinder cone ETZ1, which is west of V. Tequila (Figures 2 and 3a).

The first eruptions of andesite were all peripheral to V. Tequila and include both cinder cones and small lava flows. The oldest andesite (within the last 1 Myr) erupted ~690 ka as a cinder cone and associated flow on top of the Santa Rosa plateau (TEQ31/38). The next andesite eruptions all occurred west and south of V. Tequila between ~450 and ~225 ka as small flows and cinder cones. The main edifice of V. Tequila is predominantly andesitic and appears to have erupted over a relatively narrow time interval at ~200 ka. After an apparent hiatus of ~110 kyrs, young andesite flows

erupted ~90 ka along the northwest (TEQ123, TEQ46, TEQ48) and southeast (TAL1) flanks of V. Tequila. The youngest eruption of andesite (and the youngest feature in the Tequila volcanic field) built the small stratocone of Cerro Tomasillo ~60 ka.

Two andesite samples of nearly identical bulk composition (Table 1) are from one of the flank flows southeast of V. Tequila (TAL21 and TAL27) and were both dated; unfortunately, both resulted in highly disturbed gas spectra without a plateau, and dates are not reported. However, four different stratigraphic relations observed in the field bracket the age of this flow. Along its western margin, this flank lava flowed on top of the southernmost flows from V. Tequila (196 ± 12 ka), and it also flowed around cinder cone TAL12 (454 ± 32 ka). This flank flow is also clearly overlain by both Cerro Tomasillo (62 ± 11 ka) and the dacite domes and associated flows (> 75 ka). Thus this flank flow must have erupted sometime between ~200 and ~75 ka, and its eruption may have been broadly contemporaneous with the other andesite flank eruptions northwest and southeast of V. Tequila, all of which have $^{40}Ar/^{39}Ar$ dates that cluster ~90 ka.

Dacite first erupted ~630 ka as a series of cinder cones west of V. Tequila (ETZ4, ETZ11) and also as a flow on top of the Santa Rosa plateau (north of the town of Tequila; dated by Nixon et al. 1987). The next dacite eruptions were two small cinder cones southwest of V. Tequila ~390 ka (TAL8, TAL9). Small remnants of a dacitic airfall deposit are found underneath a small block and ash deposit of two-pyroxene andesite (TEQ23C), which has been dated at 196 ± 19 ka. Thus it appears that a small explosive eruption of dacite from the main edifice of V. Tequila occurred ~200 ka. The youngest dacite (erupted sometime between 200 and 75 ka) occurs as a series of small domes and associated flows that are immediately SE of Cerro Tomasillo.

Rhyolite domes have erupted sporadically between 1120 and 240 ka throughout the field area (on all sides of V. Tequila) with the greatest frequency of eruption between 400 and 700 ka. No rhyolite has erupted since the onset of major andesitic volcanism ~200 ka, when the main edifice of V. Tequila was built.

Samples > 1 Ma

Four dated samples are older than 1 Myr and are not included in the inventory of erupted volumes. The results for these four samples are given in Table 2c; only two have

plateau ages. The oldest (TEQ9, 5.14 ± 0.05 Ma) is a hornblende-bearing andesite ashflow erupted onto (and covered by) lake sediments and is located on the southern wall of the Rio de Santiago canyon stratigraphically beneath TEQ10, in view of the Santa Rosa dam. This is likely the same unit that was dated by Damon et al. (1979) at 4.69 Ma and described as a hornblende tuff near the town of Achio. The other three lavas are found west of V. Tequila and are all crystal-poor to aphyric. One is an andesite (ETZ2, 2.24 ± 0.02 Ma) and plots outside the field area, whereas the other two are a basaltic andesite and a rhyolite, respectively (ETZ5, 3.86 ± 0.04 Ma and ETZ7, 3.02 ± 0.05 Ma) and appear in Figures 2 and 3a.

Volumes

Methods and Errors

The total volume of magma erupted at the Tequila volcanic field over the last 1 Myr was determined from geologic field mapping combined with analysis of DEMs (1:50,000) superimposed on aerial photographs (taken at a scale of 1:20,000) using the GIS software ArcView 3.2 and ArcGIS 8.1. The Universal Transverse Mercator (UTM) projection and the Geodetic Reference System 80 (GRS 80) model are used. The DEMs have a horizontal and vertical resolution of 50 m and 2 m, respectively. In order to evaluate the volumes of volcanic cones, domes, and flows, individual units were recreated in three dimensions using ArcGIS software.

All units were assumed to have a planar base, as small variations in underlying topography were impossible to ascertain. When a cone, dome, or flow sat on a surface with a slope <1-2°, the base of the 3D unit was assumed to be horizontal at the elevation of the lowest point on the perimeter of the unit. When the underlying surface constituted a steeper slope, the base slope of the unit was programmed manually; a sloping plane was created using the points of elevation around the perimeter of the unit. If the perimeter was obscured, i.e. the flows were ponded against older units or encroached upon by younger flows, the slope and elevation of points at the base were inferred from flow thickness and adjacent areas where the underlying slope was visible. Errors were evaluated individually based on maximum and minimum possible volumes. For more details of the procedure and error analysis, see Frey et al. 2003.

The most challenging aspect of the volume calculations was determining the slope and elevation of the basal surface beneath each unit. The errors of individual units fall into three categories, ± 0 - 5 %, ± 6 - 10 %, and ± 11 - 25 % (Table 3). Errors are smallest (≤ 5 %) for units with well-exposed boundaries, including cinder cones and isolated domes and flows. Volumetric errors of 6 - 10% resulted if andesitic lava flows or rhyolitic domes ponded against older units or if overlying flows obscured the thickness at the perimeter. To estimate the thickness of a ponded flow, the underlying slope was calculated where it was visible and extended to the contact so the elevation at the base of the flow could be estimated. Where a flow was partially buried, the thickness around the exposed edge was measured and the concealed thickness estimated. Maximum and minimum volumes were estimated by varying the thickness of the flow and the elevation (degree of slope) of the underlying surface.

The most complex areas for volumetric calculations, and thus those with the largest errors (11 - 25 %), occur where rhyolitic domes are partially covered by younger andesite lavas. In these cases, the minimum volume is based on the area of the exposed dome and a horizontal base level at the lowest point of the perimeter. The sides were assumed to be vertical, which is consistent with their steep margins observed in the field. The maximum volume is calculated by assuming that the exposed area is a fraction of an idealized, circular dome where the highest elevation of the exposed dome is assumed to be the center. The volumes of the younger andesite flows that flank V. Tequila and partially cover rhyolite domes were calculated based on their well-defined perimeter and an estimate of their thickness from the elevation and topography inferred for the underlying volcanic units. Minimum volumes were calculated by assuming the flows had a constant thickness over the exposed area.

Results

The results of the volume calculations are given in Table 3; Figure 3b shows the outlines of the units used for these calculations. A relatively large volume is calculated for basalt owing to our interpretation that basalt filled the Santiago canyon ~1.0-0.9 Ma and subsequently flooded the Santa Rosa plateau at ~0.85-0.9 Ma. The volume of canyon-fill up to 20-40 m below the southern rim (~1060-1080 m) is readily calculated

with the ArcGIS software and leads to a value of ~23-25 km^3. This volume is likely a maximum, as the canyon was probably less deeply incised at 1 Ma than today. On the other hand, this calculation does not account for the volume of basalt that filled the canyon downstream, north of our defined field area. The volume of basalt that is estimated to have covered the Santa Rosa plateau ~0.9-0.85 Ma depends on its areal extent and thickness. The areal extent (~300 km^2) is estimated to be its currently exposed area (190 km^2) plus the area of the canyon at the 1100 m contour line (110 km^2). The thickness (~30 m) is based on that for the package of three flows described and dated (top and third flow) by Wopat (1990) that cap the canyon rim (MW77, MW78; Figure 2). Thickness variations of 20-40 m led to a minimum and maximum volume for the lavas of the Santa Rosa plateau of 6-12 km^3.

The sequence of dates obtained for TEQ12 (surface flow, 592 ± 20 ka) and TEQ10 (ponded flow beneath TEQ12, 671 ± 13 ka) suggest that a second infilling of the canyon occurred locally in this area. A total volume of 4.4 - 6 km^3 is estimated for this canyon-fill. The volumes of isolated basalt and basaltic andesite flows located on top of the Santa Rosa plateau are 0.40 ± 0.002 km^3 (TEQ37), 0.60 ± 0.015 km^3 (TEQ36), and 0.20 ± 0.01 km^3 (TEQ40), whereas individual cinder cones associated with the basalt flows are ≤ 0.01 km^3.

The central andesitic stratocone, Volcán Tequila, has an estimated volume of 31 ± 2.1 km^3, whereas the adjacent Cerro Tomasillo has a volume of 1.9 ± 0.02 km^3. The young andesitic flows that flank V. Tequila to the northwest have a collective volume of 8 ± 2 km^3, whereas the southeast flank lavas have an estimated volume of 5.8 ± 0.6 km^3. Peripheral andesitic flows and cones have a combined volume of 2.9 ± 0.2 km^3. The dacite flow north of V. Tequila has a volume of 1.4 ± 0.16 km^3, whereas the line of dacitic domes and associated flows southeast of Cerro Tomasillo are 1.1 ± 0.03 km^3. The peripheral dacitic cinder cones have a combined volume < 0.19 ± 0.005 km^3. There are 12 rhyolitic domes in the field area, with a total volume of 34.2 ± 6.3 km^3. The largest dome (TEQ21) has a volume of 16 ± 4.0 km^3, whereas all other rhyolite domes are significantly smaller (< 5 km^3).

Total erupted volumes, relative proportions of lava types, and eruption rates

The total volume of each lava type erupted in the Tequila volcanic field over the last 1 Myr is 34-44 km^3 basalt, ~0.7 km^3 basaltic andesite, 46-56 km^3 andesite, ~3.3 km^3 dacite, and 28-40 km^3 rhyolite (Table 3). Thus the total erupted volume is 111-144 km^3 (or 127 ± 16 km^3) over an area of ~1600 km^2 in the last 1 Myr, which leads to an average eruption rate of 79 $m^3/km^2/yr$. This is equivalent to a lava accumulation rate averaged over the entire field area of ~79 m/Myr or ~8 cm/ky. The relative proportions of lava types erupted in the Tequila volcanic field in the last 1 Myr are ~24-40 % basalt, ~0.6 % basaltic andesite, ~32-50 % andesite, ~2 % dacite and ~19-36 % rhyolite.

A combination of the $^{40}Ar/^{39}Ar$ dates with the volume estimates for individual eruptive units allows a graphical representation of how the volumes of different lava types were erupted over time (Figure 5a). The data illustrate a general trend of bimodal basalt-rhyolite volcanism between ~1.0 and 0.2 Ma, with only minor "background" eruptions of andesite and dacite occurring over this interval. At ~200 ka, a pulse of volcanism produced ~31 km^3 of andesite to create Volcán Tequila, followed by a hiatus of ~110 ka, whereupon ~14 km^3 of flank andesite lavas were erupted. The eruption of ~1 km^3 of dacite followed soon after, and the last eruptive activity occurred ~60 ka to produce ~2 km^3 of andesite in the form of Cerro Tomasillo.

The most recent and voluminous eruptions of andesite, including Volcán Tequila, its flank flows, and Cerro Tomasillo, all occurred within the last 200 kyrs. Thus the volcanism over this time period was overwhelmingly andesitic (~97 %). Because > 95 % of the total andesite erupted in the Tequila volcanic field occurred in the last 200 kyrs, the relative proportions of lava types is very different if only the first 800 kyrs of the last 1 Myr is considered. Over that time interval, the proportions are ~53 % basalt, ~1 % basaltic andesite, ~2.5 % andesite, ~2 % dacite and ~41 % rhyolite. Thus for a meaningful evaluation of eruption rates and relative proportions of lava types at an arc volcanic field, it is necessary to define the time scale of interest, as emphasized by Hildreth et al. (2003). This point is illustrated even more clearly by comparing the eruptive history of the Tequila volcanic field with that documented for the Ceboruco-San Pedro volcanic field (~75 km northwest of Tequila) over the last 1 Myr (Frey et al. 2003).

Comparison with the Ceboruco-San Pedro volcanic field

The relative proportions of magma types erupted in the Ceboruco-San Pedro volcanic field in the last 1 Myr are 0 % basalt, ~14-15 % basaltic andesite, ~62-66 % andesite, ~18-22 % dacite and ~1 % rhyolite (Frey et al. 2003). The distribution of the erupted volumes of these lava types over time is shown in Figure 5b and compared to that for the Tequila volcanic field. The most striking difference is the paucity of basalt and rhyolite in the Ceboruco-San Pedro volcanic field and their relative abundance in the Tequila volcanic field between 1 and 0.2 Ma. In contrast, low-volume eruptions of intermediate magma (andesite and dacite) constitute the "background trickle," the relatively continuous eruption of non-focal lavas as described in Hildreth and Lanphere (1994), at the Ceboruco-San Pedro volcanic field over this time period. Another difference is in the total output of erupted magma over the entire 1 Myr interval in the two volcanic fields (each 1600 km^2), ~81 ± 4 km^3 at Ceboruco-San Pedro vs. ~127 ± 16 km^3 at Tequila. Thus, the lava accumulation (volume per area) rate differs between the two volcanic fields by more than 50 % (~5 vs. ~8 cm/kyr) over the last 1 Myr.

The most striking similarity between the two volcanic fields is the voluminous intermediate (andesitic/dacitic) volcanism in the last few hundred kyrs. The relative proportions of magma types erupted in the last 200 kyrs are ~4 % basaltic andesite, ~71 % andesite, ~23 % dacite, and ~2 % rhyolite at the Ceboruco-San Pedro volcanic field and ~97 % andesite and ~3 % dacite at the Tequila volcanic field. Another similarity is that both volcanic fields record a hiatus in volcanism between the mid-Pliocene and ~1 Ma. Frey et al. (2003) document a hiatus in the Ceboruco-San Pedro volcanic field between 3.8 and 0.8 Ma. At the Tequila volcanic field, with the single exception of an andesitic lava west of the field area (ETZ2, 2.2 ± 0.02 Ma), there appears to be a hiatus between ~3 and 1 Ma. Lavas that cap the northern rim of the Santiago canyon north of Tequila have been dated at 3.7 and 3.9 Ma (Damon et al. 1979), and we report ages of 3.0 and 3.9 Ma on a rhyolite and basaltic andesite, respectively, west of V. Tequila. These are the youngest lavas prior to the eruption of the basaltic Santa Rosa plateau and the first of the rhyolite domes at ~1 Ma. This hiatus in volcanism coincides with the absence of convergence of the Rivera plate from 2.6-1.0 Ma, whereupon normal convergence resumed at a rate of ~3.2 cm/yr (DeMets and Traylen 2000). It is possible that the

initiation of volcanic activity ~1 Ma is related to the resumption of subduction of the Rivera plate, although bimodal rhyolitic and high-Ti basaltic volcanism is not generally associated with subduction. Perhaps hundreds of kyrs are required after resumption of subduction before voluminous andesitic volcanism can occur.

Comparison with volcanic fields in the Cascade arc

Additional comparisons of eruption rates, total volcanic output, and relative proportions of lava types can be made with two volcanic fields of similar areal extents (~1250 km^2) from the Cascade arc: the Mt. Adams volcanic field (Hildreth and Lanphere 1994) and the Mt. Baker volcanic field (Hildreth et al. 2003). Both areas are underlain by ~40-45 km of continental crust (Mooney and Weaver 1989) relative to the 35-40 km estimated beneath the Tequila and Ceboruco-San Pedro volcanic fields (Urrutia-Fucugauchi and Flores-Ruis 1996). Despite the erosive action of glacial activity over the last 1 Myr in the Cascade arc, especially at the Mt. Baker volcanic field, Hildreth and Lanphere (1994) and Hildreth et al. (2003) provide estimates of both total erupted volumes and relative proportions of lava types.

The 200 km^3 andesitic stratocone of Mt. Adams is significantly larger than Mt. Baker (15 ± 3 km^3), Black Buttes (30 ± 10 km^3) (part of the Mt. Baker volcanic field), V. Tequila (31 ± 2 km^3), and V. Ceboruco (51 ± 2.5 km^3). Moreover, owing to three separate cone-building events at Mt. Adams, the total volcanic output at this volcanic field over the last 1 Myr is estimated at 231-399 km^3 (Hildreth and Lanphere 1994). In contrast, the total volume of magma erupted at the Mt. Baker volcanic field over the last 1 Myr (not including 50-80 km^3 of rhyodacite that erupted between 1.0 and 1.3 Ma) is estimated at 65-137 km^3 (Hildreth et al 2003), which is closer to the total output documented for the Tequila and Ceboruco-San Pedro volcanic fields over the same time interval. At the Mt. Adams volcanic field, the relative proportions of lava types erupted in the last 1 Myr are ~9-15 % basalt, 84-89 % andesite, ~2 % dacite, and 0 % rhyolite (Hildreth and Lanphere 1994). Over this same interval at the Mt. Baker volcanic field, the relative proportions are ~2 % basalt, ~92 % andesite, ~4 % dacite, and ~3 % rhyolite, excluding the rhyodacitic volcanism between 1 and 1.3 Ma (Hildreth et al. 2003).

The dominance of andesite in all four volcanic fields is directly related to the voluminous cone-building events that build the large, predominantly andesitic stratocones. More frequent cone-building events (e.g., three at the Mt. Adams volcanic field) results in larger volcanic output. Based on data compiled from the literature, Crisp (1984) argues that volcanic output at arcs is inversely correlated with the thickness of crust. Although the crust beneath the Cascade arc is ~0-10 km thicker than that beneath western Mexico, the total volcanic output at the Mt. Adams volcanic field is 2-3 times higher than in the Tequila and Ceboruco-San Pedro volcanic fields over the last 1 Myr. Thus a clear correlation between the magnitude of volcanic output and crustal thickness is not yet established.

Cone-building eruption rates

With the aid of detailed, high-quality $^{40}Ar/^{39}Ar$ chronology, eruption rates can be determined not only for entire volcanic fields over a 1 Myr time interval but also over relatively narrow time scales (i.e., tens of kyrs) appropriate to cone-building events at individual stratocones. At V. Tequila, six samples taken from different parts of the main edifice all have ages within two sigma of each other, leading to a mean eruption age of 196 ± 12 ka. The volume of the edifice is estimated at ~31 km^3; if the two-sigma error on the eruption age (24 kyrs) is a good estimate of the maximum time interval over which the Tequila stratocone was built, then the cone-building eruption rate is ≥ 1.3 km^3/kyr, comparable to rates documented at other arc stratocones.

For example, the historically active stratocone of Volcán Colima in western Mexico (Figure 1) has erupted ~10 km^3 over the last 4300 years ago (Luhr and Prestegaard 1988), leading to an eruption rate of ~2.3 km^3/yr, nearly twice the minimum estimated for V. Tequila. The other historically-active stratocone in western Mexico, Volcán Ceboruco, is even more prodigious in its output, and has erupted ~9.5 km^3 of andesite and dacite in the last 1000 yrs (Nelson 1980, Frey et al. 2003), following a Plinian eruption of ~3-4 km^3 of dacite (Gardner and Tait 2000). The rate of effusive, cone-building volcanism at V. Ceboruco is thus ~9.5 km^3/kyr. Stratocones from the Cascade arc display a similar range of eruption rates. For example, the Mt. St. Helens volcano in the Cascade arc has erupted ~40 km^3 over the last 4000 years, leading to a

cone-building rate of ~10 km^3/kyr (Mullineaux 1986). Hildreth and Lanphere (1994) document three separate cone-building events at the Mt. Adams volcano (~50 km east of Mt. St. Helens) over the last 1 Myr with rates that range from 1.6-5.0 km^3/kyr. More recently, Hildreth et al. (2003) estimated significantly lower cone-building rates of ~0.3 ± 0.15 km^3/kyr for two andesitic centers in the Mt. Baker volcanic field, Black Buttes and Mt. Baker. Thus it appears that cone-building rates at arc stratocones can vary by approximately two orders of magnitude.

Evidence for two short-lived upper crustal magma chambers separated in time

Detailed $^{40}Ar/^{39}Ar$ chronology constrains not just the rate, but also the duration of cone-building events, and, when combined with petrologic and textural evidence, can be used to place upper limits on the longevity and depth of upper crustal magma chambers. The location of Volcán Tequila and its flank lavas along a prominent NW-SE lineament suggests that they overlie a major passageway for magmas ascending from the lower or middle crust. These magmas appear to have collected in the upper crust, forming a chamber at two discrete periods of time: ~200 ka and ~90 ka for durations of ~30 kyrs or less. These chambers are expected to be the site of mingling between different ascending magma batches that may or may not be related to one another by crystal fractionation. Ubiquitous disequilibrium textures in these lavas, described by Wallace and Carmichael (1994), confirm the mingling of at least three endmember magma compositions (andesite to dacite) prior to eruption. Importantly, the endmember magmas were already of andesitic to dacitic composition prior to their mingling within the upper crustal chambers.

The chronologic evidence for two discrete magma chambers beneath V. Tequila, separated in time by ~110 ka, is further supported by phase equilibrium data. Most of the lavas erupted ~90 ka from the flanks of V. Tequila are distinguished from those erupted ~200 ka from the main edifice by the addition of hornblende to an otherwise similar phenocryst assemblage of plagioclase and two pyroxenes. Wallace and Carmichael (1994) performed a detailed petrologic study of both sets of lavas and show a systematic difference in their pre-eruptive temperatures and water concentrations. On the basis of both iron oxide and two-pyroxene thermometry, they calculated temperatures of ~910-960°C for the hornblende-bearing magmas and ~990-1045°C for the hornblende-free

magmas. Wallace and Carmichael (1994) used these temperatures in conjunction with the plagioclase-melt equilibria of Housh and Luhr (1991) to estimate pre-eruptive water concentrations in the two groups: 3.3-4.7 and 2.5-3.0 wt % for those with and without hornblende, respectively. In Figure 6, we combine these results with the experimentally determined water-saturated phase diagram of Moore and Carmichael (1998) for an andesite from western Mexico (similar to those erupted from V. Tequila) to locate the position of two discrete magma chambers in P-T space (Figure 6). The results suggest that the earlier magma chamber that fed the eruptions of V. Tequila ~200 ka (for a duration of $\leq$ 24 kyrs) was located at a relatively shallow depth of ~2-3 km (~50-70 MPa) and was injected by magmas $\geq$ 990°C. The absence of hornblende phenocrysts reflects higher magmatic temperatures, i.e., above the thermal stability limit of hornblende. In contrast, the second chamber, which formed ~110 ka later, appears to have been located at a depth of ~5.0-6.5 km (130-170 MPa) and was injected by relatively cooler magmas (910-960°C), thus allowing hornblende to crystallize.

The peripheral andesites and dacites, especially those erupted from the nine cinder and lava cones along the southern margin of V. Tequila, have very few phenocrysts, which suggests that they ascended rapidly through the upper crust and did not stall within an upper crustal chamber. Nor is there any textural evidence of magma mingling, which is consistent with the monogenetic character of each cone and flow. The absence of any upper crustal magma chamber feeding these small-volume eruptions of andesite and dacite (total volume is ~4.5 km^3) is further supported by the distribution of their eruption ages over a 460 kyr interval (~685-225 ka), with no pattern of increasing silica content with time (Figure 7). These peripheral eruptions give further evidence that hydrous andesitic and dacitic magmas are emplaced into the upper crust as crystal-poor *liquids* and that significant crystallization of these magmas occurs only if they stall and degas within upper crustal chambers (Cashman and Blundy 2000; Carmichael 2002).

The plagioclase phenocrysts in most of the andesites and dacites (both peripheral and focal eruptions) have cores, and sometimes bands, that are riddled with melt inclusions. This texture is often interpreted in the literature as a resorption feature. An alternative hypothesis (Anderson 1984) is that this texture reflects extremely rapid crystal growth under conditions of strong undercooling ($\Delta T > 100$ degrees), similar to that

documented in experiments by Lofgren (1974). Such strong undercooling is fully expected if crystallization of these andesites and dacites is driven by degassing of water during decompression, causing the liquidus for plagioclase to abruptly increase by > 100 degrees (Figure 6). If this texture is a reflection of degassing-induced crystallization, then it further underscores the conclusion that the andesites and dacites were emplaced into the upper crust as crystal-poor liquids.

Petrogenesis of lavas within the Tequila volcanic field

The detailed eruptive chronology of the diverse lavas within the Tequila volcanic field, combined with their relative volumes, places strict constraints on models of their collective petrogenesis. Proposed models must be consistent with the following observations: (1) The basalts and rhyolites are broadly associated in time (1-0.2 Ma) and do not appear to be directly related to the voluminous eruptions of andesite over the last 200 kyrs. (2) The compositional spectrum of andesite through dacite (59-69 wt % SiO_2) was erupted from small-volume, isolated flows and cinder cones over a period of ~460 kyrs (~685-225 ka) with no time progression in their compositions. (3) The compositional spectrum of andesite through dacite (mostly 59-63 wt % SiO_2) was erupted in relatively large volumes in a relatively short time (tens of kyrs) at V. Tequila at two discrete times, separated by a hiatus of ~110 kyrs. (4) Hydrous andesitic and dacitic liquids were emplaced into the upper crust (either into short-lived chambers or directly onto the surface) as crystal-poor liquids, and therefore must have been generated in the middle or lower crust by a process that produces a crystal-poor liquid.

Further constraints on the genetic relationships among the lavas are provided by simple plots of two incompatible trace elements, Ba (large ion lithophile) and Zr (high field strength) as a function of silica concentration (Figure 8). The lavas are divided into four groups: (1) basalt/basaltic andesite, (2) andesite/dacite from V. Tequila and its flanks, including C. Tomasillo, (3) peripheral andesite/dacite, and (4) rhyolites. The basalts and basaltic andesites show a wide spread in these two incompatible elements and indicate considerable geochemical diversity among the mafic lavas. Therefore, any relationship among the basalts and basaltic andesites likely involved numerous parental liquids following limited differentiation trends, similar to the conclusions drawn by

Dungan et al. (2001) for lavas at the Tataro-San Pedro volcanic field. The rhyolites, with which the basalts and basaltic andesites are associated in time, have an equally large spread in Ba and Zr, and thus clearly were not all derived from a single, homogenous rhyolitic magma body with a long residence time in the upper crust (i.e., over ~800 kyrs of eruptive history). A more plausible scenario is that the individual rhyolite domes each were produced during discrete episodes of partial melting of upper sialic crust, most likely driven by the episodic emplacement of hot, basaltic magmas into the upper crust between 1.0 and 0.2 Ma; some of these basalts erupted along NW-SE fractures and faults. It is unclear whether this bimodal volcanism of rhyolite and high-Ti basalt is a consequence of the renewed subduction of the Rivera plate ~1 Ma or merely reflects extensional tectonics.

The andesites and dacites, especially those erupted in significant volumes from V. Tequila and its flanks, are not obviously linked to the basalts and basaltic andesites in terms of their eruptive history. If they are related by a crystal fractionation process to parental liquids similar to these more mafic lavas, then the scatter in Ba and Zr indicates that such a process must have operated on numerous parental liquids, each of which was geochemically distinct and likely of modest volume. Thus, the image of a single or only a few large chambers of initially homogeneous magma undergoing crystal-fractionation (e.g., á la Skaergaard) is probably unrealistic. Nor is mixing of the rhyolites and basalts to produce the andesites and dacites a reasonable hypothesis because: (1) such mingled basalt/rhyolite lavas have not been identified in the Tequila volcanic field despite their coexistence for ~800 kyrs, (2) there is no evidence of a single olivine crystal in more than 150 thin sections of andesite/dacite lavas from the Tequila volcanic field examined petrographically by Wallace and Carmichael (1994) (and 28 more in this study), and (3) textural evidence suggests that andesitic and dacitic magmas were emplaced into the upper crust as homogenous, crystal-poor liquids, and therefore mingling and crystallization occurs largely in upper crustal chambers. Therefore, of the four principal mechanisms commonly invoked to explain the generation of andesite/dacite magmas at subduction zones (i.e., crystal fractionation, crustal assimilation, magma mixing, partial melting), the one that appears to be most consistent with the evidence provided in this study is partial melting of an amphibolitized mafic lower crust.

Many authors (e.g., Hildreth and Moorbath 1988; Atherton and Petford 1993; Tepper et al. 1993; Lange and Carmichael 1996) have suggested that mantle-derived arc magmas solidify near the base of the arc crust, causing crustal thickening through magma accretion. During solidification, hydrous basaltic magmas lose some water, allowing a hydrous fluid to ascend through fractures and amphibolitize previously solidified mafic rocks. The introduction of new additions of basaltic magma from the mantle may then heat and partially melt variably hydrated (amphibolitized) portions of the mafic lower crust. Melting experiments on mafic amphibolite at ~1 GPa indicate that initial partial melts are broadly dacitic in composition for as long as hornblende is residual; melts move to andesitic compositions as the amphibole-out curve is crossed (e.g., Wolf and Wyllie 1994).

Although it is beyond the scope of this paper to provide a rigorous evaluation of the partial melting hypothesis, it appears to be the process that is most consistent with the detailed eruptive history documented for two different volcanic fields (Tequila and Ceboruco-San Pedro) in the western Mexican arc. The recurring theme is a persistent background leakage to the upper crust of geochemically diverse, small-volume batches of crystal-poor magma with a compositional range over basaltic andesite/basalt, andesite, and dacite. The magmas undergo significant crystallization only after emplacement in the upper crust, have no progressive sequence in their composition over time, and are periodically punctuated by voluminous bursts of andesitic magmatism.

Acknowledgement

This study was supported by NSF grant EAR-9909567. We thank Marcus Johnson for his assistance in the geochronology lab. We very much appreciate the field assistance of Marcos Luna Alonso and Miguel Angel Alatorre Ibarguengoitia. We also thank Ian Carmichael for spending a few days with us in the field and sharing his 30+ years of experience of the volcanic geology of western Mexico. Discussions with Holli Frey about the ArcGIS software are also greatly appreciated. We especially thank Paul Wallace for sending us several samples from his collection, four of which were dated for this study.

References

Allan JF, Nelson SA, Luhr JF, Carmichael ISE, Wopat M, and Wallace PJ (1991) Pliocene-Holocene rifting and associated volcanism in southwest Mexico: an exotic terrane in the making. In: Dauphin JP, Simoneit BA (eds) The gulf and peninsular province of the Californias. Am Assoc Petrol Geol Mem 47:425-445

Atherton MP and Petford N (1993) Generation of sodium-rich magmas from newly underplated basaltic crust. Nature 362: 144-146

Baksi AK, Archibald DA, Farrar E (1996) Intercalibration of 40Ar/39Ar dating standards. Chem Geol 129:307-324

Carmichael ISE (2002) The andesite aqueduct: perspectives on the evolution of intermediate magmatism in west-central (105-99°W) Mexico. Contrib Mineral Petrol 143:641-663

Cashman K, Blundy J (2000) Degassing and crystallization of ascending andesite and dacite. Phil Trans Roy Soc Lond Ser A 358: 1487-1513

Conway FM, Ferrill DA, Hall CM, Morris AP, Stamatakos JA, Connor CB, Halliday AN, Condit C (1997) Timing of basaltic volcanism along the Mesa Butte fault in the San Francisco volcanic field, Arizona, from $^{40}Ar/^{39}Ar$ dates: implications for longevity of cinder cone alignments. J Geophys Res 102:815-824

Crisp JA (1984) Rates of magma emplacement and volcanic output. J Volcanol Geotherm Res 20:177-211

Damon PE, Nieto-Obregon J, Delgado-Argote LA (1979) Un plegamiento neogénico en Nayarit y Jalicso y evolución geomórphica del Río Grande de Santiago. Asoc Ing Min Met Geol Mex Memoria Técnica 12: 156-191.

Delgado Granados H (1993) Late Cenozoic tectonics offshore western Mexico and its relation to the structure and volcanic activity in the western Trans-Mexican volcanic belt. Geofis Int 32:543-559

Demant A (1979) Vulcanologia y petrografia del sector occidental del eje neovolcanico. UNAM Inst Geol Revista 3:39-57

DeMets C, Traylen S (2000) Motion of the Rivera plate since 10 Ma relative to the Pacific and North American plates and the mantle. Tectonophysics 318:119-159

DeMets C, Wilson DS (1997) Relative motions of the Pacific, Rivera, North American and Cocos plates since 0.78 Ma. J Geophys Res 102:2789-2806

Druitt TH, Edwards R, Mellors M, Pyle DM, Sparks RSJ, Lanphere MA, Davies M, Barriero B (1999) Santorini Volcano. Geol Soc Mem 19, London Geol Soc, pp 1-165

Dungan MA, Wulff A, Thompson R (2001) Eruptive stratigraphy of the Tatara-San Pedro complex, 36°S, southern volcanic zone, Chilean Andes: reconstruction method and implications for magma evolution at long-lived arc volcanic centers. J Petrol 42:555-626

Frey HM, Lange RA, Hall CM, Delgado Granados H (2003) Magma eruption rates constrained by 40Ar/39Ar chronology and GIS for the Ceboruco-San Pedro volcanic field, western Mexico. Geol Soc Am Bull: in press

Gilbert CM, Mahood GA, Carmichael ISE (1985) Volcanic stratigraphy of the Guadalajara area, Mexico. Geofís Int 24: 169-192

Gill J (1981) Orogenic andesites and plate tectonics. Springer-Verlag, Berlin-Heidelberg-New York, pp 1-385

Hall CM, Farrell JW (1995) Laser $^{40}Ar/^{39}Ar$ ages of tephra from Indian Ocean deep-sea sediments: tie points for the astronomical and geomagnetic polarity time scales. Earth Planet Sci Lett 133:327-338
Hall CM, York D (1978) K-Ar and $^{40}Ar/^{39}Ar$ age of the Laschamp geomagnetic polarity reversal. Nature 274:462-464
Hall CM, York D (1984) The applicability of 40Ar/39Ar dating to young volcanics: Quaternary Dating Methods 67-74
Harris, JM (1986) Silicic volcanics of Volcán Tequila, Jalisco, Mexico. MS thesis University of California, Berkeley
Heizler MT, Perry FV, Crowe BM, Peters L, Appelt R (1999) The age of Lathrop Wells volcanic center: an Ar-40/Ar-39 dating investigation. J Geophys Res 104:767-804
Hildreth W, Fierstein J, Lanphere M (2003) Eruptive history and geochronology of the Mount Baker volcanic field, Washington. Geol Soc Am Bull 115: 729-764
Hildreth W, Lanphere MA (1994) Potassium-argon geochronology of a basalt-andesite-dacite arc system: the Mount Adams volcanic field, Cascade Range of southern Washington. Geol Soc Am Bull 106:1413-1429
Hildreth W, Moorbath S (1988) Crustal contributions to arc magmatism in the Andes of central Chile. Contrib Mineral Petrol 98:455-489
Housh TB, Luhr JF (1991) Plagioclase-melt equilibria in hydrous systems. Am Mineral 78: 477-492
Klitgord KD, Mammerickx J (1982) Northern East Pacific Rise: magnetic anomaly and bathymetric framework. J Geophys Res 87:6725-6750
Lange RA and Carmichael ISE (1996) The Aurora volcanic field, California-Nevada: oxygen fugacity constraints on the development of andesitic magma. Contrib Mineral Petrol 125: 167-185.
Lanphere MA (2000) Comparison of conventional K-Ar and 40Ar/39Ar dating of young mafic volcanic rocks. Quaternary Res 53: 294-301
Luhr JF, Prestegaard KL (1988) Caldera formation at Volcano Colima, Mexico by a large Holocene volcanic debris avalanche. J Volcanol Geotherm Res 35: 335-348
Mahood GA (1981) A summary of the geology and petrology of the Sierra La Primavera, Jalisco, Mexico. J Geophys Res 86: 10137-10152
Mooney WD, Weaver CS (1989) Regional crustal structure and tectonics of Pacific coastal states: California, Oregon, and Washington. GSA Memoir 172:129-161
Moore G, Carmichael ISE (1998) The hydrous phase equilibria (to 3 kbar) of an andesite and basaltic andesite from western Mexico: constraints on water content and conditions of phenocryst growth. Contrib Mineral Petrol 130:304-319
Mullineaux DM (1986) Summary of pre-1980 tephra-fall deposits erupted from Mount St. Helens, Washington State, USA: Bull Volcanol 48: 17-26
Nelson SA (1980) Geology and petrology of Volcán Ceboruco, Nayarit, Mexico. Geol Soc Am Bull 91: 2290-2431
Nieto-Obregón J, Delgado L, Damon PE (1985) Geochronologic, petrologic, and structural data related to large morphologic features between the Sierra Madre Occidental and the Mexican volcanic belt. Geofís Int 24:623-663
Nixon GT, Demant A, Armstrong RL, Harakal JE (1987) K-Ar and geologic data bearing on the age and evolution of the Trans-Mexican volcanic belt. Geofís Int 26:109-158

Pardo M, Suárez G (1993) Steep subduction geometry of the Rivera plate beneath the Jalisco block in western Mexico. Geophys Res Lett 20:2391-2394

Renne PR, Sharp WD, Deino AL, Orsi G, Civetta L (1997) $^{40}Ar/^{39}Ar$ dating into the historical realm: calibration against Pliny the Younger. Science 277:1279-1280

Renne PR, Swisher CC, Deino AL, Karner DB, Owens TL, DePaolo DJ (1998) Intercalibration of standards, absolute ages, and uncertainties in 40Ar/39Ar dating. Chem Geol 145:117-152

Samson SD, Alexander EC (1987) Calibration of the interlaboratory $^{40}Ar/^{39}Ar$ dating standard, Mmhb-1. Chem Geol 66:27-34

Singer BS, Thompson RA, Dungan MA, Feeley TC, Nelson ST, Pickens JC, Brown LL, Wulff AW, Davidson JP, Metzger J (1997) Volcanism and erosion during the past 930 k.y. at the Tatara-San Pedro complex, Chilean Andes. Geol Soc Am Bull 109:127-142

Steiger RH, Jäger E (1977) Subcommission on geochronology: convention on the use of decay constants in geo- and cosmochronology. Earth Planet Sci Lett 36:359-362

Taylor (1982) An Introduction to Error Analysis: The Studies of Uncertainty in Physical Measurements. Mill Valley, CA, University Science Books, pp 1-270

Tepper JH, Nelson BK, Bergantz GW, Irving AJ (1993) Petrology of the Chilliwack Batholith, North Cascades, Washington: generation of calc-alkaline granitoids by melting of mafic lower crust with variable water fugacity. Contrib Mineral Petrol 113: 333-351

Urrutia-Fucugauchi J, Flores-Ruis JH (1996) Bouguer gravity anomalies and regional crustal structure in central Mexico. Int Geol Rev 38:176-194

Wallace PJ, Carmichael ISE (1994) Petrology of Volcán Tequila, Jalisco, Mexico: disequilibrium phenocryst assemblages and evolution of the subvolcanic magma system. Contrib Mineral Petrol 117: 345-361

Wolf MB and Wyllie PJ (1994) Dehydration-melting of amphibolite at 10 kbar: the effects of temperature and time. Contrib Mineral Petrol 115: 369-383

Wopat MA (1990) Quaternary alkaline volcanism and tectonics in the Mexican volcanic belt near Tequila, Jalisco, southwestern Mexico. PhD dissertation University of California, Berkeley

Table 1 Whole-rock major and trace element compositions and modal analyses of dated samples

	Basalts						Basaltic Andesites					
	TEQ 12	TEQ 10	TAL 3	ETZ 1	TEQ 36	TEQ 39	ETZ 6	TAL 26	TEQ 40	TEQ 37	TEQ 32	TEQ 33
Whole-rock composition, major elements (wt. %)												
SiO_2	49.02	49.09	49.46	50.01	50.49	50.59	52.55	53.19	53.85	53.98	55.71	55.96
TiO_2	2.46	2.46	2.04	2.31	2.33	2.59	1.29	1.72	1.39	1.77	1.74	1.61
Al_2O_3	16.21	15.81	16.48	15.83	16.10	15.65	17.07	16.53	17.90	16.35	16.24	16.61
Fe_2O_3*	12.16	12.45	11.32	10.12	11.26	11.71	7.94	9.81	8.08	8.95	9.04	8.80
MnO	0.19	0.19	0.17	0.19	0.18	0.16	0.17	0.17	0.12	0.14	0.16	0.13
MgO	5.55	5.76	5.76	5.45	5.28	3.44	5.78	4.52	3.76	4.29	3.25	3.28
CaO	8.92	8.91	9.00	8.11	7.43	6.97	8.28	7.22	7.70	7.15	6.34	6.56
Na_2O	3.76	3.79	3.56	3.73	3.48	3.59	3.64	3.85	3.62	3.82	4.13	4.10
K_2O	1.14	1.12	1.01	1.66	1.69	1.73	1.26	1.91	1.71	2.19	2.14	1.94
P_2O_5	0.52	0.53	0.43	0.99	1.06	0.61	0.39	0.92	0.36	0.60	0.65	0.55
LOI	-0.17	-0.59	0.11	0.18	1.19	1.46	0.39	0.24	0.48	0.87	0.60	0.60
TOTAL	99.76	99.51	99.34	98.58	100.49	98.49	98.75	100.08	98.97	100.12	99.99	100.14
Whole-rock composition, trace elements (ppm)												
Zr	192	185	175	205	262	210	171	320	175	133	113	207
Ba	358	337	414	684	923	670	655	826	626	824	795	791
Modal % analyses												
plag ph	18.5	16.3	4.2	5.0	0.7	0.2	4.8	22.0	23.4	2.9	1.0	3.1
mph	13.9	8.5	5.8	5.4	3.7	2.5	5.6	10.0	7.0	7.9	2.8	7.4
opx ph	-	-	-	-	-	-	-	-	-	-	-	-
mph	-	-	-	-	-	-	-	-	-	-	-	-
cpx ph	-	-	-	-	-	-	1.0	-	2.4	-	-	0.4
mph	0.2	0.7	-	-	-	-	-	-	2.5	-	0.3	1.4
ol ph	5.5	4.5	2.6	3.3	0.2	-	6.6	0.3	1.2	0.7	2.5	0.2
mph	3.5	4.3	2.6	0.5	3.9	0.5	0.5	3.6	1.0	1.3	0.7	0.8
hbd ph	-	-	-	-	-	-	-	-	-	-	-	-
mph	-	-	-	-	-	-	-	-	-	-	-	0.8
oxide	0.5	0.6	-	-	0.9	0.6	0.4	-	0.2	-	-	0.5
xls	42.1	34.9	15.2	14.2	9.4	3.8	18.9	35.9	37.7	12.8	7.3	14.6
gmass	57.9	65.1	84.8	85.8	90.6	96.2	81.1	64.1	62.3	87.2	92.7	85.4

Notes:

Fe_2O_3* is total Fe as Fe_2O_3

Modal analyses are given in vol.% and were determined by point counting >1500 points. Abbreviations: ph = phenocrysts (> 0.3 mm); mph = microphenocrysts (> 0.03 mm); xls = total crystals; gmass = groundmass;

Major elements analyzed by ICP at Activation Laboratories of Ancaster, Ontario

Trace elements analyzed by ICP-MS at Activation Laboratories of Ancaster, Ontario

Table 1 cont. Whole-rock major and trace element compositions and modal analyses of dated samples

	Andesites												
	Volcán Tequila							Flank Flows of Volcán Tequila					
	TEQ 15	TEQ 23C	TEQ 25	TEQ 60	TEQ 17	TEQ 6	TEQ 23*	TEQ-48	TEQ 46	TAL 27	TAL 21	TEQ 53	TAL 1
Whole-rock composition, major elements (wt. %)													
SiO_2	57.64	60.75	61.18	61.56	62.70	63.05	63.56	58.55	58.91	59.08	59.44	60.95	60.58
TiO_2	0.78	0.75	0.77	0.76	0.69	0.69	0.62	0.98	1.02	0.87	0.87	0.74	0.77
Al_2O_3	18.86	16.60	16.95	16.60	16.57	16.35	15.77	16.91	17.20	17.19	17.23	16.99	17.34
Fe_2O_3*	5.61	5.29	5.49	5.15	4.28	4.85	3.70	6.45	6.58	6.22	6.18	5.51	5.75
MnO	0.09	0.08	0.09	0.08	0.08	0.08	0.06	0.11	0.11	0.11	0.11	0.09	0.10
MgO	2.91	3.09	2.93	2.90	2.63	2.52	1.10	3.65	3.49	3.39	3.37	2.84	3.06
CaO	6.11	5.81	5.93	5.76	5.30	5.54	3.47	6.26	6.25	6.34	6.35	5.82	6.06
Na_2O	3.44	3.70	3.74	3.73	3.54	3.90	3.19	3.68	4.11	3.81	3.78	3.72	4.01
K_2O	1.68	2.28	2.12	2.16	2.34	2.19	2.50	2.50	1.99	1.89	2.09	2.39	1.97
P_2O_5	0.17	0.19	0.24	0.18	0.13	0.15	0.16	0.31	0.32	0.32	0.32	0.23	0.25
LOI	2.53	1.24	0.90	1.05	1.75	0.55	6.04	0.48	-0.03	0.71	0.66	0.77	0.41
TOTAL	99.81	99.79	100.34	99.93	100.00	99.86	100.16	99.86	99.94	99.95	100.39	100.06	100.30
Whole-rock composition, trace elements (ppm)													
Zr	155	155	155	168	145	137	189	236	234	207	196	189	184
Ba	920	736	736	789	713	776	930	785	792	677	694	717	687
Modal % analyses													
plag ph	6.2	13.3	2.6	10.1	14.5	5.9	1.0	6.9	5.5	7.8	0.5	8.7	8.1
mph	10.7	7.2	14.1	5.3	6.7	11.4	0.3	5.0	9.4	10.2	13.1	9.3	3.9
opx ph	1.5	2.4	1.5	3.2	2.0	1.2	0.1	1.0	1.2	0.9	0.5	2.4	1.1
mph	1.5	2.3	0.7	0.9	1.4	5.5	0.4	2.1	0.8	1.1	0.5	1.5	0.9
cpx ph	1.0	1.7	0.3	2.0	1.2	1.0	-	1.4	2.0	1.1	0.3	0.6	2.0
mph	0.6	0.6	1.3	1.6	0.2	0.5	0.2	2.0	1.2	-	0.1	1.2	1.7
hbd ph	-	-	-	-	-	-	1.2	0.5	1.2	-	-	-	-
mph	-	-	-	-	-	-	0.5	0.3	2.6	-	-	-	trace
oxide	0.5	0.2	0.8	0.3	0.1	0.1	-	0.6	1.5	0.6	0.3	0.5	-
xls	22.0	27.7	21.3	23.4	26.1	25.6	3.7	19.8	25.4	21.7	15.3	23.7	17.7
gmass	78.0	72.3	78.7	76.6	73.9	74.4	96.3	80.2	74.6	78.3	84.7	76.3	82.3

Notes:

Fe_2O_3* is total Fe as Fe_2O_3

Modal analyses are given in vol.% and were determined by point counting >1500 points. Abbreviations: ph = phenocrysts (> 0.3 mm); mph = microphenocrysts (> 0.03 mm); xls = total crystals; gmass = groundmass

Major elements analyzed by ICP at Activation Laboratories of Ancaster, Ontario

Trace elements analyzed by ICP-MS at Activation Laboratories of Ancaster, Ontario

*Note the large LOI on pumice sample

Table 1 cont. Whole-rock major and trace element compositions and modal analyses of dated samples

	Andesites									
	Peripheral Flows and Cones around Volcan Tequila									
	TEQ 31	TEQ 38	ETZ 10A	TEQ 67	ETZ 3	TAL 11	TAL 25	TAL 7	TAL 13	TAL 12
Whole-rock composition, major elements (wt. %)										
SiO_2	58.12	58.23	58.78	58.96	59.40	59.54	59.70	59.79	60.67	62.04
TiO_2	1.18	1.15	1.46	1.28	1.23	1.42	1.44	1.42	1.27	1.14
Al_2O_3	17.07	16.92	16.09	16.71	16.51	16.37	16.33	16.18	16.21	16.18
Fe_2O_3*	7.35	7.24	8.05	6.71	7.13	7.11	7.02	7.23	6.85	5.77
MnO	0.12	0.11	0.12	0.11	0.11	0.12	0.12	0.12	0.11	0.11
MgO	3.11	3.05	2.78	3.11	3.00	2.54	2.40	2.44	2.51	2.50
CaO	6.14	6.12	5.81	6.11	6.01	5.38	5.19	5.32	5.39	5.25
Na_2O	4.18	3.99	4.28	4.12	4.20	4.16	4.13	4.49	4.37	4.28
K_2O	1.91	2.06	2.20	2.05	2.07	2.57	2.79	2.31	2.35	2.44
P_2O_5	0.31	0.32	0.38	0.39	0.43	0.49	0.52	0.52	0.41	0.36
LOI	0.43	0.77	-0.23	0.10	0.02	0.62	0.44	-0.01	-0.19	-0.01
TOTAL	99.90	99.95	99.73	99.65	100.10	100.33	100.09	99.74	99.94	100.03
Whole-rock composition, trace elements (ppm)										
Zr	170	151	168	187	182	222	236	206	156	191
Ba	721	740	685	734	776	829	874	776	832	766
Modal % analyses										
plag ph	0.8	0.3	0.8	1.4	1.9	1.0	1.1	0.5	1.0	2.6
mph	4.3	6.5	2.2	3.1	1.3	4.5	0.6	9.4	1.9	3.2
opx ph	-	0.1	-	-	0.8	0.3	-	-	-	0.2
mph	-	-	-	0.3	0.1	-	-	0.1	-	0.8
cpx ph	0.2	-	-	-	0.2	-	0.1	-	0.7	0.6
mph	0.3	0.3	0.3	0.3	1.0	0.5	-	0.4	-	1.2
hbd ph	-	-	-	-	-	-	0.7	-	1.3	-
mph	-	-	-	-	-	0.9	0.5	0.7	0.4	trace
oxide	1.0	0.7	-	0.4	-	0.5	0.6	0.6	0.2	-
xls	6.6	7.9	3.3	5.5	5.3	7.7	3.6	11.7	3.6	8.6
gmass	93.4	92.1	96.7	94.5	94.7	92.3	96.4	88.3	96.4	91.4

Notes:

Fe_2O_3* is total Fe as Fe_2O_3

Modal analyses are given in vol.% and were determined by point counting >1500 points. Abbreviations: ph = phenocrysts (> 0.3 mm); mph = microphenocrysts (> 0.03 mm); xls = total crystals; gmass = groundmass; values for Fe-Ti oxides include all crystals > 0.03 mm

Major elements analyzed by ICP at Activation Laboratories of Ancaster, Ontario

Trace elements analyzed by ICP-MS at Activation Laboratories of Ancaster, Ontario

Table 1 cont. Whole-rock major and trace element compositions and modal analyses of dated samples

	Dacites					Rhyolites						Flows >1Ma			
	TAL 8	TAL 9	ETZ 11	ETZ 4	TEQ 66	TEQ 29*	TEQ 21A	TEQ 18	TEQ 22	TEQ 45B	TEQ 35	ETZ 7	ETZ 5	TEQ 9*	ETZ 2
Whole-rock composition, major elements (wt. %)															
SiO_2	64.62	66.31	66.63	67.46	68.44	73.70	74.11	74.14	74.50	75.04	75.41	75.78	55.16	55.20	61.41
TiO_2	0.93	0.77	0.71	0.53	0.68	0.09	0.15	0.11	0.15	0.12	0.11	0.16	1.79	1.21	0.67
Al_2O_3	15.66	15.44	15.51	15.26	14.59	12.63	13.33	12.26	13.39	13.11	12.56	13.10	16.79	16.24	17.40
Fe_2O_3*	4.75	4.39	3.95	3.44	3.41	1.35	1.62	1.50	1.47	1.47	1.49	1.28	9.61	6.32	5.24
MnO	0.09	0.08	0.09	0.10	0.07	0.05	0.06	0.05	0.04	0.06	0.06	0.04	0.14	0.13	0.07
MgO	1.33	1.56	0.94	0.50	0.92	0.05	0.11	0.08	0.13	0.07	0.06	0.17	2.44	2.40	2.07
CaO	3.46	3.55	2.57	1.48	2.33	0.48	0.51	0.42	0.63	0.42	0.39	0.86	5.82	5.48	5.89
Na_2O	4.75	4.48	5.06	5.47	4.44	3.69	4.61	4.35	4.50	4.67	4.45	4.20	4.62	2.79	4.00
K_2O	3.00	3.30	3.65	4.29	3.89	4.60	4.83	4.62	4.71	4.77	4.66	4.31	1.99	1.71	1.49
P_2O_5	0.32	0.23	0.22	0.13	0.22	0.02	0.03	0.02	0.03	0.02	0.02	0.04	0.58	0.37	0.19
LOI	0.28	0.02	0.16	0.52	-0.06	3.81	1.14	0.67	0.87	0.20	1.25	0.43	1.08	8.12	1.59
TOTAL	99.18	100.14	99.50	99.19	98.94	100.48	100.50	98.22	100.43	99.94	100.46	100.35	100.02	99.96	100.02
Whole-rock composition, trace elements (ppm)															
Zr	249	259	404	811	237	163	263	234	183	254	228	157	251	207	129
Ba	913	927	957	1,370	852	166	342	55	940	81	53	911	820	823	666
Modal % analyses															
plag ph	1.9	1.1	2.3	-	1.2	9.0	0.6	-	-	-	-				
mph	3.4	1.0	6.0	3.4	6	0.5	0.3	-	-	-	-				
opx ph	-	0.3	-	1.8	-	-	-	-	-	-	-				
mph	0.2	0.1	-	0.1	0.3	-	-	-	-	-	-				
cpx ph	0.7	0.1	-	0.1	0.5	-	-	-	-	-	-				
mph	0.3	0.2	0.2	0.2	0.3	-	-	-	-	-	-				
hbd ph	1.2	-	1.3	-	-	0.1	-	-	-	-	-				
mph	0.2	0.9	0.4	-	1.5	-	-	-	-	-	-				
alk fspar ph	-	0.2	-	-	-	3.9	1.2	-	-	-	-				
mph	-	-	-	-	-	-	0.4	-	-	-	-				
qz ph	-	0.2	-	-	-	-	-	-	-	-	-				
xls	7.9	4.1	10.2	5.6	9.8	13.5	2.5	0.0	0.0	0.0	0.0				
gmass	92.1	95.9	89.8	94.4	90.2	86.5	97.5	100.0	100.0	100.0	100.0				

Notes:

Fe_2O_3* is total Fe as Fe_2O_3

Modal analyses are given in vol.% and were determined by point counting >1500 points. Abbreviations: ph = phenocrysts (> 0.3 mm); mph = microphenocrysts (> 0.03 mm); xls = total crystals; gmass = groundmass

Major elements analyzed by ICP at Activation Laboratories of Ancaster, Ontario

Trace elements analyzed by ICP-MS at Activation Laboratories of Ancaster, Ontario

All dacites are from cinder cones; all rhyolites are obsidian samples

*Note the large LOI on pumice/ashflow samples

Table 2a $^{40}Ar/^{39}Ar$ incremental heating ages, Tequila volcanic field

Sample #	Coordinates	Total Gas Age (ka)	Correlation Age (ka)	Correlation MSWD	$(^{40}Ar/^{36}Ar)_I$	Points fitted	Plateau Age (ka)	Plateau MSWD	Plateau % ^{39}Ar
TEQ 29	20°54.80 103°58.50	978 ± 283	1137 ± 152	0.44	295 ± 2	17 of 17	1121 ± 149*	0.43	100
TEQ 31	20°47.68 103°42.43	617 ± 20	730 ± 31	0.83	289 ± 2	9 of 13	691 ± 26*	1.89	85
TEQ 38	20°50.30 103°43.50	616 ± 29	524 ± 73	0.675	301 ± 2	9 of 13	683 ± 32*	1.30	70
TEQ 10	20°53.88 103°44.18	700 ± 21	668 ± 13	1.79	299 ± 3	13 of 13	671 ± 13*	1.99	89
TEQ 18	20°53.42 103°56.60	634 ± 8	608 ± 7	1.66	282 ± 13	13 of 13	642 ± 6*	0.37	96
TEQ 35	20°51.81 103°58.65	612 ± 12	595 ± 11	0.85	294 ± 23	7 of 13	632 ± 8*	0.71	97
ETZ 4	20°48.35 104°01.43	642 ± 6	601 ± 4	0.89	294 ± 2	7 of 13	635 ± 4*	0.87	93
TEQ 21A	20°51.26 103°51.86	615 ± 5	584 ± 4	2.23	301 ± 31	13 of 13	622 ± 3*	0.67	84
ETZ11	20°47.00 103°00.46	624 ± 10	609 ± 31	0.46	289 ± 8	13 of 13	619 ± 8*	0.48	100
TEQ 45B	20°54.76 103°53.44	603 ± 6	603 ± 4	0.54	296 ± 1	13 of 13	604 ± 3*	0.51	100
TEQ 12	20°53.99 103°43.71	631 ± 27	595 ± 26	0.32	294 ± 7	8 of 13	592 ± 20*	0.28	88
TAL 12	20°41.98 103°47.78	458 ± 36	499 ± 32	0.65	282 ± 6	8 of 13	454 ± 32*	1.38	93
TEQ 37	20°51.60 103°55.25	429 ± 25	363 ± 39	0.75	299 ± 2	13 of 13	427 ± 20*	1.00	100
TEQ 22	20°50.46 103°49.66	420 ± 7	379 ± 5	0.96	356 ± 123	13 of 13	416 ± 3*	1.10	85
TAL 9	20°44.91 103°55.24	375 ± 24	393 ± 24	2.52	299 ± 3	13 of 13	404 ± 15*	0.90	88
TEQ 66	20°48.15 103°59.02	378 ± 7	384 ± 3	0.54	261 ± 20	13 of 13	383 ± 4*	0.69	100
TAL 8	20°44.85 103°55.82	339 ± 14	381 ± 7	0.96	235 ± 21	13 of 13	374 ± 11*	1.94	94
TAL 13	20°44.70 103°49.50	354 ± 36	356 ± 28	0.48	305 ± 13	5 of 13	372 ± 18*	0.50	88
TEQ 33	20°49.75 103°59.69	371 ± 14	320 ± 59	0.95	300 ± 6	13 of 13	362 ± 13*	0.92	100
TAL 25	20°41.34 103°55.06	394 ± 13	346 ± 16	2.06	302 ± 3	13 of 13	354 ± 15*	2.28	81
ETZ 3	20°46.50 103°00.30	351 ± 45	367 ± 60	1.06	294 ± 3	13 of 13	339 ± 35*	0.86	86
TEQ 36	20°53.03 103°53.96	261 ± 11	268 ± 18	1.42	292 ± 5	13 of 13	261 ± 11*	1.33	100
TAL 11	20°40.79 103°56.05	271 ± 19	287 ± 10	1.01	292 ± 5	5 of 13	224 ± 19*	0.86	67
TEQ 6	20°47.38 103°50.96	227 ± 16	173 ± 14	1.01	312 ± 19	13 of 13	216 ± 11*	0.71	92
JH009‡	20°47.27 103°50.57	211 ± 12	149 ± 16	0.57	322 ± 18	13 of 13	198 ± 11*	0.64	98
TEQ 23C	20°50.02 103°48.79	211 ± 11	153 ± 22	5.49	299 ± 8	13 of 13	196 ± 19*	5.13	96
TEQ 15	20°47.41 103°51.08	223 ± 9	151 ± 17	2.93	312 ± 28	6 of 13	196 ± 8*	2.56	87
TEQ 40	20°50.70 103°46.10	233 ± 18	214 ± 17	0.96	291 ± 2	5 of 13	194 ± 15*	1.36	77
TEQ 17	20°48.60 103°50.70	162 ± 16	158 ± 52	0.58	295 ± 13	9 of 13	191 ± 13*	0.47	61
TEQ 60	20°51.96 103°50.42	187 ± 11	176 ± 13	0.91	298 ± 14	10 of 13	178 ± 8*	0.82	97
TEQ 25	20°49.26 103°47.79	167 ± 15	162 ± 20	2.38	291 ± 6	13 of 13	150 ± 18*	2.47	95
ETZ1	20°49.60 104°05.00	145 ± 15	147 ± 38	0.51	293 ± 13	13 of 13	140 ± 12*	0.47	100
TEQ 48	20°49.15 103°58.43	135 ± 18	108 ± 27*	1.59	296 ± 1	13 of 13	119 ± 18	1.51	100
TEQ 46	20°50.06 103°58.81	56 ± 20	73 ± 24*	0.71	293 ± 3	13 of 13	53 ± 16*	0.75	100
TAL 1	20°41.32 103°41.83	55 ± 11	93 ± 11	1.75	284 ± 9	13 of 13	87 ± 11*	1.83	100

PW 123**	20°47.59	103°53.11	96 ± 16	82 ± 14	0.54	299 ± 4	13 of 13	87 ± 12*	0.44	99
PW 391**	20°45.51	103°47.77	85 ± 27	51 ± 37	0.81	297 ± 3	13 of 13	66 ± 20*	0.39	69
PW 143**	20°45.32	103°46.71	85 ± 13	53 ± 16	1.80	298 ± 7	7 of 13	58 ± 10*	1.56	86

All errors are ± 1 sigma

*Preferred age

**collected by Wallace and Carmichael 1994

‡collected by Harris 1986

All correlation diagrams with MSWD > 1.8 are considered errorchrons.

Plateau ages are error weighted averages with scatter included in the error estimate.

Groundmass was dated in all samples except for TEQ29 for which hornblende was used

Table 2b $^{40}Ar/^{39}Ar$ total fusion ages, Tequila volcanic field

Sample #	Coordinates		Total Gas Age (ka)	Correlation age (ka)	Points fitted	Correlation MSWD	$(^{40}Ar/^{36}Ar)_I$	Volume
ETZ 6	20°49.60	104°02.60	956 ± 48*	1130 ± 159	6 of 13	0.94	293 ± 3	individual flow
TEQ 39	20°50.85	103°45.45	970 ± 34	949 ± 68*	13 of 13	6.38	294 ± 1	0.01 ± 0.001
TEQ 32	20°46.23	103°40.52	960 ± 42	625 ± 60*	13 of 13	1.74	297 ± 1	0.08 ± 0.002
ETZ 10	20°45.40	104°00.70	124 ± 134	444 ± 140*	13 of 13	1.89	295 ± 1	0.07 ± 0.002
TAL 26	20°41.10	103°52.79	248 ± 15	343 ± 38*	13 of 13	1.99	288 ± 3	0.03 ± 0.001
TEQ 67	20°48.16	103°58.94	626 ± 110	312 ± 32*	13 of 13	0.93	297 ± 1	1.3 ± 0.13
PW133**	20°49.57	103°56.87	95 ± 42*	114 ± 79	13 of 13	6.92	298 ± 3	individual flow

All errors are ± 1 sigma

*Preferred age

**collected by Wallace and Carmichael 1994

Correlation diagrams with MSWD > 1.8 are considered errorchrons.

Groundmass was dated for all samples

Table 2c $^{40}Ar/^{39}Ar$ incremental heating and total fusion ages >1Ma, Tequila volcanic field

Sample #	Coordinates	Total Gas Age (ka)	Correlation Age (ka)	Correlation MSWD	Points fitted	$(^{40}Ar/^{36}Ar)_I$	Plateau Age (ka)	Plateau MSWD	Plateau % ^{39}Ar
TEQ 9	20°54.60 103°43.20	5118 ± 62	5120 ± 51	0.57	17 of 17	300 ± 9	5137 ± 47*	0.45	96
ETZ 5	20°49.89 104°02.12	3911 ± 37	3855 ± 35*	3.06	13 of 13	295 ± 3	-	-	-
ETZ 7	20°46.97 104°05.66	2905 ± 12*	3023 ± 45	3.89	13 of 13	282 ± 4	-	-	-
ETZ 2	20°46.20 104°10.50	2306 ± 34	2213 ± 32	2.92	13 of 13	297 ± 2	2238 ± 24*	1.52	86

All errors are ± 1 sigma

*Preferred age

All correlation diagrams with MSWD > 1.8 are considered errorchrons.

Plateau ages are error weighted averages with scatter included in the error estimate.

Groundmass was dated in all samples except for TEQ9 for which hornblende was used

Table 3 Volumes of dated units at the Tequila volcanic field

	Sample	Volume km3	% error	Min km3	Max km3	% of Total
Andesites	Cerro Tomasillo	1.9 ± 0.02	1.10	1.88	1.92	
	ETZ3	0.04 ± 0.001	2.50	0.039	0.041	
	ETZ10	0.07 ± 0.002	2.86	0.068	0.072	
	PICA	0.22 ± 0.01	4.55	0.21	0.23	
	PW123	8 ± 2.00	25.00	6.00	10.00	
	TAL5	0.20 ± 0.01	5.00	0.19	0.21	
	TAL7	0.08 ± 0.002	2.50	0.078	0.082	
	TAL12	0.04 ± 0.001	2.50	0.039	0.041	
	TAL13	0.02 ± 0.001	5.00	0.019	0.021	
	TAL21	4.6 ± 0.60	13.04	4.00	5.20	
	TAL23	1.04 ± 0.12	11.00	0.92	1.16	
	TAL25	0.41 ± 0.01	2.44	0.40	0.42	
	TEQ31	0.20 ± 0.02	11.00	0.18	0.22	
	TEQ52	0.48 ± 0.05	10.42	0.43	0.53	
	TEQ53	1 ± 0.01	1.00	0.99	1.01	
	TEQ67	1.3 ± 0.13	10.0	1.17	1.43	
	Volcán Tequila	31 ± 2.1	7.00	28.90	33.10	
Total		**50.60 ± 5.09**	**10.05**	**45.51**	**55.69**	**(31.6 - 50.3)**
Basaltic Andesites	TAL26	0.03 ± 0.001	3.00	0.029	0.031	
	TEQ32	0.08 ± 0.002	2.50	0.078	0.082	
	TEQ33	0.01 ± 0.001	5.00	0.010	0.011	
	TEQ37flow	0.4 ± 0.02	5.00	0.398	0.402	
	TEQ37	0.01 ± 0.001	5.00	0.010	0.011	
	TEQ40	0.2 ± 0.01	5.00	0.199	0.201	
Total		**0.73 ± 0.04**	**3.56**	**0.70**	**0.76**	**(0.49 - 0.68)**
Basalts	ETZ1	0.03 ± 0.001	3.3	0.029	0.031	
	TAL3	0.01 ± 0.001	5.0	0.010	0.011	
	TEQ36	0.01 ± 0.001	5.0	0.010	0.011	
	TEQ36flow	0.6 ± 0.015	2.5	0.59	0.62	
	TEQ39	0.01 ± 0.001	5.0	0.010	0.011	
	~1 Ma	24 ± 1.00	4.2	23.00	25.00	
	~850 ka	9.0 ± 3.00	33.3	6.00	12.00	
	~670 ka	4.4 ± 0.41	9.4	3.97	4.79	
	~590 ka	0.83 ± 0.40	48.2	0.43	1.23	
Total		**38.84 ± 4.81**	**12.4**	**34.03**	**43.65**	**(23.7 - 39.5)**
Dacites	DOMES	1.1 ± 0.025	2.3	1.08	1.13	
	ETZ4	0.04 ± 0.001	2.5	0.039	0.041	
	ETZ11	0.07 ± 0.002	2.9	0.068	0.072	
	GN624	1.2 ± 0.14	12.0	1.06	1.34	
	GN624a	0.15 ± 0.015	10.0	0.14	0.17	
	GN624b	0.09 ± 0.008	9.0	0.08	0.10	
	TAL8	0.04 ± 0.001	2.5	0.040	0.040	
	TAL9	0.04 ± 0.001	2.5	0.039	0.041	
	TAL17	0.21 ± 0.01	4.76	0.20	0.22	
Total		**2.94 ± 0.40**	**13.7**	**2.54**	**3.34**	**(1.8 - 3.0)**
Rhyolites	ANESRHYO	0.12 ± 0.03	25.0	0.09	0.15	
	ERHYO	0.37 ± 0.04	10.8	0.33	0.41	
	JH147	0.57 ± 0.03	5.3	0.54	0.60	
	JH182	1 ± 0.25	25.0	0.75	1.25	
	JH201	2 ± 0.2	10.0	1.80	2.20	
	JH257	3 ± 0.6	20.0	2.40	3.60	
	JH260	2 ± 0.1	5.0	1.90	2.10	
	TEQ21	16 ± 4	25.0	12.00	20.00	
	TEQ22	2.1 ± 0.2	10.0	1.90	2.30	
	TEQ29	1.2 ± 0.06	5.0	1.14	1.28	
	TEQ34	0.05 ± 0.003	5.0	0.048	0.053	
	TEQ35	4.7 ± 0.5	10.6	4.20	5.20	
	TEQ45	1 ± 0.25	25.0	0.75	1.25	
Total		**34.1 ± 6.26**	**18.4**	**27.85**	**40.37**	**(19.4 - 36.4)**
Total volume erupted		**127.2 ± 16.6**	**13.0**	**110.6**	**143.8**	

Figure Captions

Fig. 1 Tectonic framework and overview of western Mexico, modified from Delgado Granados (1993). Numbered triangles in the Tepic-Zacoalco and Colima grabens refer to central volcanoes: (1) Sierra La Primavera, (2) V. Tequila, (3) V. Ceboruco, (4) V. Tepetiltic, (5) V. Sangangüey, (6) V. Las Navajas, (7) V. San Juan, and (8) V. Colima-Nevado.

Fig. 2 Aerial photograph of the field area with the geologic units outlined as on the geologic map. Major features and sample locations are labeled. Stars represent dacitic airfall deposits.

Fig. 3 Geologic map of the Tequila volcanic field. Numbers are dates in millions of years.

Fig. 4 Eruption frequency diagram for lava erupted over the last one million years. Included in this diagram are five K-Ar dates from Harris (1986), one from Nieto-Obregón et al. (1985), three from Nixon et al. (1987) and six from Wopat (1990) on samples in the volcanic field not dated in this study, as well as the $^{40}Ar/^{39}Ar$ dates from this study.

Fig. 5 a Relative volumes of lavas erupted ≤ 1 Ma in the Tequila volcanic field. The apex of each peak represents the $^{40}Ar/^{39}Ar$ age (x-axis) and the volume of the erupted lava (y-axis). The width of each distribution curve represents a uniform error of ± 40 kyrs. Both the height and area under each curve display the relative volumes of each volcanic feature. **b** The same diagram as in **a**, but for the Ceboruco-San Pedro volcanic field (Frey et al. 2003).

Fig. 6 Water-saturated phase diagram for an andesite modified from Moore and Carmichael (1998). The dashed lines are isopleths of wt. % water calculated from Moore et al. (1998). The shaded areas indicate the P-T conditions of the two magma chambers beneath V. Tequila, separated in time by ~110 kyrs.

Fig. 7 a The age (and 2 sigma error) of each dated eruptive unit ≤ 1 Myr as a function of silica concentration; there is no correlation. **b** Same as **a**, but only the peripheral cinder cones and flows of andesite and dacite are shown; there is no trend of increasing silica with time.

Fig. 8 a Plot of incompatible element Ba as a function of silica concentration for basalts through rhyolites. **b** Same as in **a**, but a blow-up of only basaltic andesites through dacites. **c** Same as in **a**, but for incompatible element Zr. Basalts and basaltic andesites are shown by crosses enclosed by squares, andesites and dacites from the main edifice and flanks of V. Tequila are shown by solid dots, andesites and dacites from peripheral cinder cones and flows are shown by the symbol X, and rhyolites are shown by open squares.

Figure 1

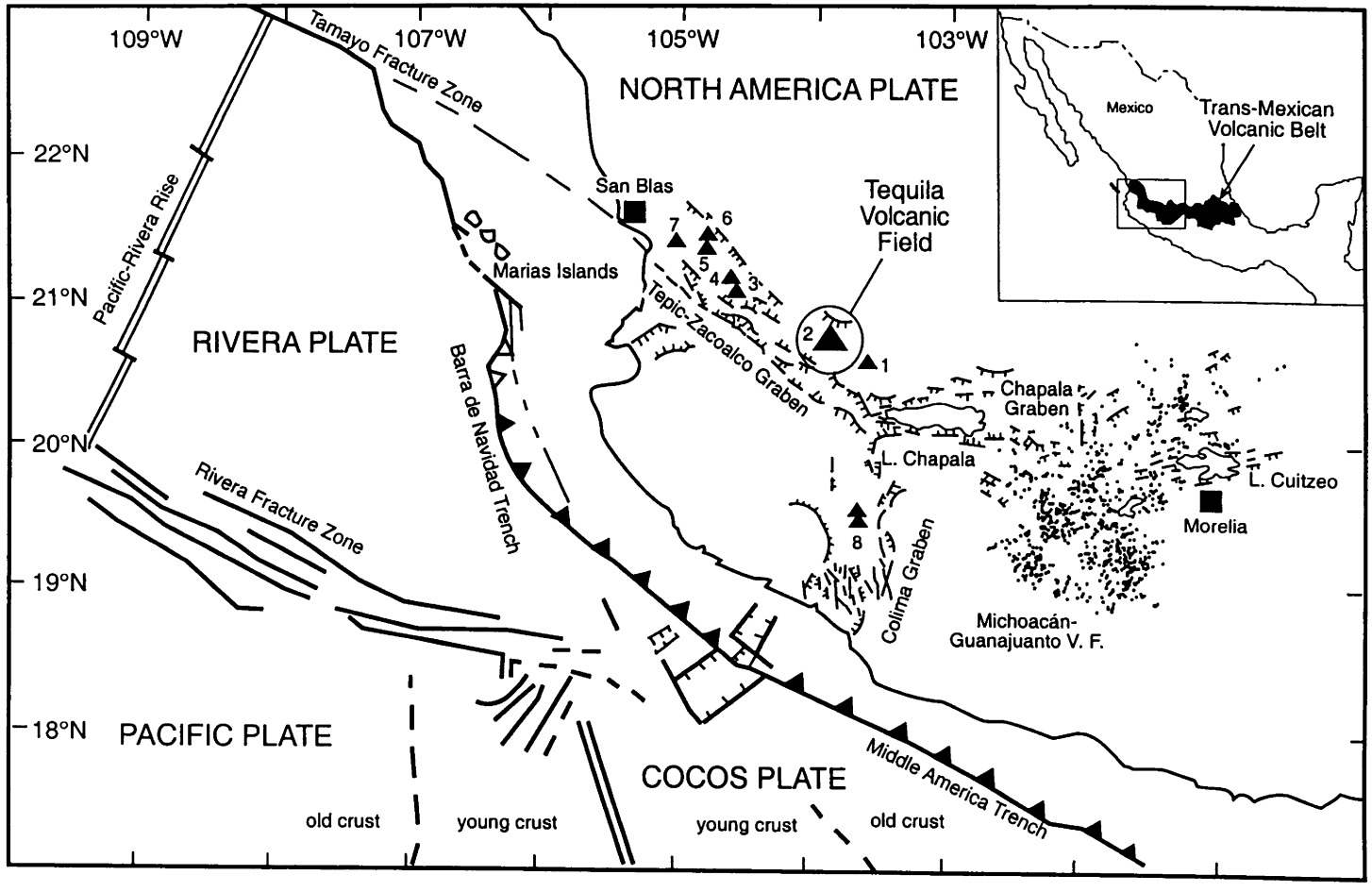
109°W
107°W
105°W
103°W
22°N
21°N
20°N
19°N
18°N
NORTH AMERICA PLATE
RIVERA PLATE
PACIFIC PLATE
COCOS PLATE
Tamayo Fracture Zone
Pacific-Rivera Rise
Rivera Fracture Zone
Barra de Navidad Trench
Middle America Trench
San Blas
Marias Islands
Tepic-Zacoalco Graben
Tequila Volcanic Field
Chapala Graben
L. Chapala
Colima Graben
Michoacán-Guanajuanto V. F.
Morelia
L. Cuitzeo
Mexico
Trans-Mexican Volcanic Belt
old crust
young crust
young crust
old crust

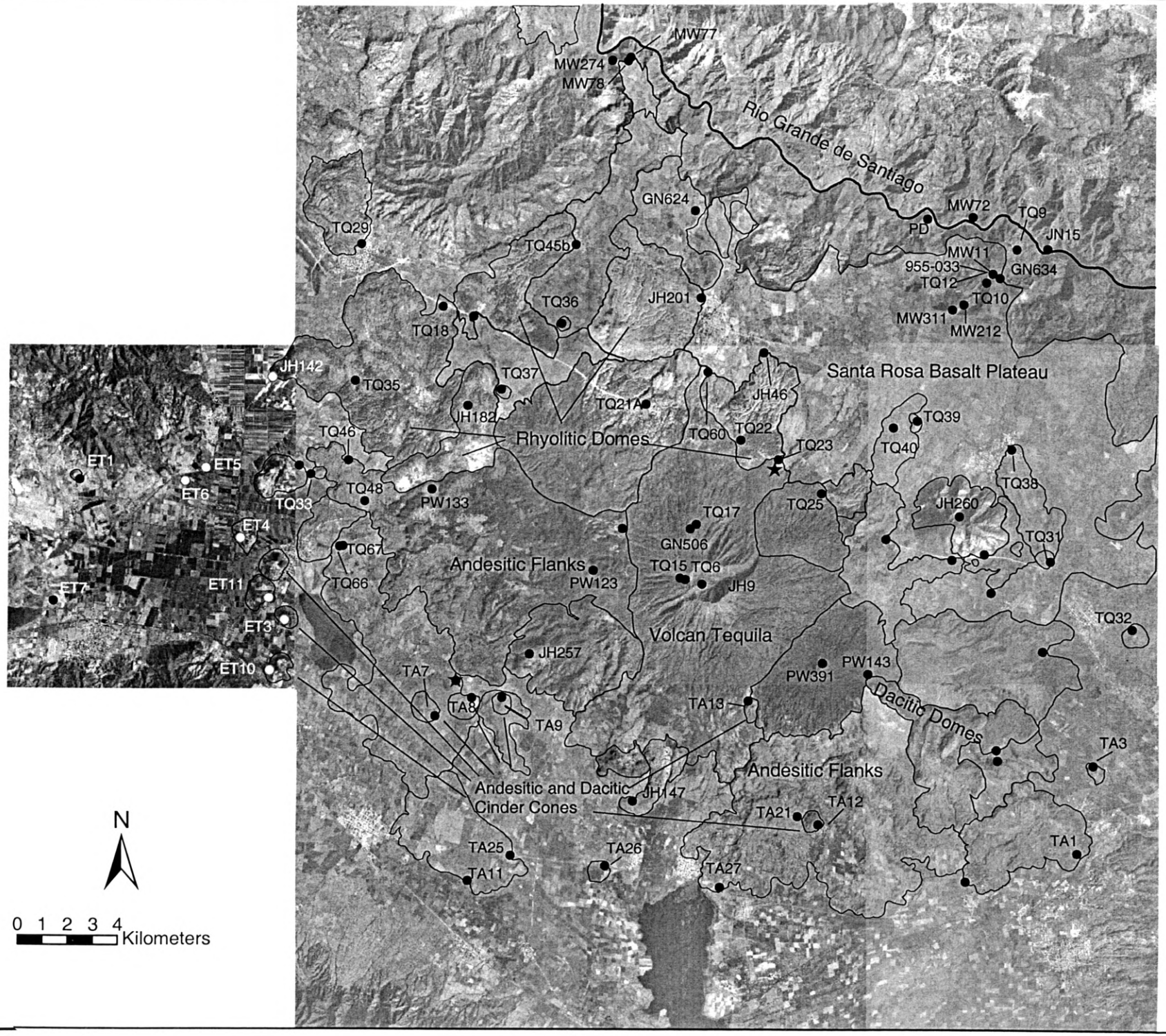
MW77
MW274
MW78
Rio Grande de Santiago
GN624
MW72
TQ9
PD
JN15
TQ29
TQ45b
MW11
955-033
GN634
TQ12
TQ10
TQ36
JH201
MW311
MW212
TQ18
JH142
TQ35
TQ37
Santa Rosa Basalt Plateau
JH46
TQ21A
JH182
TQ39
TQ46
Rhyolitic Domes
TQ60
TQ22
TQ23
TQ40
ET1
ET5
ET6
TQ48
PW133
TQ33
TQ25
JH260
TQ38
TQ17
ET4
GN506
TQ31
TQ67
Andesitic Flanks
TQ15
TQ6
PW123
JH9
TQ66
ET7
ET11
TQ32
ET3
Volcan Tequila
JH257
PW391
PW143
TA7
TA13
TA8
TA9
Dacitic Domes
TA3
Andesitic Flanks
Andesitic and Dacitic
Cinder Cones
JH147
TA21
TA12
TA25
TA26
TA1
TA11
TA27
ET10
N
0 1 2 3 4
Kilometers

Fig 2

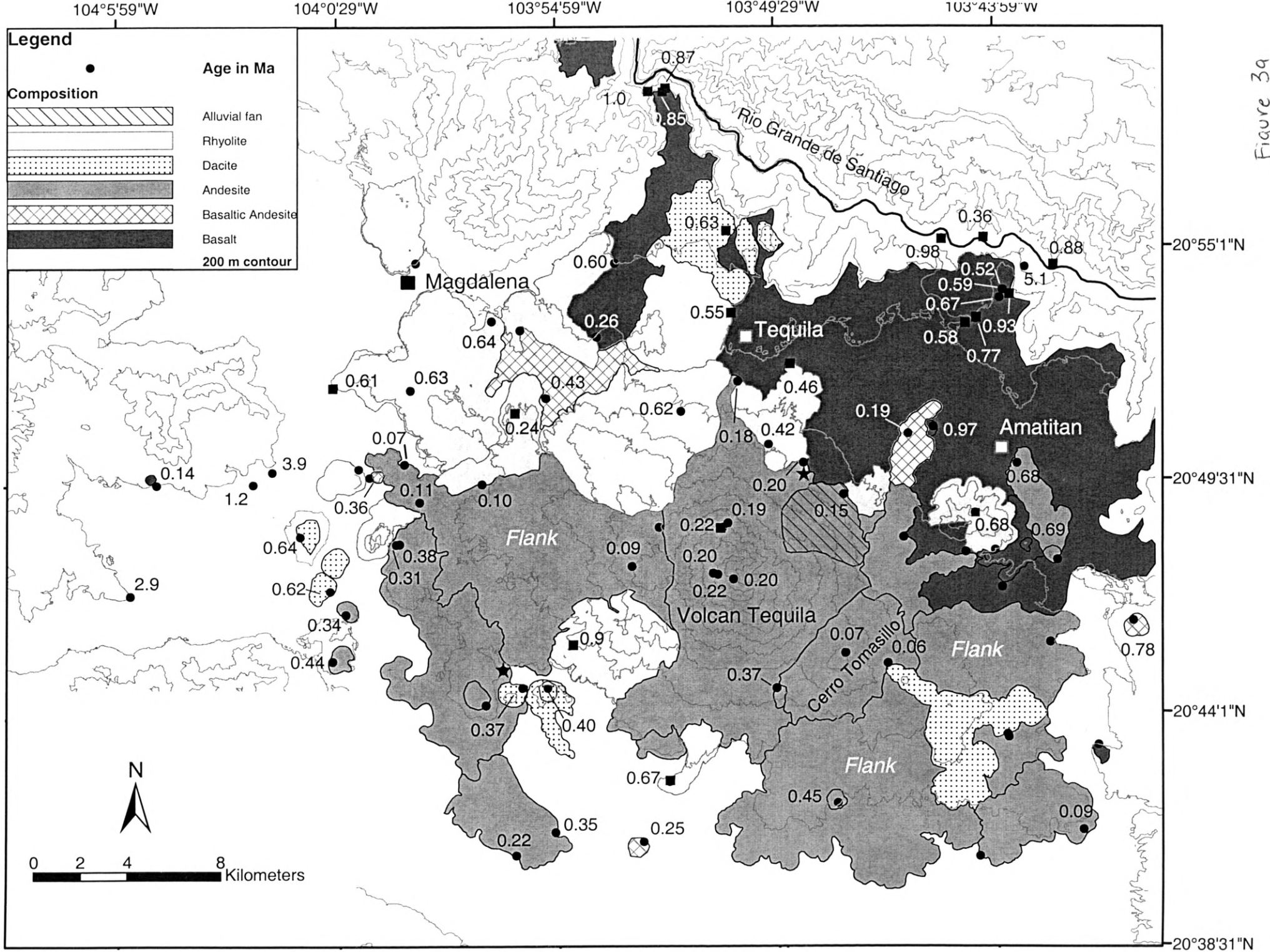
Legend
Age in Ma
Composition
Alluvial fan
Rhyolite
Dacite
Andesite
Basaltic Andesite
Basalt
200 m contour
104°5'59"W
104°0'29"W
103°54'59"W
103°49'29"W
103°43'59"W
20°55'1"N
20°49'31"N
20°44'1"N
20°38'31"N
Rio Grande de Santiago
Magdalena
Tequila
Amatitan
Volcan Tequila
Flank
Flank
Flank
Cerro Tomasillo
N
0 2 4 8 Kilometers
0.87
1.0
0.85
0.63
0.60
0.36
0.98
0.88
0.52
0.59
0.67
5.1
0.93
0.58
0.77
0.55
0.26
0.64
0.61
0.63
0.43
0.24
0.62
0.46
0.19
0.97
0.18
0.42
0.07
0.14
3.9
1.2
0.36
0.11
0.10
0.20
0.15
0.68
0.69
0.22
0.19
0.64
0.38
0.31
0.09
0.20
2.9
0.62
0.22
0.20
0.34
0.9
0.07
0.06
0.78
0.44
0.37
0.40
0.67
0.45
0.09
0.35
0.22
0.25

Figure 39

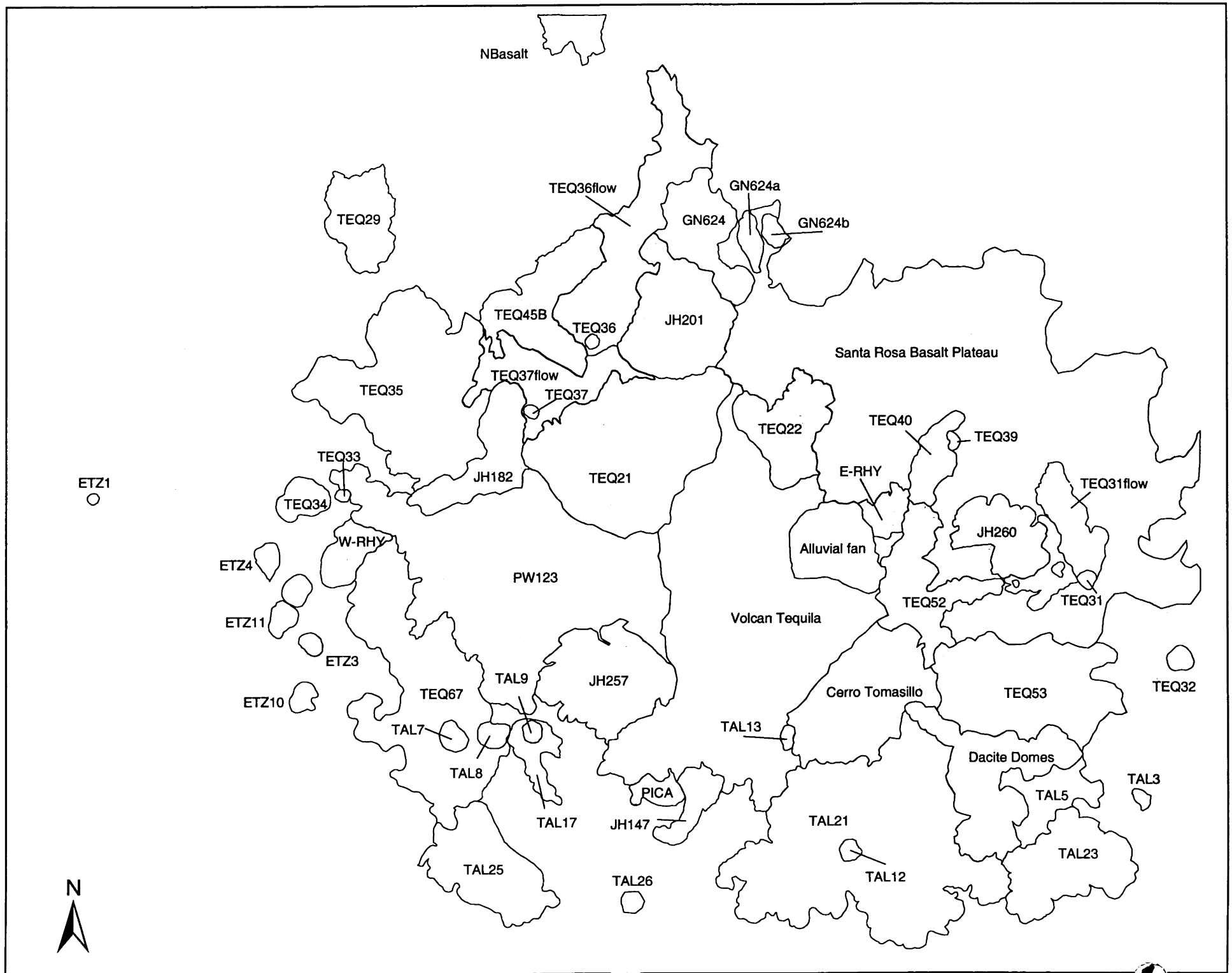
NBasalt
TEQ36flow
GN624a
GN624
GN624b
TEQ29
TEQ45B
TEQ36
JH201
Santa Rosa Basalt Plateau
TEQ37flow
TEQ35
TEQ37
TEQ22
TEQ40
TEQ39
TEQ33
JH182
TEQ21
E-RHY
TEQ31flow
ETZ1
TEQ34
JH260
W-RHY
Alluvial fan
ETZ4
PW123
TEQ52
TEQ31
ETZ11
Volcan Tequila
ETZ3
TAL9
JH257
TEQ32
ETZ10
TEQ67
Cerro Tomasillo
TEQ53
TAL13
TAL7
Dacite Domes
TAL3
TAL8
PICA
TAL5
TAL17
JH147
TAL21
TAL23
TAL25
TAL12
TAL26
N

Figure 3b

Figure 4

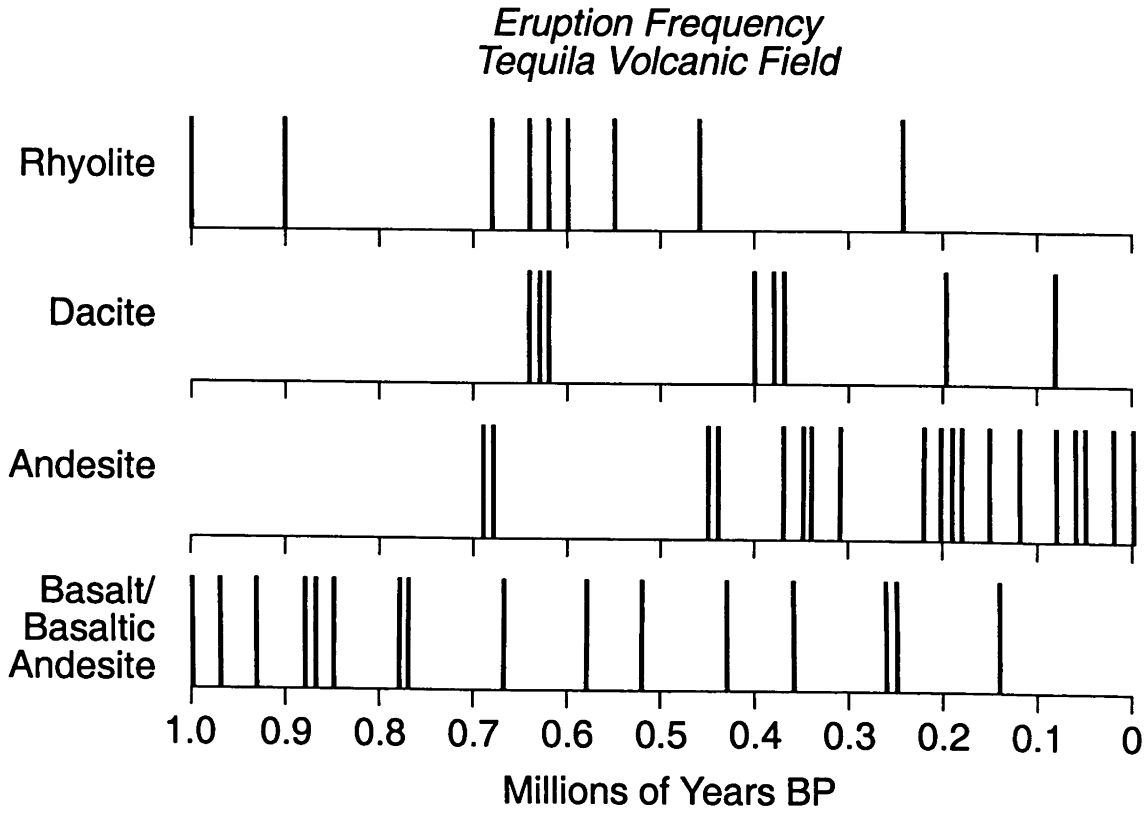
Eruption Frequency
Tequila Volcanic Field
Rhyolite
Dacite
Andesite
Basalt/
Basaltic
Andesite
1.0
0.9
0.8
0.7
0.6
0.5
0.4
0.3
0.2
0.1
0
Millions of Years BP

Figure 5a

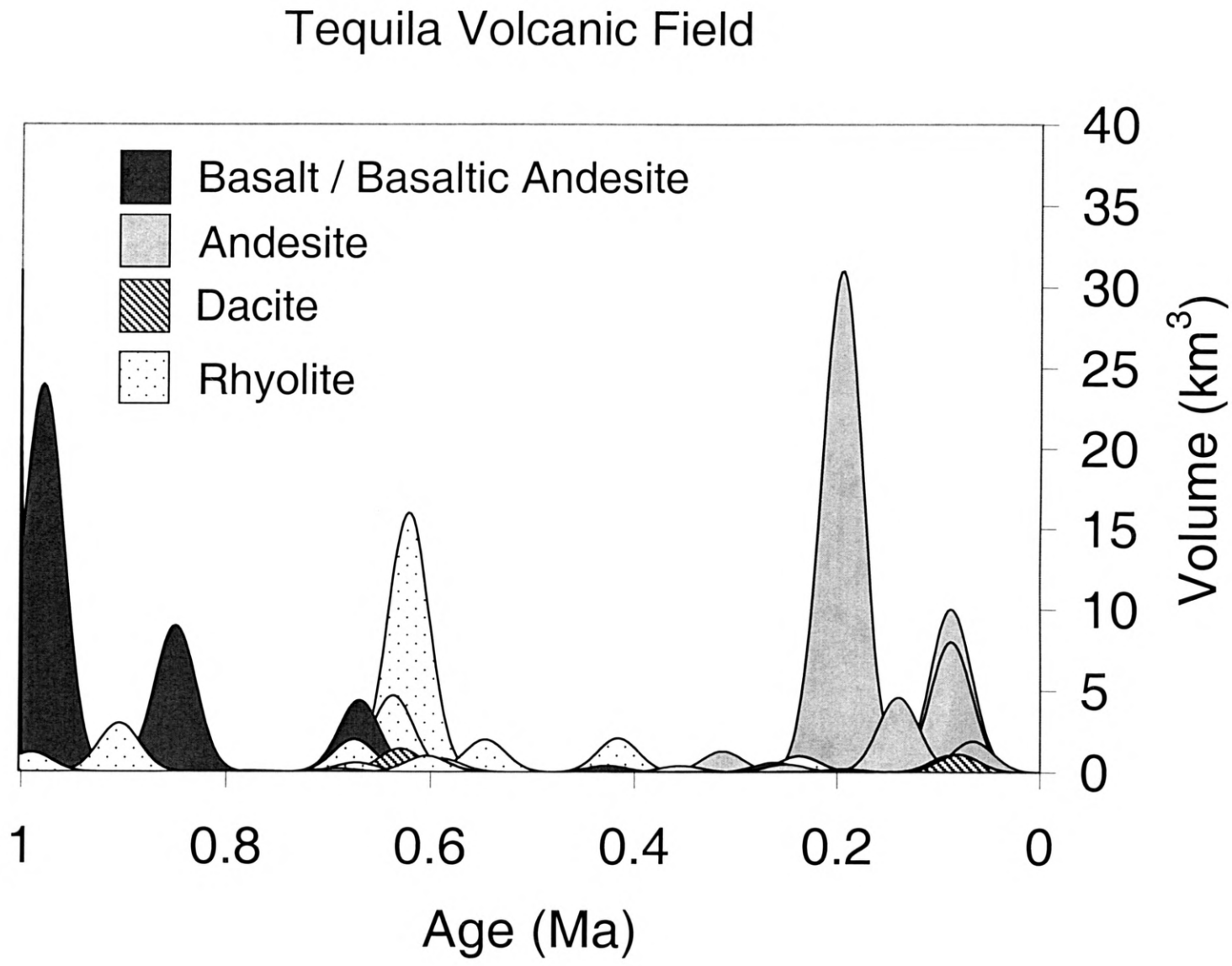
Tequila Volcanic Field
Basalt / Basaltic Andesite
Andesite
Dacite
Rhyolite
40
35
30
25
20
15
10
5
0
Volume (km3)
1
0.8
0.6
0.4
0.2
0
Age (Ma)

Figure 5b

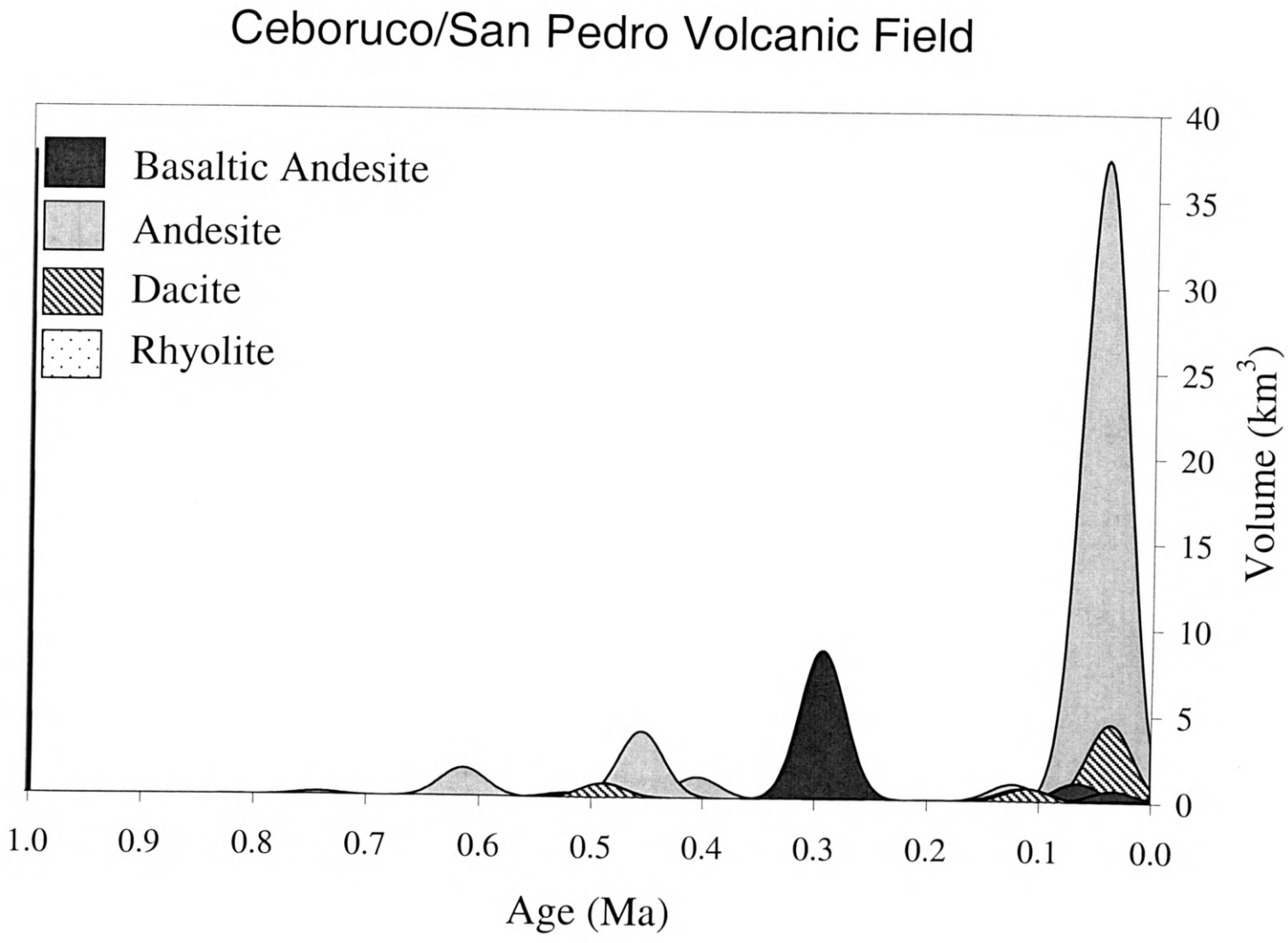
Ceboruco/San Pedro Volcanic Field
Basaltic Andesite
Andesite
Dacite
Rhyolite
40
35
30
25
20
15
10
5
0
Volume (km3)
1.0
0.9
0.8
0.7
0.6
0.5
0.4
0.3
0.2
0.1
0.0
Age (Ma)

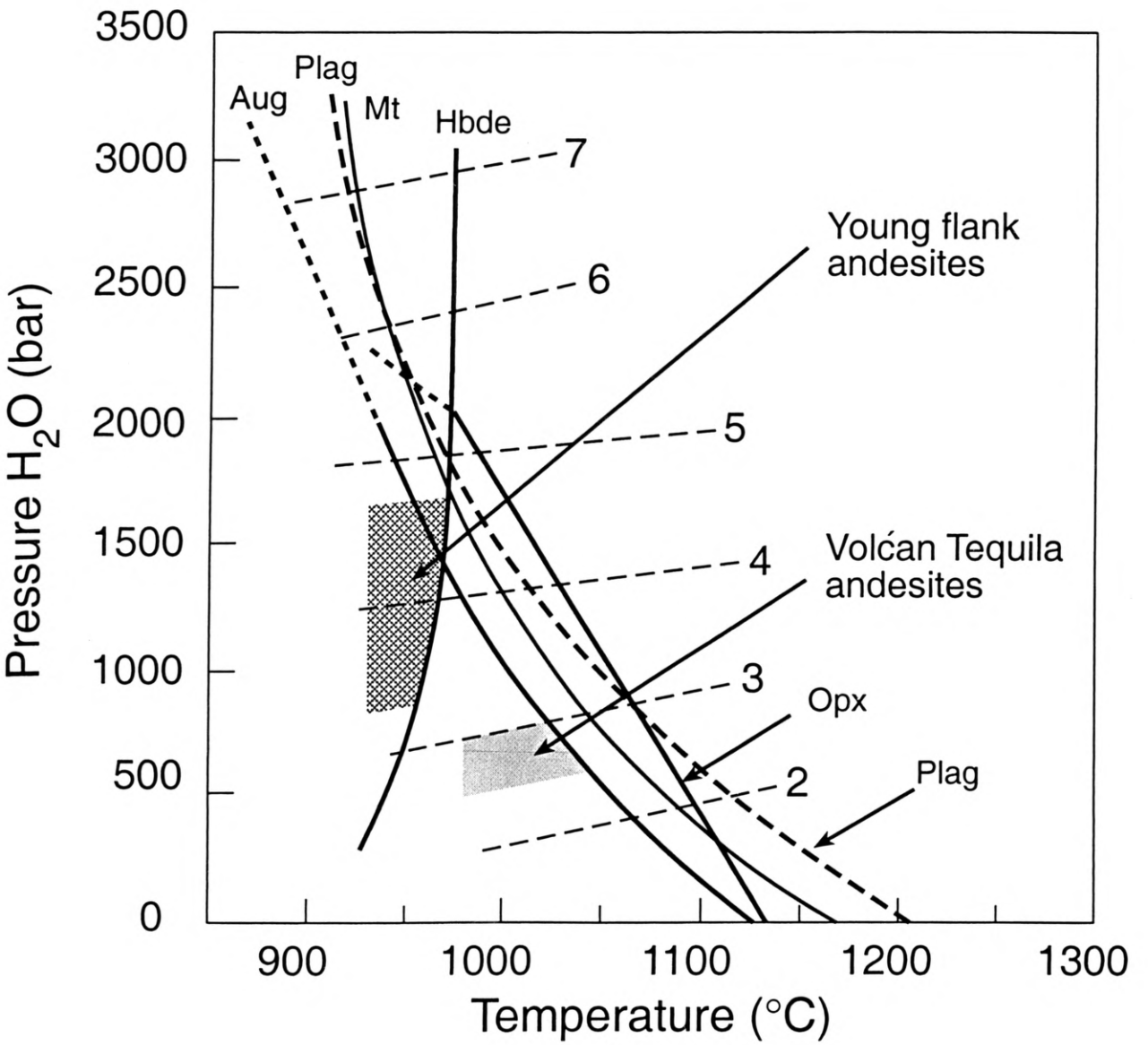
3500
3000
2500
2000
1500
1000
500
0
Pressure H_2O (bar)
900
1000
1100
1200
1300
Temperature (°C)
Aug
Plag
Mt
Hbde
7
6
5
4
3
2
Young flank andesites
Volćan Tequila andesites
Opx
Plag

Figure 6

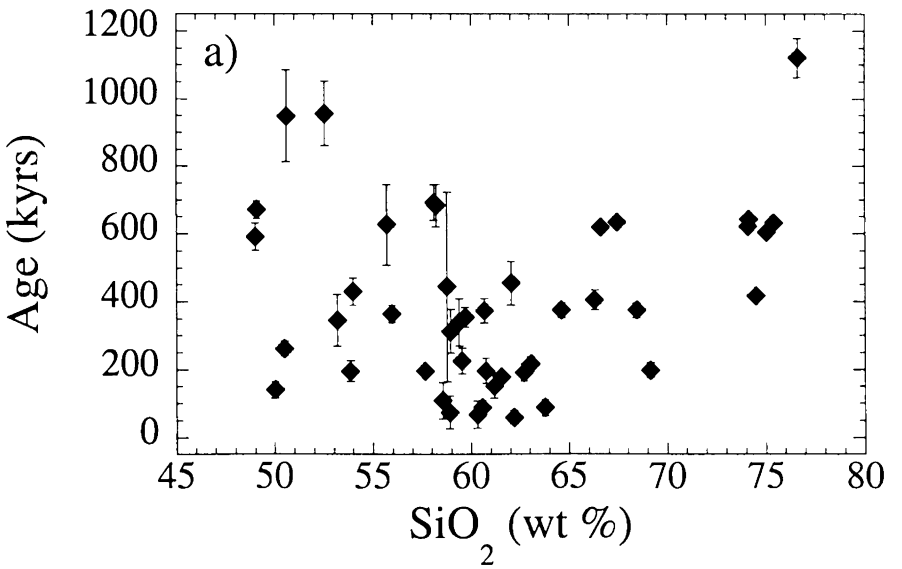
a)
1200
1000
800
600
400
200
0
Age (kyrs)
45
50
55
60
65
70
75
80
SiO2 (wt %)

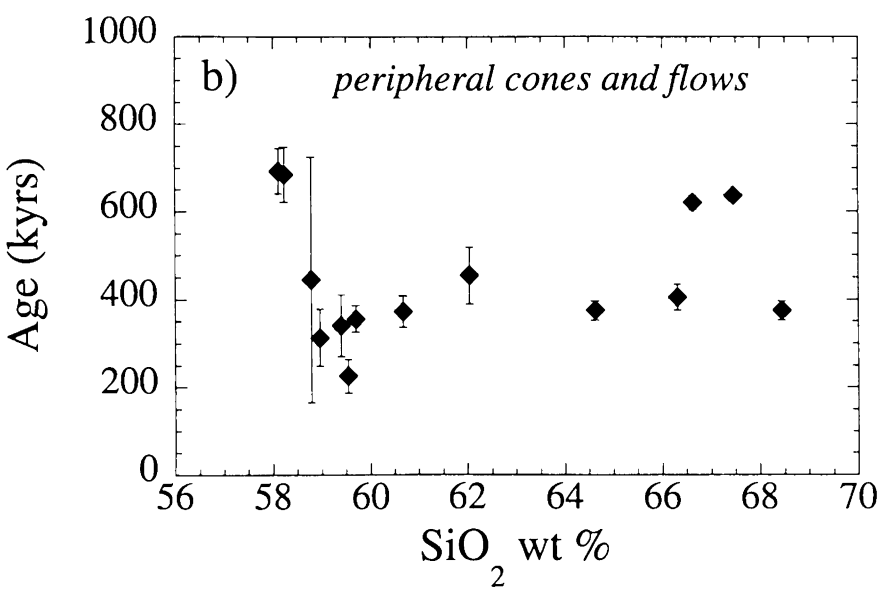
b)
peripheral cones and flows
1000
800
600
400
200
0
Age (kyrs)
56
58
60
62
64
66
68
70
SiO2 wt %

Figure 7

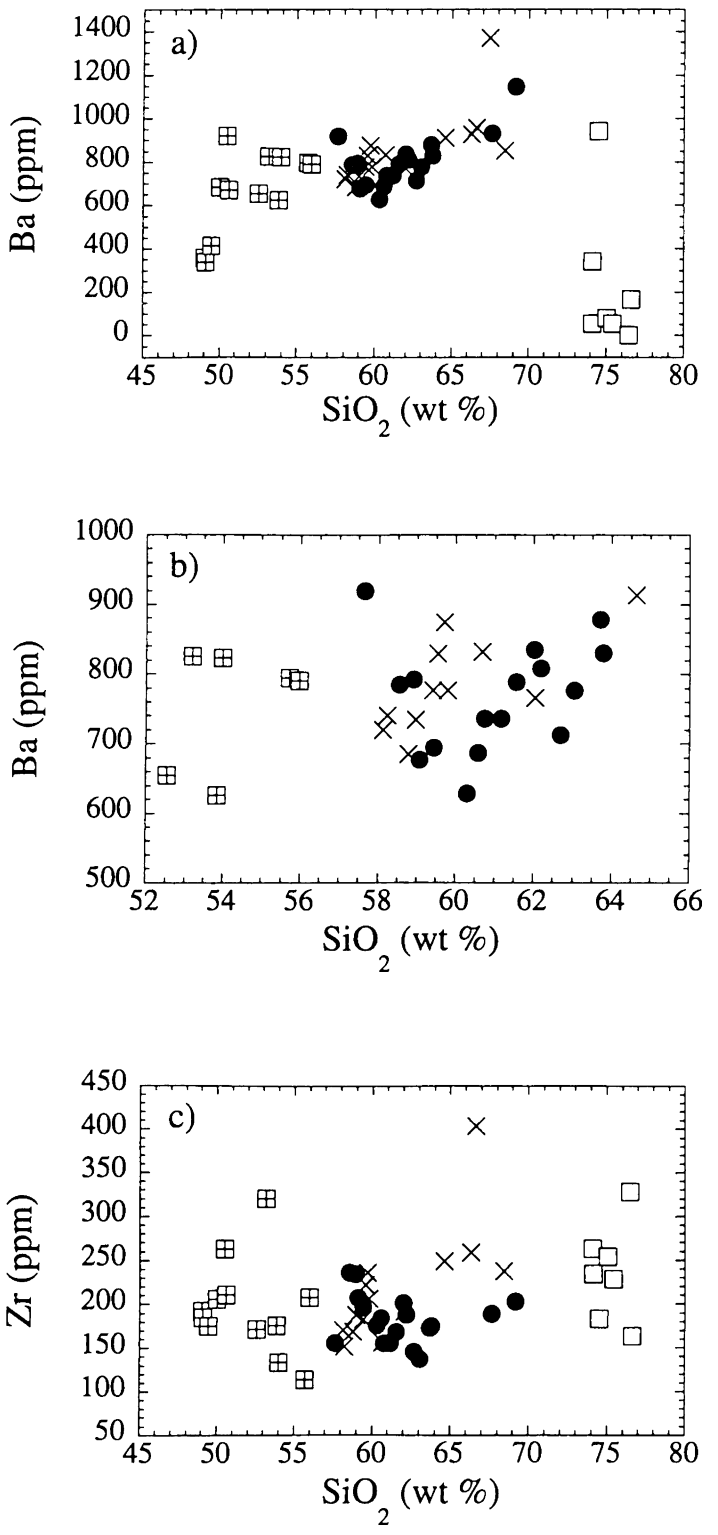
a)
Ba (ppm)
1400
1200
1000
800
600
400
200
0
45
50
55
60
65
70
75
80
SiO2 (wt %)
b)
Ba (ppm)
1000
900
800
700
600
500
52
54
56
58
60
62
64
66
SiO2 (wt %)
c)
Zr (ppm)
450
400
350
300
250
200
150
100
50
45
50
55
60
65
70
75
80
SiO2 (wt %)

Figure 8

Data Repository: Discussion of incremental step-heating results

Age spectra and inverse isochron diagrams are included for each sample, and errors are reported at the 1σ value. The criteria for determining whether the plateau and isochron ages from an incremental heating experiment are meaningful are as follows: 1) a plateau includes >50% of the ^{39}Ar gas released in at least three consecutive heating fractions, 2) the plateau passes a null hypothesis test such that for a heating experiment with 13 steps the MSWD is a maximum of 1.8, 3) the plateau and isochron ages are concordant at the 95% confidence level, and 4) the $^{40}Ar/^{36}Ar$ intercept of the isochron agrees with the atmospheric value of 295.5 at the 95% confidence level. The error on the plateau age is a standard weighted error for the individual steps of the plateau by variance (Taylor 1982), i.e. release fractions with more precise results carry greater weight in the age calculation. Seven samples ≤ 1 Ma had disturbed spectra that did not result in a plateau; correlation and total gas ages are presented in Table 2b.

In the isochron diagrams, a dotted line indicates that all the heating fractions were included in the regression, and a dashed-dotted line indicates that only heating fractions associated with the plateau were included.

TEQ29 – Hornblende from R hyolite

The plateau includes all the heating fractions; there are large errors on the low and high-temperature fractions but the ages are consistent throughout the run. The isochron includes all the heating fractions and agrees with the plateau age at the 1σ level.

ETZ6 Basaltic Andesite

Anomalously young ages in the lowest temperature heating fractions suggest minor argon loss and were excluded from the plateau. The highest temperature fractions also were excluded due to the likelihood that xenocrystic pyroxene degassed and caused anomalous ages as well as sudden increases in calcium and chlorine. The plateau points were used to construct the isochron, which agrees with the plateau age at the1σ level.

TEQ32 Basaltic Andesite

A plateau exists that fits the criteria, but the sample contains a high initial argon content with inherent uncertainty about the exact value. Therefore the isochron age using points from all the heating fractions has been designated as the more reliable age and agrees with the plateau age at the 2σ level.

TEQ31 Andesite

The stair step pattern in the initial heating fractions suggests that argon was lost due to slight alteration; these fractions were excluded from the plateau. The plateau points were used to construct the isochron, which agrees with the plateau age at the1σ level.

TEQ38 Andesite

The sample has an initial, low temperature heating fraction of an anomalously old age, followed by three fractions of young age that may be due to argon loss/alteration. Minor alteration is also suggested by changing chlorine and calcium concentrations over the

course of the experiment, but nine of 13 steps form a plateau with an MSWD of 1.30. The sample contains a high level of atmospheric argon. The plateau points were used to construct the isochron, which agrees with the plateau age at the 2σ level.

TEQ10 Basalt
The plateau excludes anomalously old ages in both low and high temperature fractions. The low temperature discrepancy is most likely due to release of atmospheric argon, which may be expected in a young, vesicular sample. The high temperature discrepancy is most likely due to the fusion of Ca-rich pyroxene or augite, which corresponds with the jump in calcium concentrations. All of the heating fractions were used to construct the isochron, which shows a wide spread of points and is consistent with the plateau age at the 1σ level.

TEQ18 Rhyolite
High levels of atmospheric argon in the sample may cause anomalously old ages in the low temperature heating fractions; the plateau excludes these fractions. The isochron is based on all heating fractions and is not within error of the plateau age. The MSWD of the isochron age is 1.66 and of the plateau age is 0.37.

TEQ35 Rhyolite
Slight alteration of the obsidian may have led to argon loss and anomalously young ages in some of the low temperature heating fractions; these fractions are excluded from the plateau. The plateau points were used to construct the isochron, which agrees with the plateau age at the 2σ level.

ETZ4 Dacite
High levels of atmospheric argon in the sample may cause anomalously old ages in the low temperature heating fractions. These fractions have been excluded from the plateau. The plateau points were used to construct the isochron, which is not within error of the plateau age. The MSWD of the isochron age is 0.89 and of the plateau age is 0.87.

TEQ21A Rhyolite
Slight alteration of the obsidian may have led to large errors on heating fractions in the low temperatures. The plateau excludes these fractions although the ages are consistent with the higher temperature results. Isochrons were constructed using both the plateau points and all the points, but the isochron and plateau ages are not within error. The reported isochron age uses all the points and is an errorchron with an MSWD of 2.23. The plateau age has an MSWD of 0.67.

ETZ11 Dacite
High levels of atmospheric argon caused large errors on the low temperature heating fractions, but the ages are internally consistent and thus all have been included in the plateau. All of the heating fractions were used to construct the isochron, which is consistent with the plateau age at the 1σ level.

TEQ45B Rhyolite
Large errors on heating fractions in the low temperatures may have been caused by slight alteration of the obsidian, but the ages are consistent and all results are included in the plateau. All of the heating fractions were used to construct the isochron, which shows a wide spread of points and is consistent with the plateau age at the 1σ level.

TEQ12 Basalt
The plateau excludes anomalously old ages in both low and high temperature fractions. The low temperature discrepancy is most likely due to release of atmospheric argon, which may be expected in a young, vesicular sample. The high temperature discrepancy is most likely due to the fusion of Ca-rich pyroxene or augite xenocrysts, which corresponds with the jump in calcium concentrations. The plateau points were used to construct the isochron, which agrees with the plateau age at the 1σ level.

TAL12 Andesite
The plateau excludes anomalously old ages in low temperature fractions. The low temperature discrepancy is most likely due to release of atmospheric argon, which may be expected in a young, vesicular sample. The first heating fraction gives an anomalously young age, suggesting minor argon loss at the grain rims. The plateau points were used to construct the isochron, which agrees with the plateau age at the 1σ level.

TEQ37 Basaltic Andesite
The fourth heating fraction gives an anomalously low age that is not reflected in change in calcium or chlorine concentrations; the other steps result in consistent ages, so the plateau includes all of the heating fractions. The isochron age is based on all fractions and is consistent with the plateau age at the 2σ level.

TEQ22 Rhyolite
Slight alteration of the obsidian may have led to large errors on heating fractions in the low temperatures, so the plateau excludes these results. Isochrons were constructed using all the points and using only the plateau points, but the isochron and plateau ages are not within error. The reported isochron age uses all the heating fractions and has an MSWD of 0.96. The plateau age has an MSWD of 1.10.

TAL9 Dacite
Anomalously young ages as well as a spike in chlorine concentration in the low heating fractions suggest minor alteration and argon loss. The plateau excludes these fractions. The isochron age is based on all fractions and is consistent with the plateau age at the 1σ level.

TEQ66 Dacite
Slight alteration of the glass may have led to irregular values in calcium concentrations as well as argon loss that produced slightly young ages in the low temperature heating fractions. The plateau includes these fractions and results in a MSWD of 0.69. The isochron age is based on all fractions and is consistent with the plateau age at the 1σ level.

TAL8 Dacite
Slight alteration of the glass may have led to irregular values in the calcium concentrations as well as argon loss that resulted in large errors in the low temperature heating fractions. These fractions have been excluded from the plateau. The isochron age is based on all fractions and is consistent with the plateau age at the 1σ level.

TAL13 Andesite
The initial heating fractions have large errors and old ages that suggest alteration and release of atmospheric argon; these fractions were excluded from the plateau. This is consistent with irregular values (at low temperatures) in the calcium and chlorine concentrations. The plateau points were used to construct the isochron, which is consistent with the plateau age at the 1σ level.

TEQ33 Basaltic Andesite
The heating fractions have low errors and consistent ages, so all of the steps were used in calculating the plateau age. The total gas, plateau, and isochron ages are all within 1σ error of each other.

TAL25 Andesite
The plateau excludes anomalous ages in both low and high temperature fractions. The low temperature discrepancy of an old age is most likely due to release of atmospheric argon, which may be expected in a young, vesicular sample. The high temperature discrepancy, which corresponds with the jump in chlorine and calcium concentrations, is most likely due to the fusion of pyroxene (Ca), Ca-rich augite, and hornblende (Ca and Cl) xenocrysts. All the heating fractions were used to construct the isochron, which is consistent with the plateau age at the 1σ level.

ETZ3 Andesite
The heating fractions have large errors, most likely due to the large volume of atmospheric argon, but the ages used for the plateau are internally consistent. All the heating fractions were used to construct the isochron, which is consistent with the plateau age at the 1σ level.

TEQ36 Basalt
The heating fractions have low errors and consistent ages, so all the steps were used in calculating the plateau. The total gas, plateau, and isochron ages are all within 1σ error of each other.

TAL11 Andesite
The anomalously low age in the first heating fraction indicates slight argon loss due to alteration. The jump in calcium and chlorine concentrations at the highest temperature fractions suggests degassing of pyroxene, Ca-rich augite or hornblende xenocrysts. The sample contains very high levels of atmospheric argon. Isochrons were constructed using all the points and using only the plateau points, but the isochron and plateau ages are not

within error. The reported isochron age uses the plateau fractions and has an MSWD of 1.01. The plateau age has an MSWD of 0.86.

TEQ6 Andesite
Large errors in the initial heating fractions suggest minor alteration, but the plateau excludes these fractions and uses ~90% of the ^{39}Ar released. All of the heating fractions were used to construct the isochron, which shows a wide spread of points and is consistent with the plateau age at the 2σ level.

JH009 Andesite
The plateau excludes anomalously old ages in the high temperature heating fractions. The high temperature discrepancy is most likely due to the fusion of pyroxene, Ca-rich augite, or hornblende xenocrysts, which corresponds with a rise in calcium and chlorine concentrations. All of the heating fractions were used to construct the isochron, which shows a wide spread of points and is consistent with the plateau age at the 2σ level.

TEQ23C Andesite
The plateau excludes anomalously young ages in the high temperature heating fractions. The high temperature discrepancy is most likely due to the fusion of pyroxene, Ca-rich augite, or hornblende xenocrysts, which corresponds with a rise in calcium and chlorine concentrations. The isochron has a MSWD of 5.49 and so is an errorchron.

TEQ15 Andesite
The plateau excludes anomalously old ages in both low and high temperature fractions. The low temperature discrepancy is most likely due to release of atmospheric argon, which may be expected in a young, vesicular sample. The high temperature discrepancy is probably due to the fusion of pyroxene, Ca-rich augite, or hornblende xenocrysts, which corresponds with a rise in calcium and chlorine concentrations. The plateau fractions were used to construct the isochron, which is consistent with the plateau age at the 2σ level.

TEQ40 Basaltic Andesite
The plateau excludes high temperature heating fractions with anomalously old ages that are most likely due to fusion of pyroxene or Ca-rich augite xenocrysts. The plateau points were used to construct the isochron, which is the same as the plateau age at the 1σ level.

TEQ17 Andesite
The stair step pattern in the initial heating fractions suggests that $^{40}Ar^*$ argon was lost due to slight alteration; these fractions were excluded from the plateau. Although there were large errors in the highest temperature heating fractions, the steps were included because these ages did not change the age of the plateau. The plateau points were used to construct the isochron, which is the same as the plateau age at the 1σ level.

TEQ60 Andesite
The plateau excludes the first and last heating fractions of the experiment. The anomalously low age in the first step indicates slight $^{40}Ar^*$ loss due to alteration. The jump in calcium concentrations at the highest temperature fractions suggests degassing of Ca-rich augite or pyroxene xenocrysts. The plateau points were used to construct the isochron, which results in an age the same as the plateau age at the 1σ level.

TEQ25 Andesite
The plateau excludes high temperature, anomalously old ages that are most likely due to fusion of Ca-rich pyroxene or plagioclase. The isochron is based on all the heating fractions and the age corresponds with the plateau age at the 1σ level.

ETZ1 Basalt
The heating fractions have low errors and consistent ages, so 100% of the ^{39}Ar was used in calculating the plateau. The total gas, plateau, and isochron ages are all within 1σ error of each other. All the heating fractions were used to construct the isochron.

TEQ48 Andesite
Although there were relatively large errors in the highest temperature heating fractions the ages did not affect the age of the plateau and were included. All the points were used to construct the isochron, which resulted in an age within a 1σ error of the plateau age. The sample contains a high concentration of atmospheric argon, which results in a cluster of points near the Y-axis of the isochron.

TEQ46 Andesite
The heating fractions have low errors and consistent ages, so 100% of the ^{39}Ar was used in calculating the plateau. The sample contains a high concentration of atmospheric argon, which results in a cluster of points near the Y-axis of the isochron. All the points were used to construct the isochron. The total gas, plateau, and isochron ages are all within 1σ error of each other.

TAL1 Andesite
The heating fractions have low errors and consistent ages, so 100% of the ^{39}Ar released was used in calculating the plateau. All points were used to construct the isochron; the plateau and isochron ages are within 1σ error of each other.

PW123 Andesite
The plateau excludes an anomalously old age in the lowest temperature fraction. The low temperature discrepancy is most likely due to release of atmospheric argon, which may be expected in a young, vesicular sample. The isochron age is based on all of the step-heating fractions and is the same as the plateau age within 1σ error.

PW391 Andesite
The plateau excludes anomalous ages in the high temperature heating fractions that may result from degassing of xenocrysts. The sample contains a high concentration of atmospheric argon, which results in a cluster of points near the Y-axis of the isochron.

The isochron age is based on all of the step-heating fractions and is the same as the plateau age at the 1σ level.

PW143 Andesite
The plateau excludes anomalously old ages in the high temperature heating fractions that are most likely due to fusion of pyroxene xenocrysts, which corresponds with the jump in calcium concentrations. The plateau points were used to construct the isochron, which has the same age as the plateau age at the 1σ level.

TEQ39 Basalt
There is no plateau age for the sample. The descending stair step pattern in ages that corresponds with increasing calcium concentration may indicate recoil effects. The sample has a high concentration of atmospheric argon, which may affect the errors on the analysis.

ETZ10 Andesite
The sample contains high concentrations of atmospheric argon, which has resulted in large errors on the heating fractions of the plateau diagram and a cluster of points near the y-axis on the isochron diagram. Because the isochron has an MSWD of 1.89, close to the minimum of 1.8, the isochron age has been reported. No plateau age can be calculated for this sample.

TAL26 Basaltic Andesite
There is no plateau age due to the appearance of two clusters of ages that may indicate two phases of degassing of the sample. Each group of fractions contains 50% of the gas released, so neither fits the requirement to form a plateau of >50% of the ^{39}Ar. The calculated average age of each group is within error of the isochron age. This sample has a high concentration of atmospheric argon, so samples are clustered near the y-axis of the isochron.

TEQ67 Andesite
There is no plateau age for this sample due to inconsistent ages calculated at the different heating temperatures. The large errors are likely due to the high concentration of atmospheric argon in the sample. The gas from all the step-heating fractions was used to construct the isochron.

PW133 Andesite
The plateau age of this sample is negative, so it has not been reported in the tables in the paper. A negative age indicates youth, supporting the ages (~100 ka) obtained for the total gas and isochron ages. The anomalously old ages at high temperatures are most likely due to fusion of Ca-rich pyroxene, plagioclase, or hornblende, which corresponds with the jump in calcium and slight rise in chlorine concentrations. The sample is rich in atmospheric argon, which explains the cluster of points by the y-axis on the isochron diagram. All points were used in calculating the isochron age, which is consistent with the plateau age at the 1σ level.

TEQ9 Hornblende from Dacite
The plateau age includes gas from all except the final gas fraction. The last step had a low age that corresponds to a jump in calcium, suggestive of degassing of xenocrystic plagioclase, pyroxene, or hornblende. The isochron has a wide spread of points, all of which were used in its construction. The isochron and plateau ages correspond at the 1σ level.

ETZ5 Basaltic Andesite
A plateau age could not be determined for this sample. The descending stair step pattern in ages combined with the high concentration of calcium suggests possible recoil effects. The gas from all the step-heating fractions was used to calculate the isochron age, which has a good spread of points along the isochron and a well-defined y-intercept.

ETZ7 Basaltic Andesite
There is no plateau age for this sample due to inconsistent ages calculated at the different heating temperatures. The correlation diagram has an errorchron based on all the heating fractions.

ETZ2 Andesite
The plateau excludes anomalously old ages in both low and high temperature fractions. The low temperature discrepancy is most likely due to release of atmospheric argon. The high temperature discrepancy is most likely due to fusion of Ca-rich pyroxene or plagioclase, which corresponds with a slight increase in calcium concentrations. All of the heating fractions were used to construct the isochron, which shows a good spread of points and is consistent with the plateau age at the 1σ level.

MI84-o8a TEQ-29 Rhyolite (Hornblende)

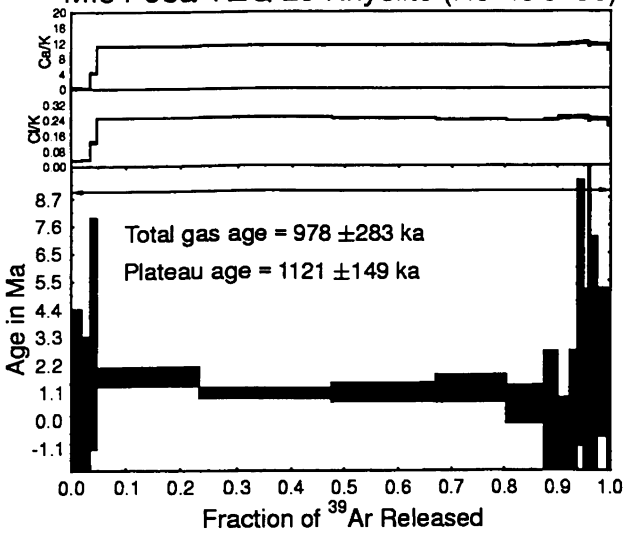

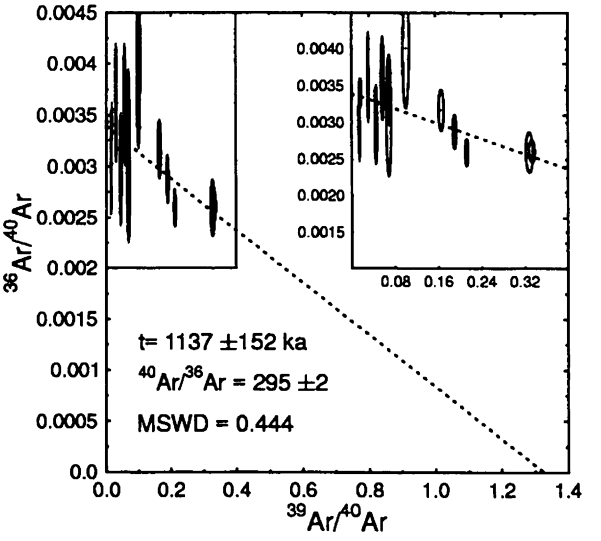

MI79-r3a ETZ-6 Basaltic Andesite

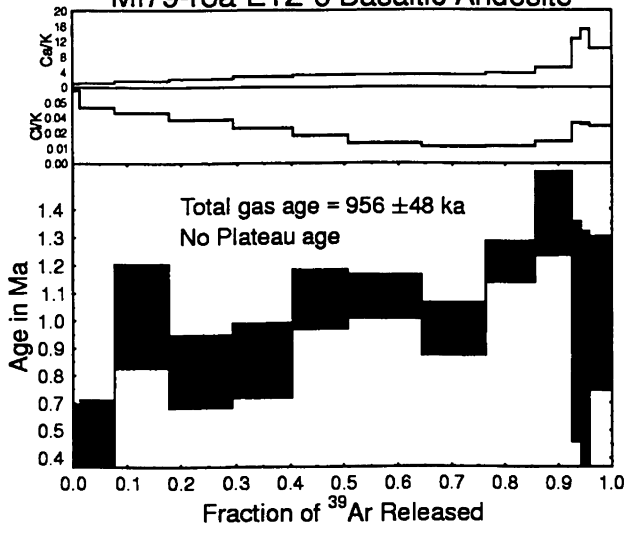

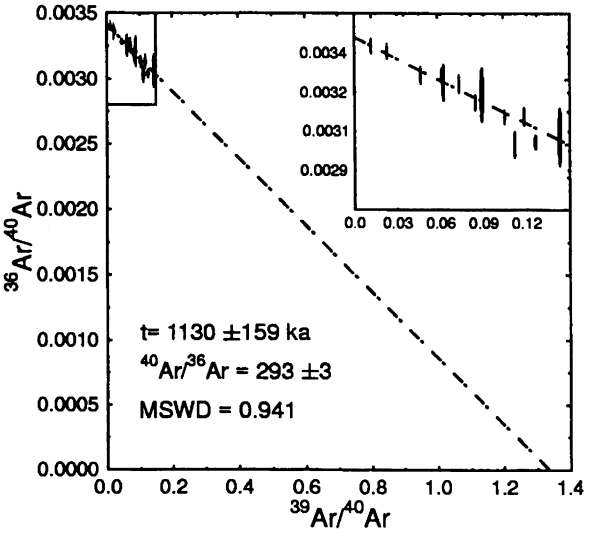

MI84-a48a TEQ-32 Basaltic Andesite

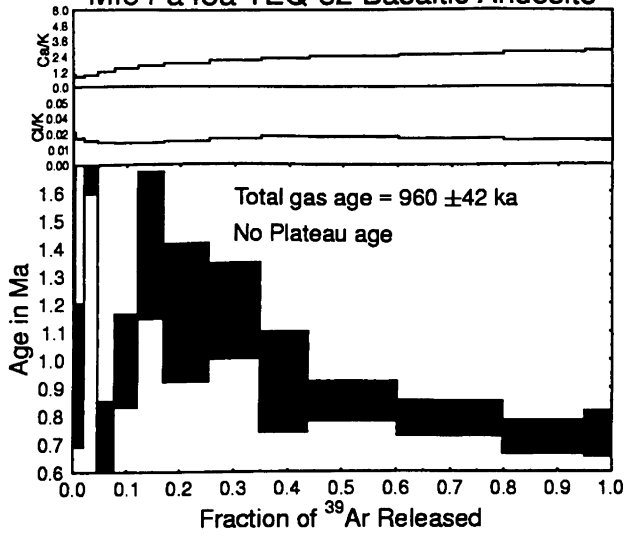

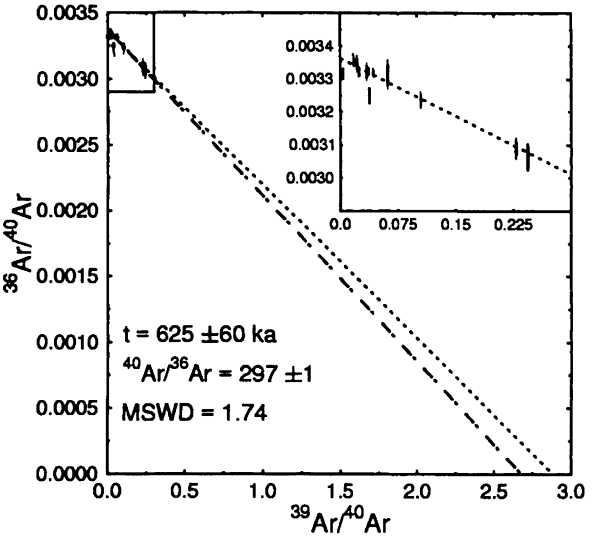

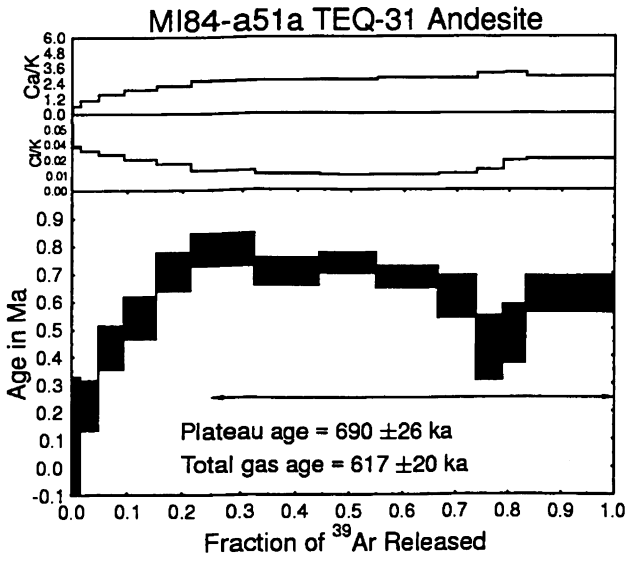
MI84-a51a TEQ-31 Andesite
Ca/K
Cl/K
Age in Ma
Plateau age = 690 ±26 ka
Total gas age = 617 ±20 ka
Fraction of ^{39}Ar Released

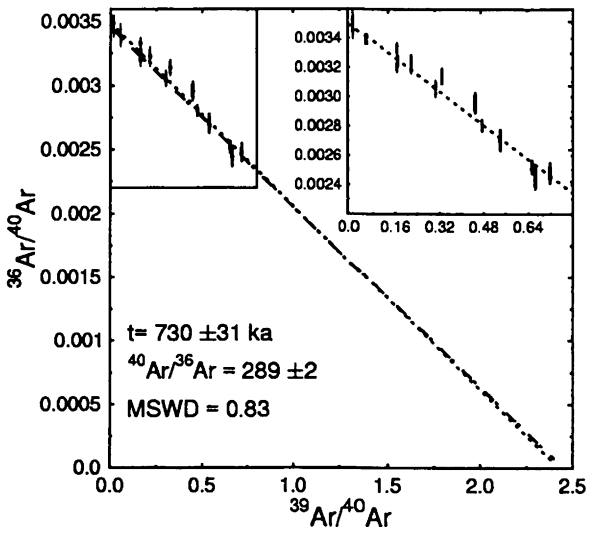
^{36}Ar/^{40}Ar
t= 730 ±31 ka
^{40}Ar/^{36}Ar = 289 ±2
MSWD = 0.83
^{39}Ar/^{40}Ar

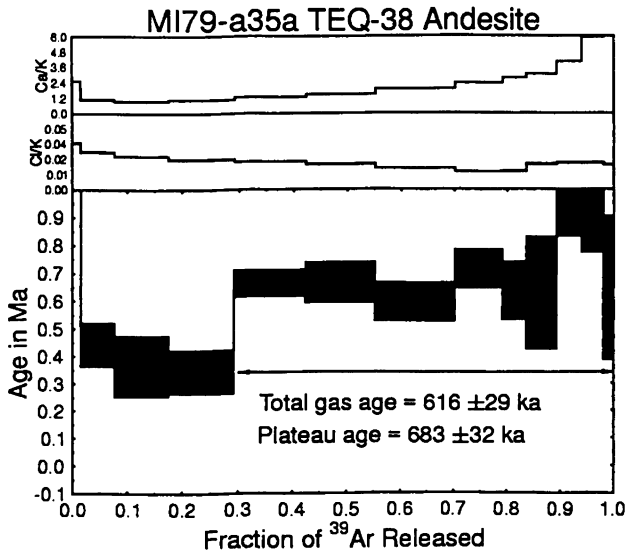
MI79-a35a TEQ-38 Andesite
Ca/K
Cl/K
Age in Ma
Total gas age = 616 ±29 ka
Plateau age = 683 ±32 ka
Fraction of ^{39}Ar Released

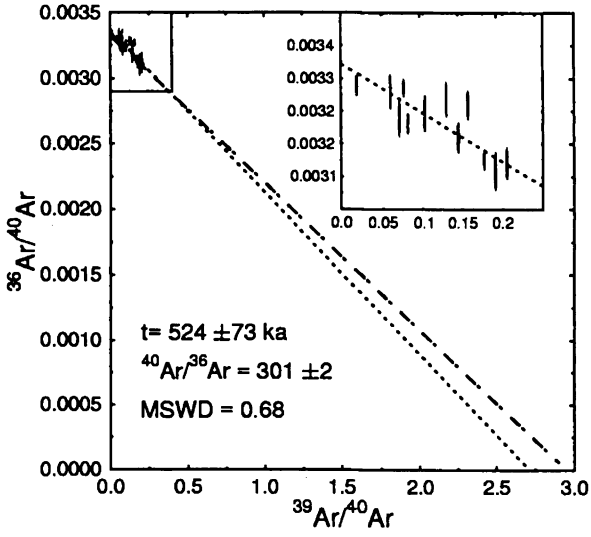
^{36}Ar/^{40}Ar
t= 524 ±73 ka
^{40}Ar/^{36}Ar = 301 ±2
MSWD = 0.68
^{39}Ar/^{40}Ar

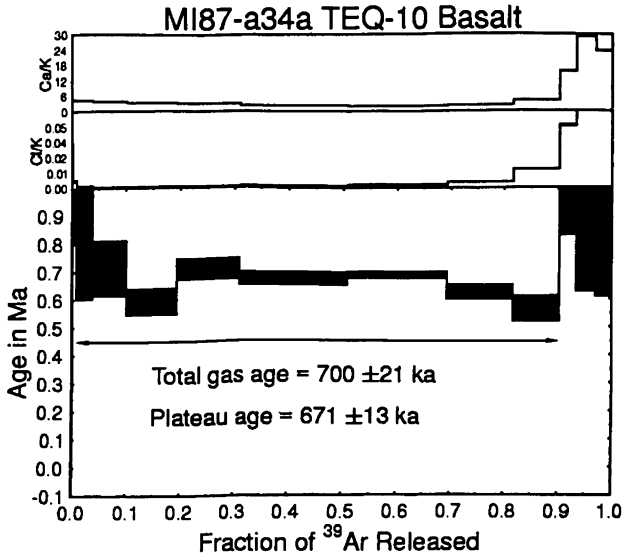
MI87-a34a TEQ-10 Basalt
Ca/K
Cl/K
Age in Ma
Total gas age = 700 ±21 ka
Plateau age = 671 ±13 ka
Fraction of ^{39}Ar Released

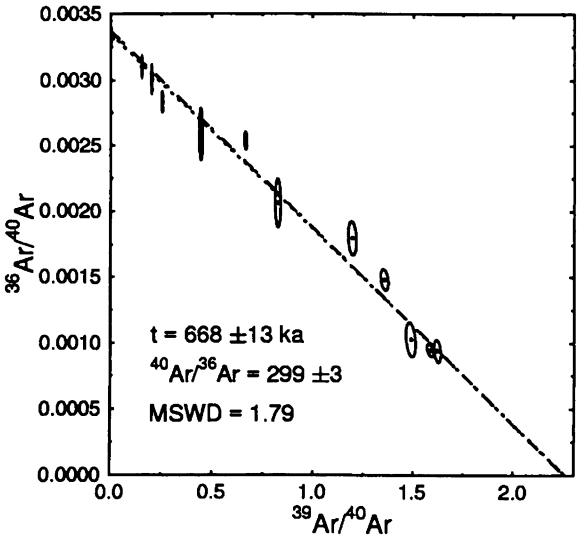
^{36}Ar/^{40}Ar
t = 668 ±13 ka
^{40}Ar/^{36}Ar = 299 ±3
MSWD = 1.79
^{39}Ar/^{40}Ar

MI84-a35a TEQ-18 Rhyolite

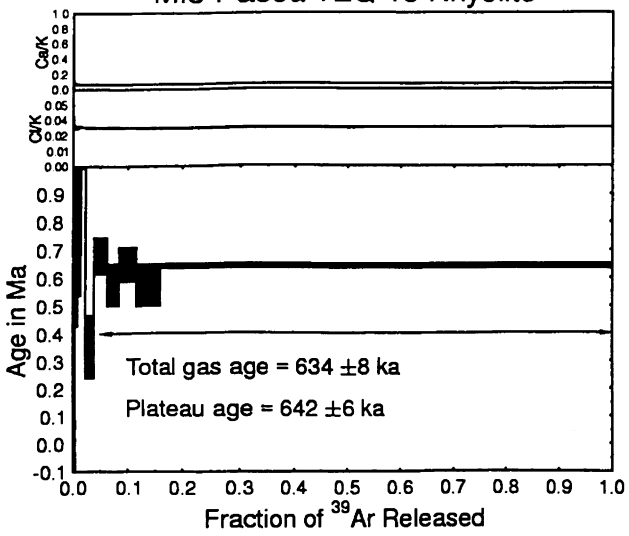

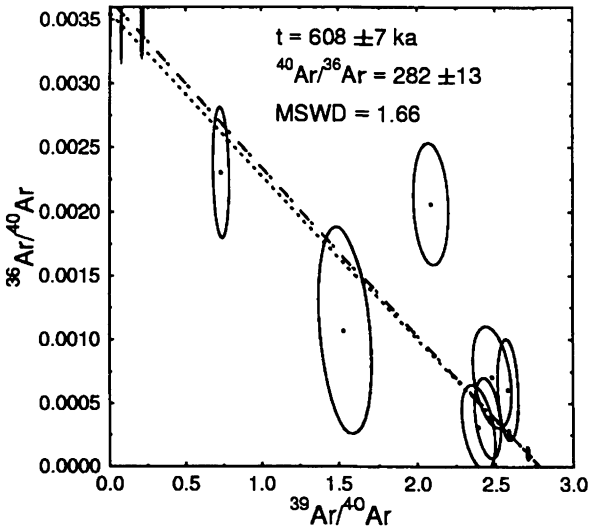

MI84-a40a TEQ-35 Rhyolite

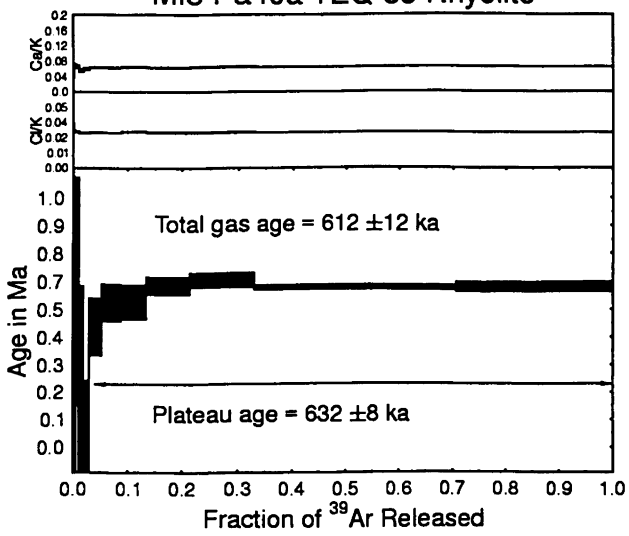

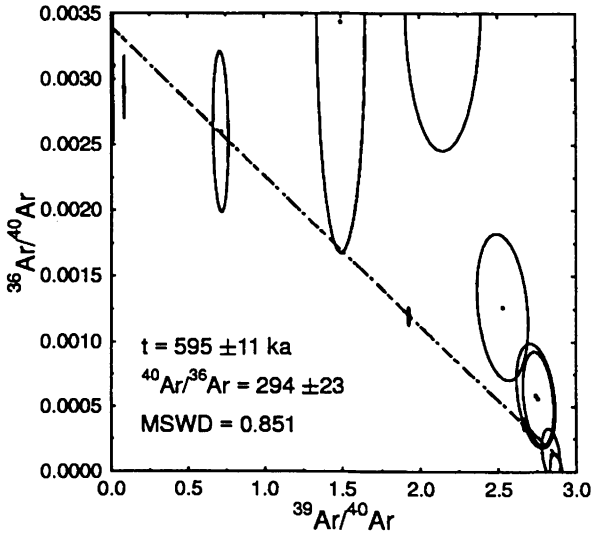

MI84-a41a ETZ-4 Dacite

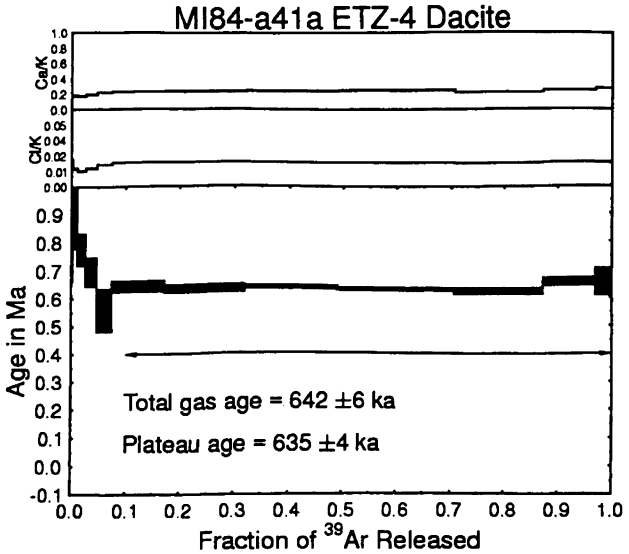

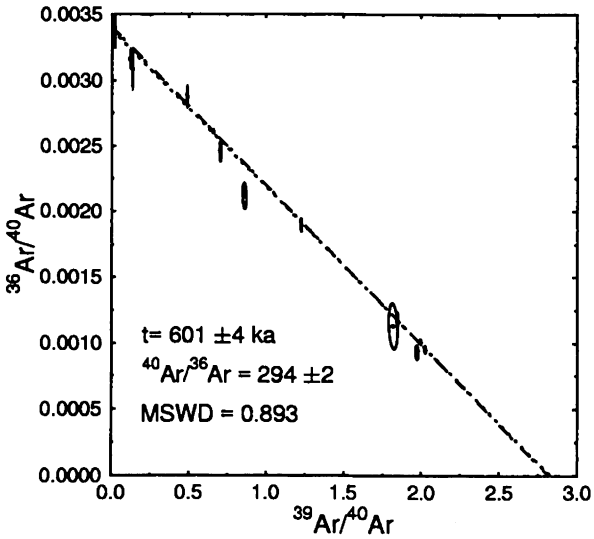

MI79-a54a TEQ-21A Rhyolite

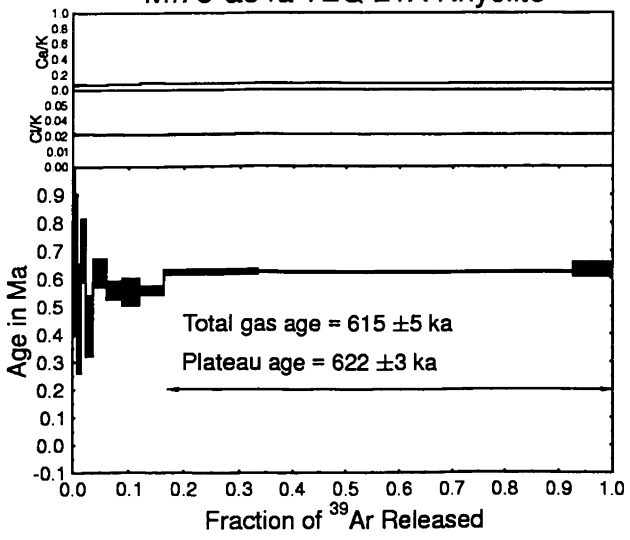

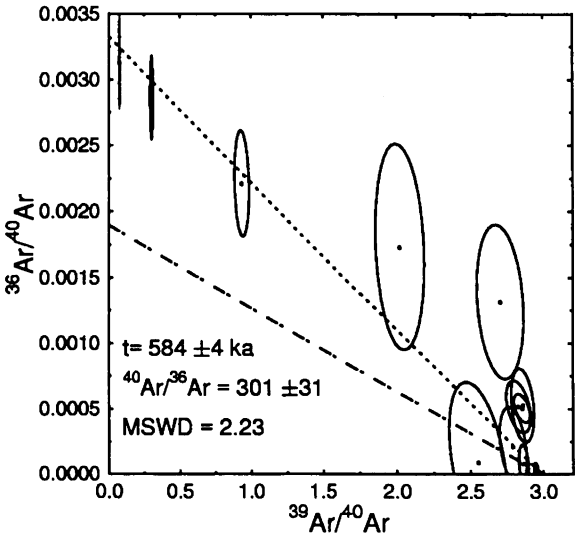

MI79-a56a ETZ-11 Dacite

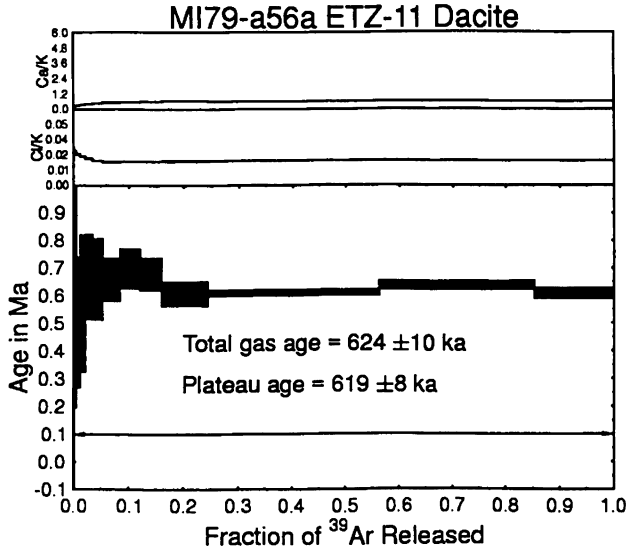

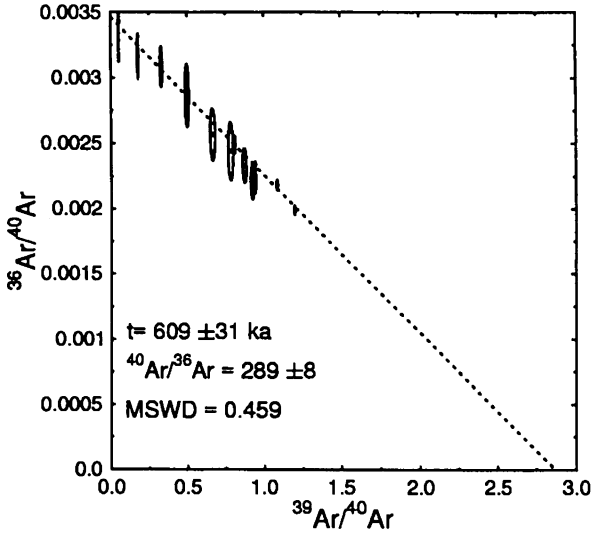

MI87-a26a TEQ-45b Rhyolite

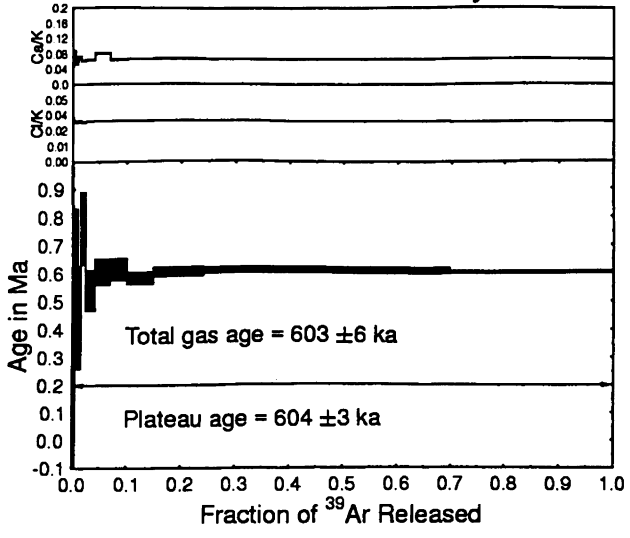

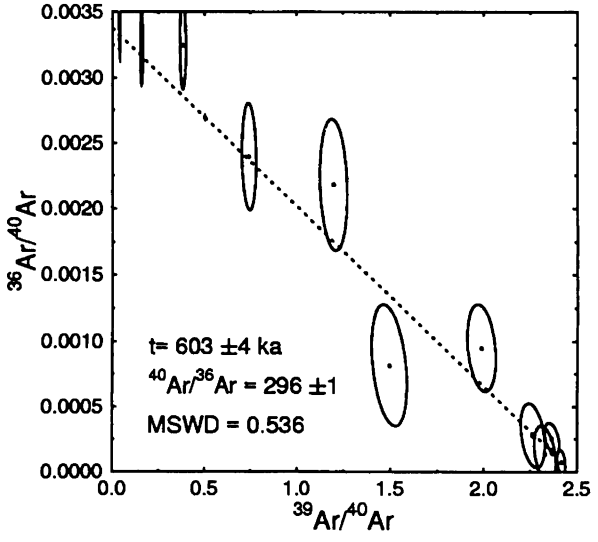

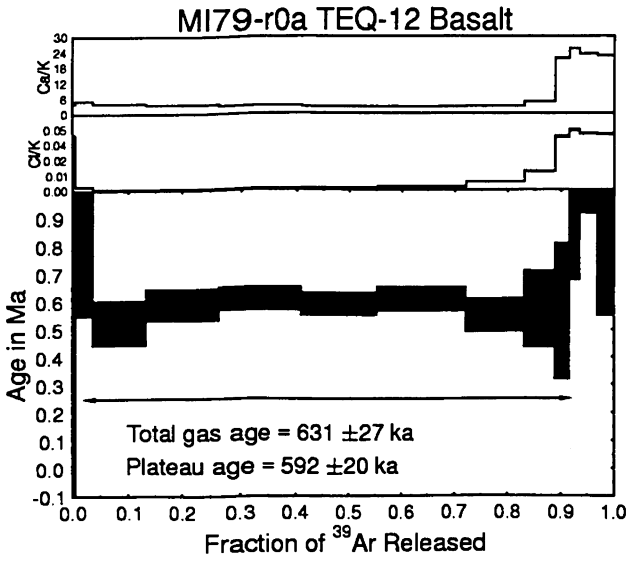
MI79-r0a TEQ-12 Basalt
Ca/K
Cl/K
Age in Ma
Total gas age = 631 ±27 ka
Plateau age = 592 ±20 ka
Fraction of ^{39}Ar Released

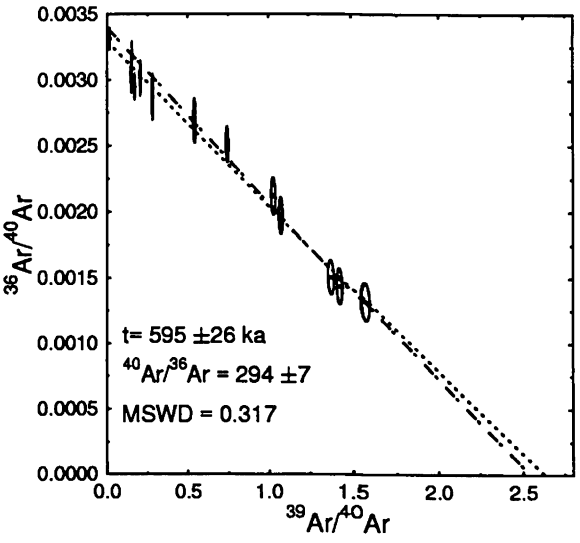
t= 595 ±26 ka
^{40}Ar/^{36}Ar = 294 ±7
MSWD = 0.317
^{36}Ar/^{40}Ar
^{39}Ar/^{40}Ar

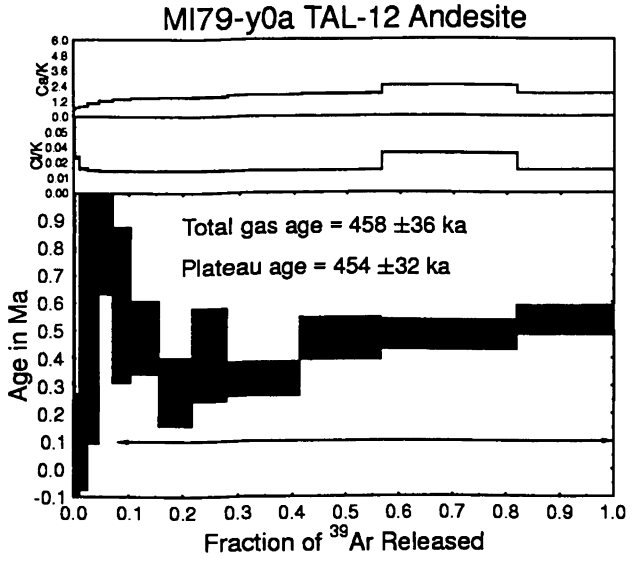
MI79-y0a TAL-12 Andesite
Ca/K
Cl/K
Age in Ma
Total gas age = 458 ±36 ka
Plateau age = 454 ±32 ka
Fraction of ^{39}Ar Released

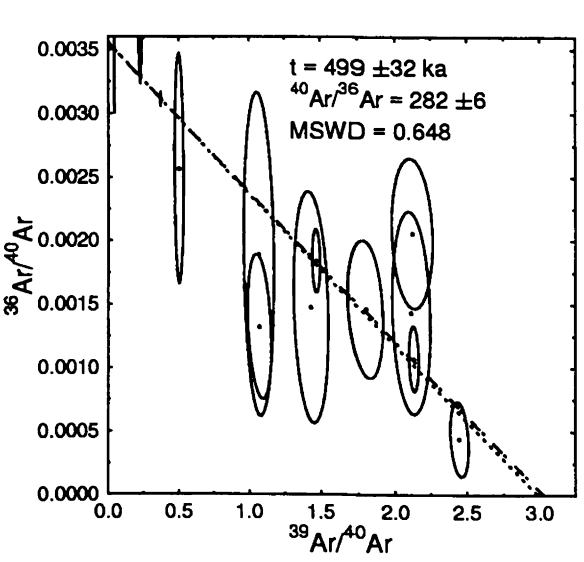
t = 499 ±32 ka
^{40}Ar/^{36}Ar = 282 ±6
MSWD = 0.648
^{36}Ar/^{40}Ar
^{39}Ar/^{40}Ar

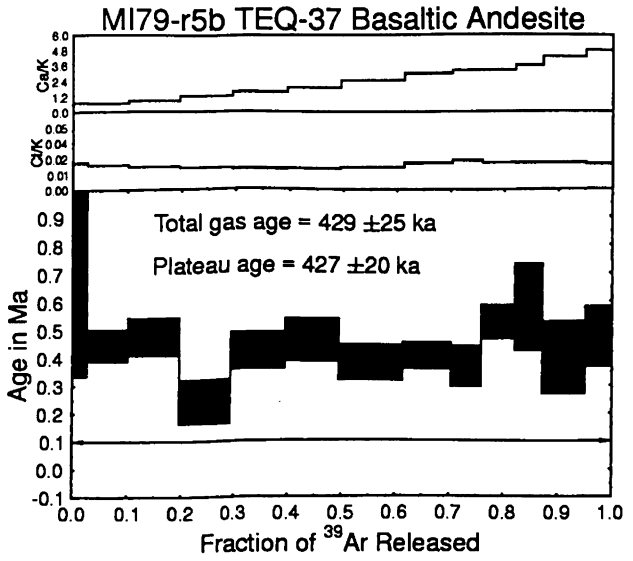
MI79-r5b TEQ-37 Basaltic Andesite
Ca/K
Cl/K
Age in Ma
Total gas age = 429 ±25 ka
Plateau age = 427 ±20 ka
Fraction of ^{39}Ar Released

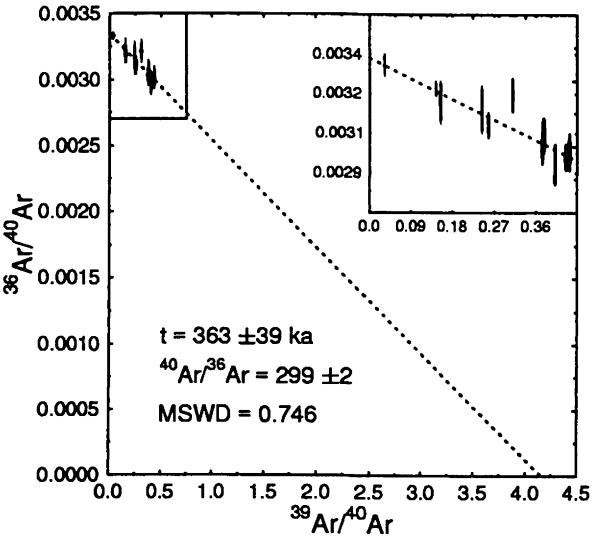
t = 363 ±39 ka
^{40}Ar/^{36}Ar = 299 ±2
MSWD = 0.746
^{36}Ar/^{40}Ar
^{39}Ar/^{40}Ar

MI84-a47a TEQ-22 Rhyolite

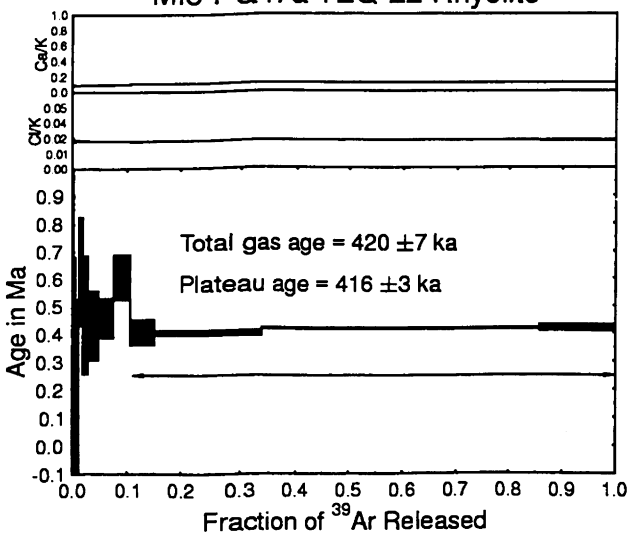

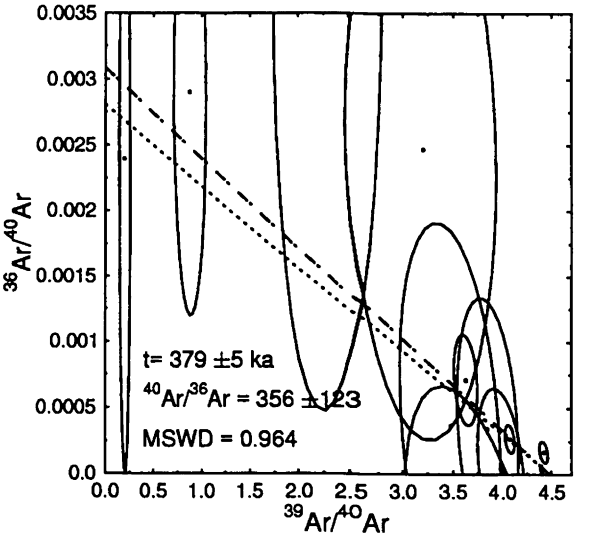

MI84-q4a TAL-9 Dacite

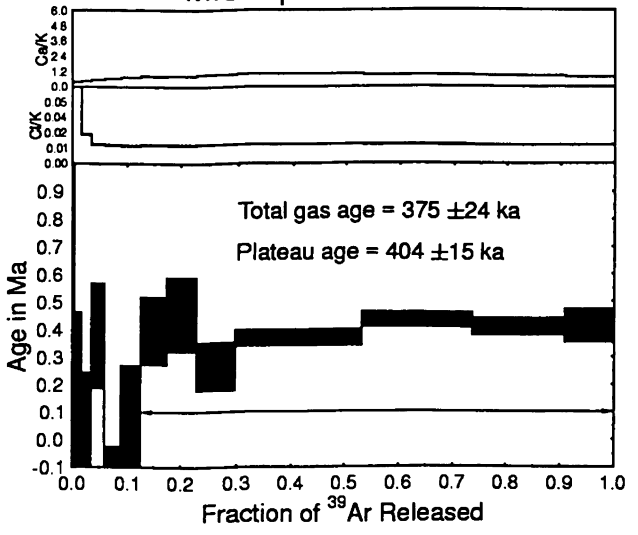

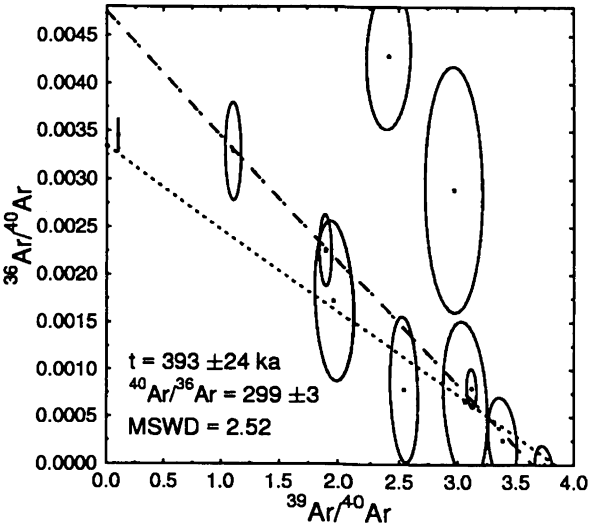

MI87-a44a TEQ-66 Dacite

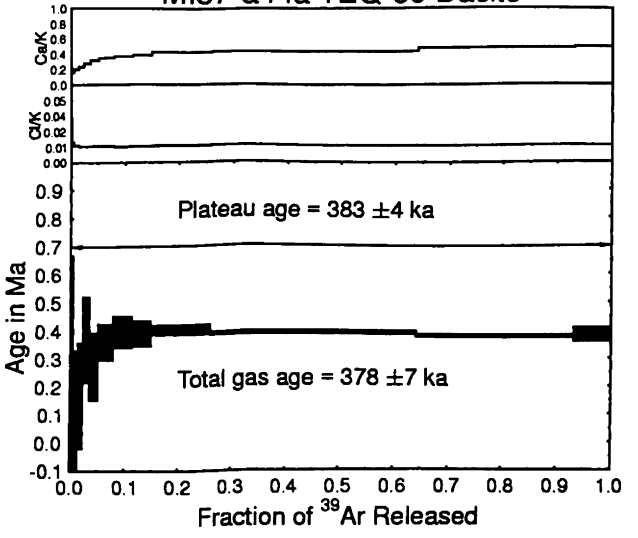

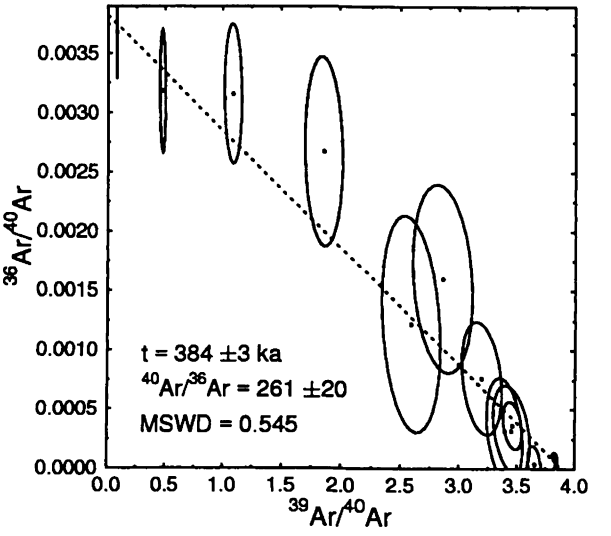

MI84-a45a TAL-8 Dacite

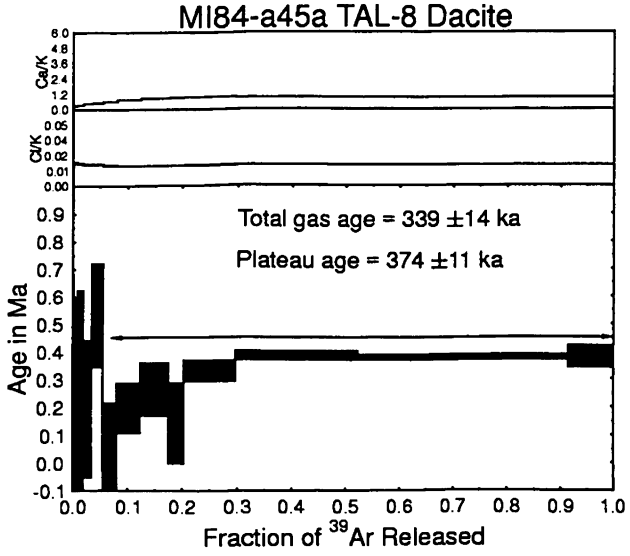

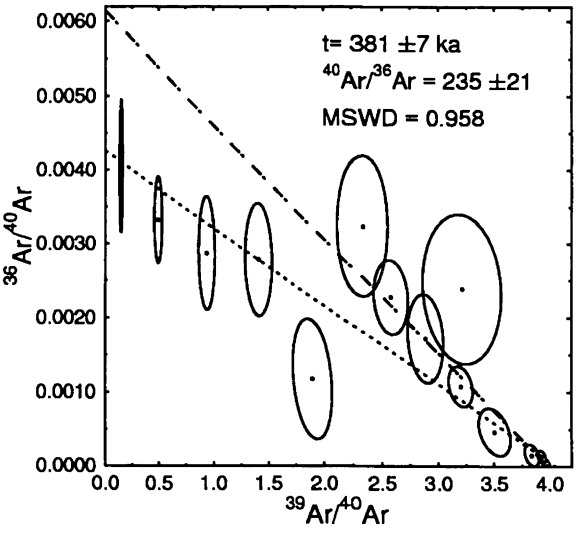

MI79-q6a TAL-13 Andesite

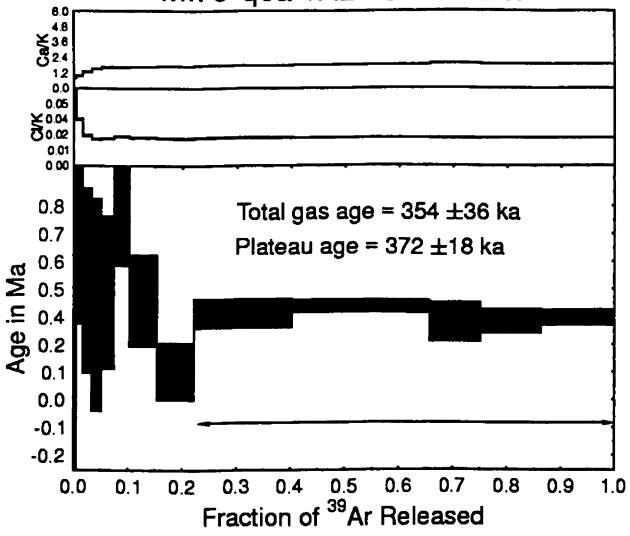

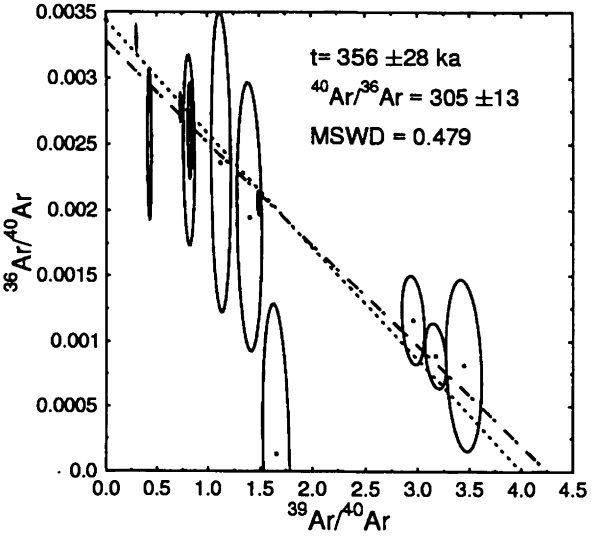

MI79-q7a TEQ-33 Basaltic Andesite

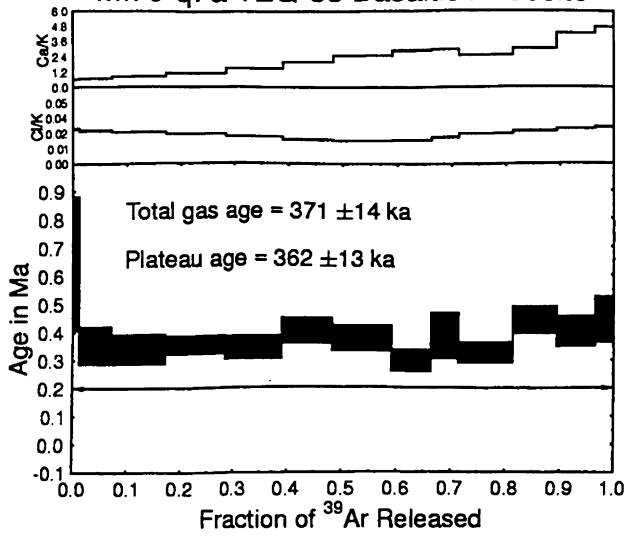

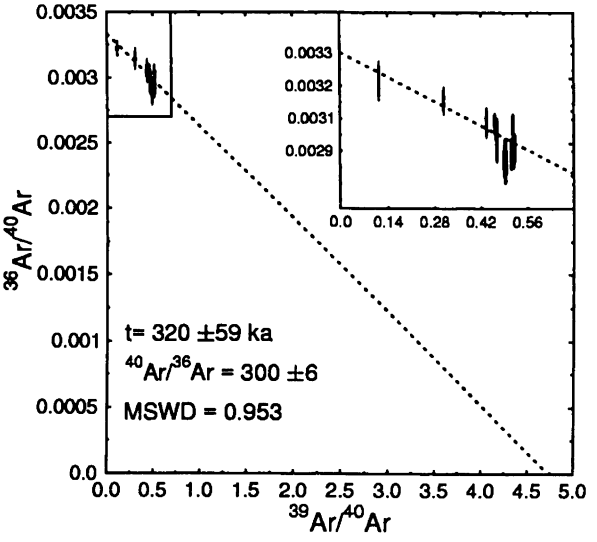

MI84-a23a TAL-25 Andesite

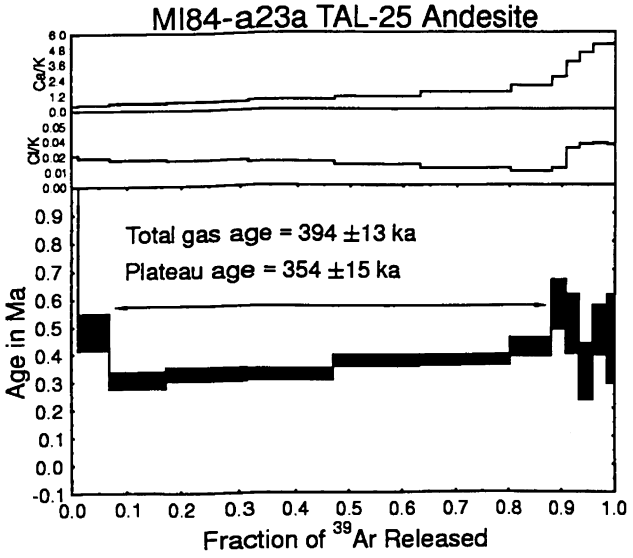

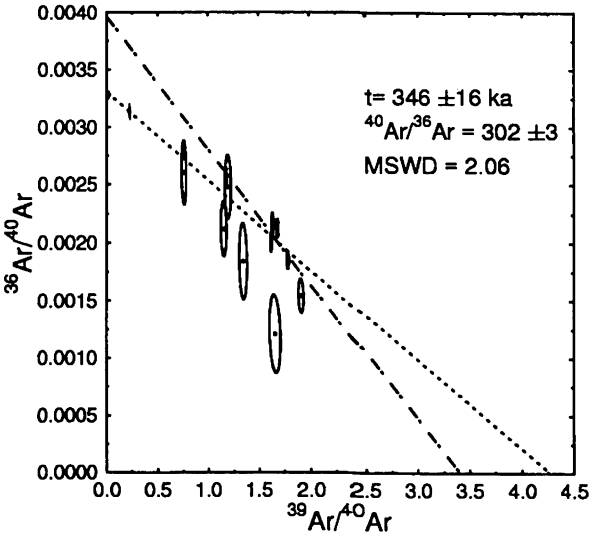

MI79-s2a ETZ-3 Andesite

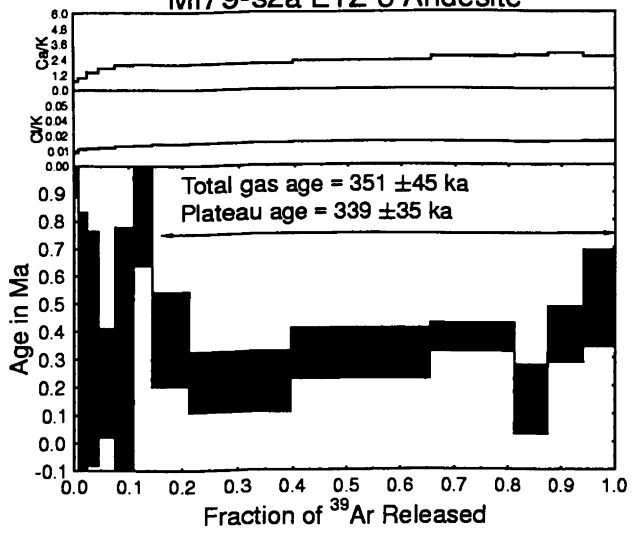

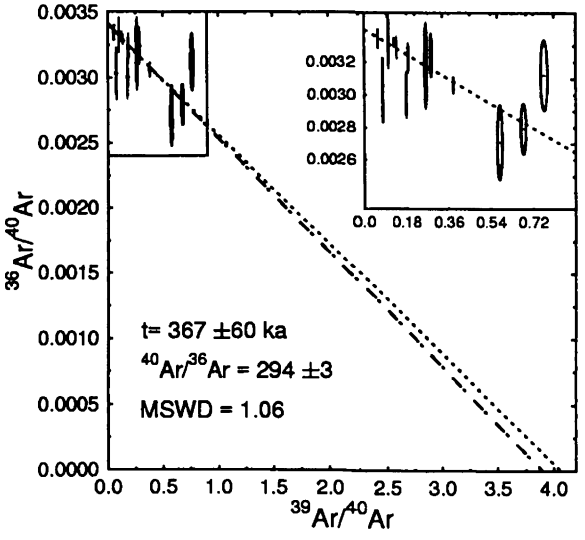

MI79-r6a TEQ-36 Basalt

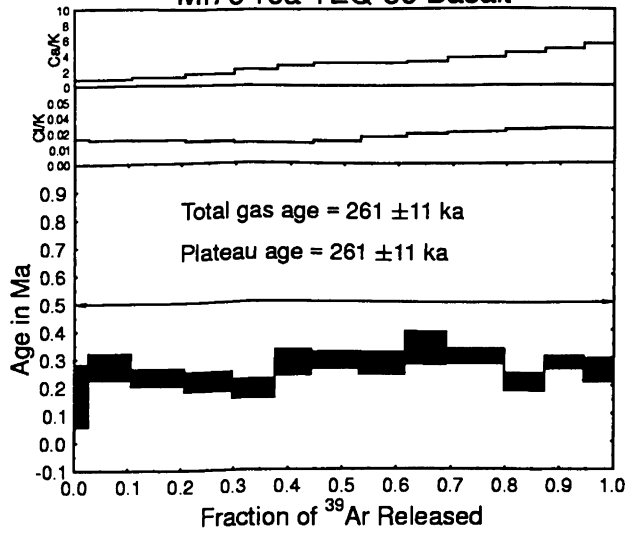

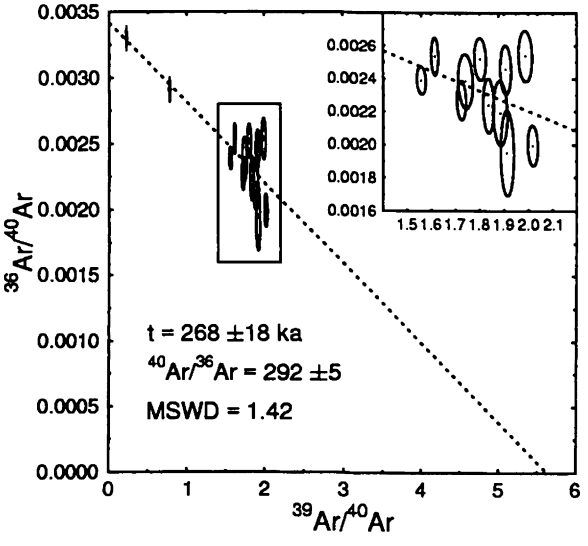

MI87-a41a TAL-11 Andesite

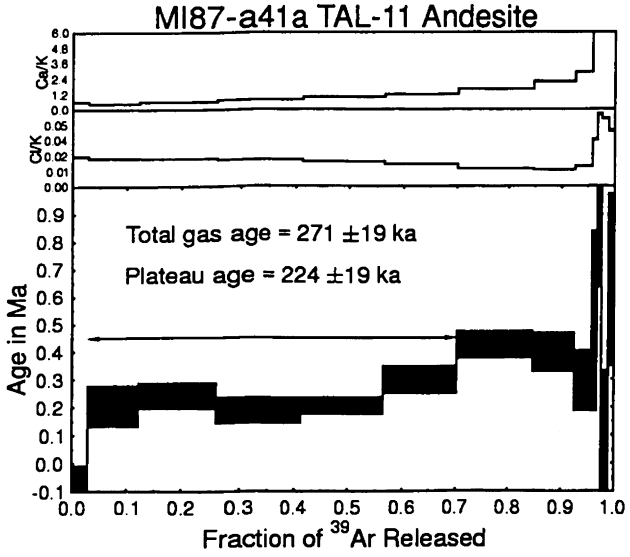

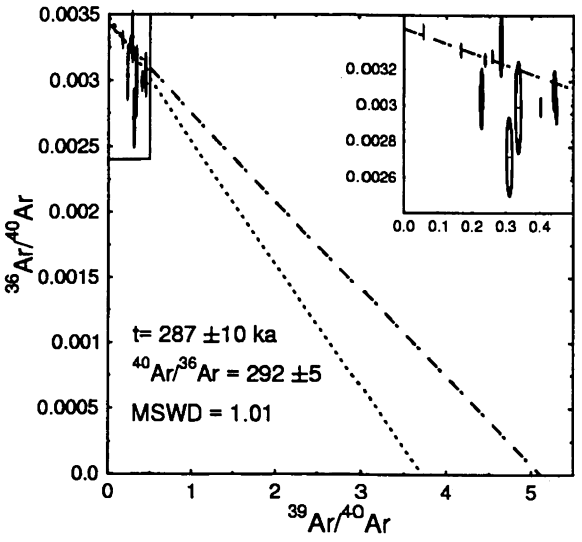

MI79-a32a TEQ-6 Andesite

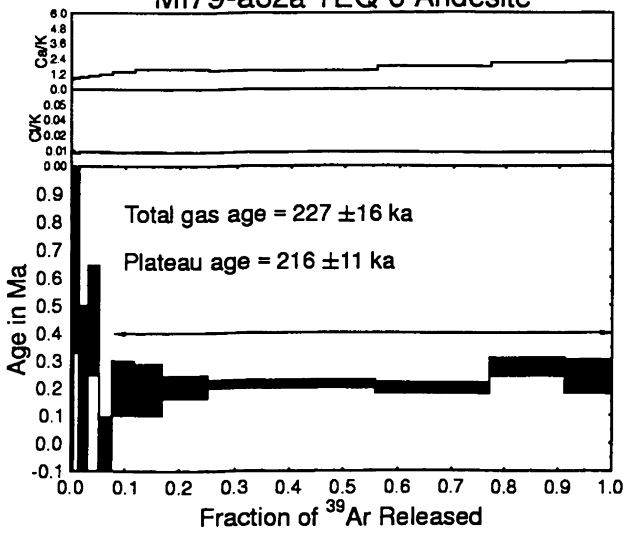

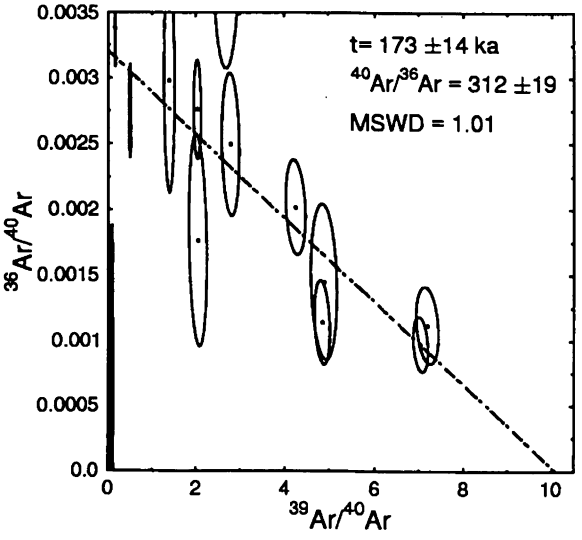

MI84-a65a JH009 Andesite

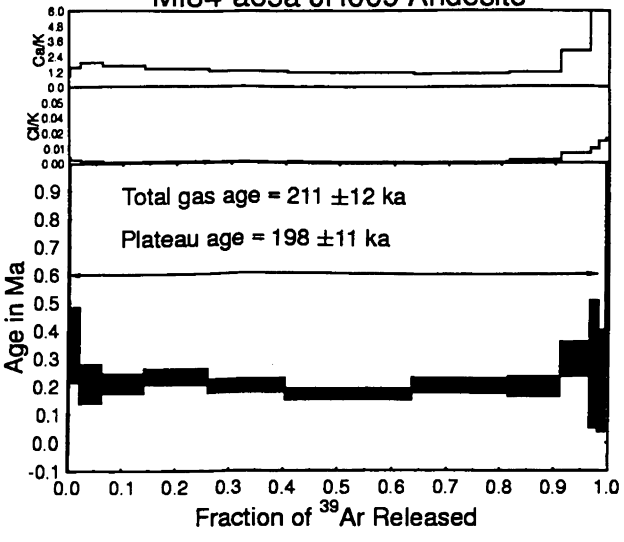

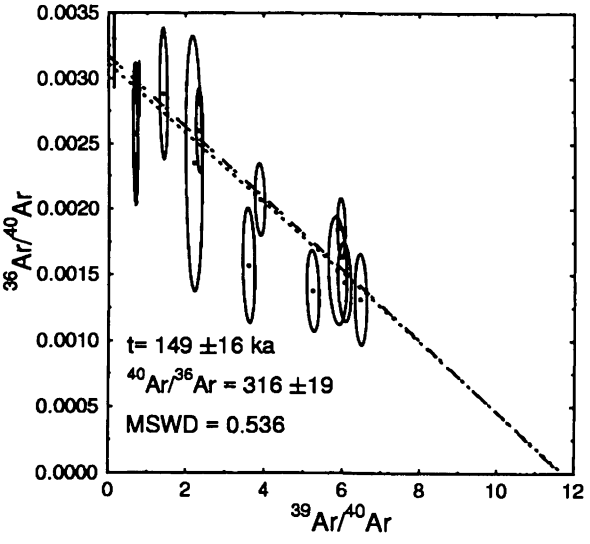

MI84-a50a TEQ-23C Andesite

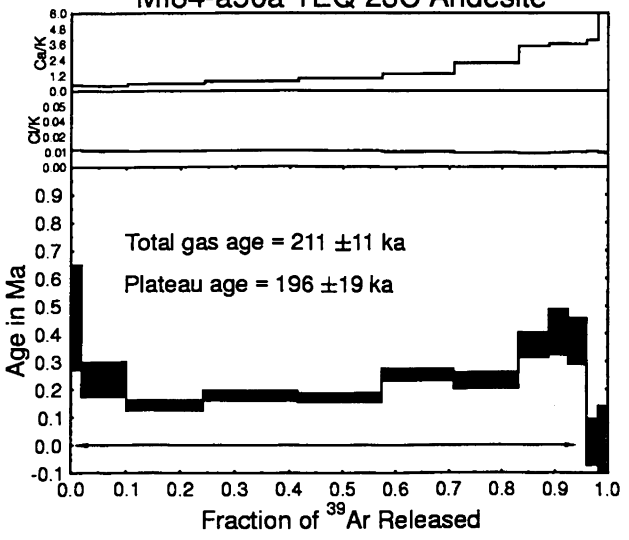

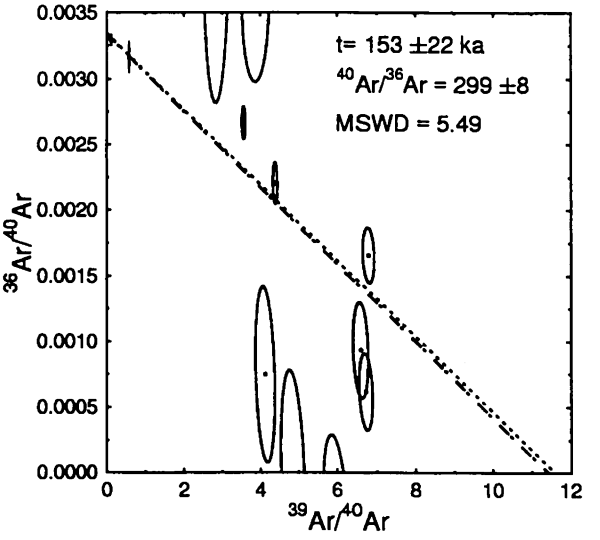

MI79-a39a TEQ-15 Andesite

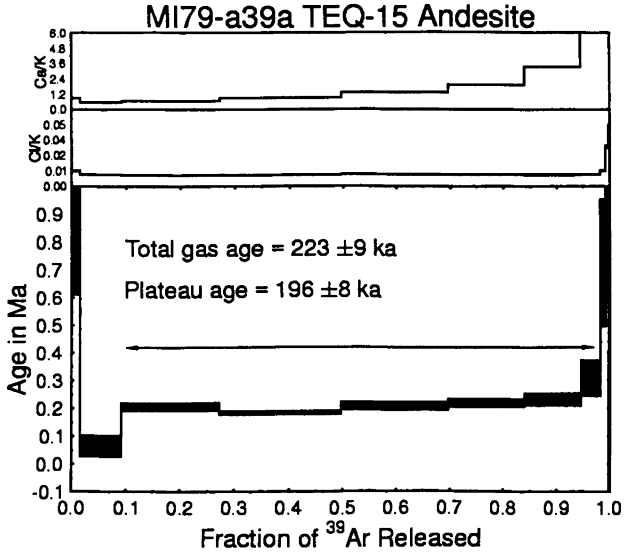

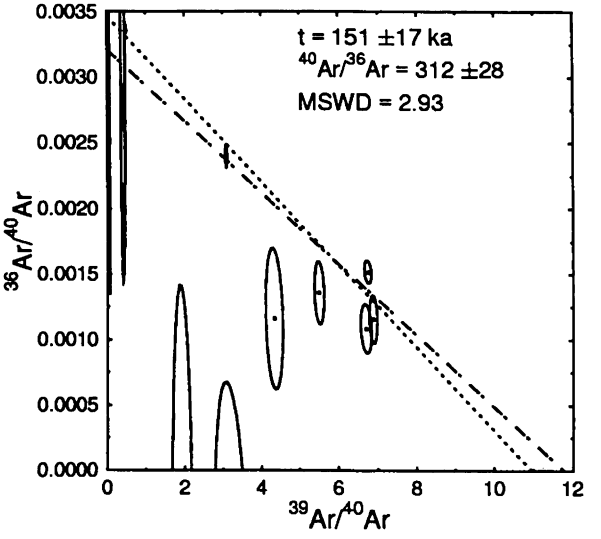

MI79-s0a TEQ-40 Basaltic Andesite

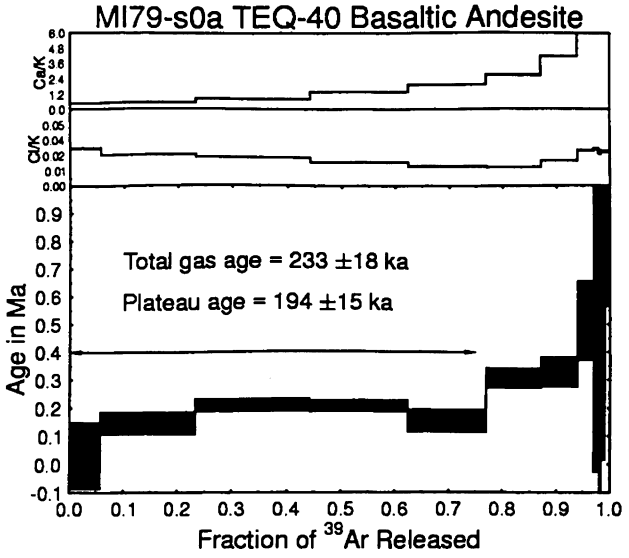

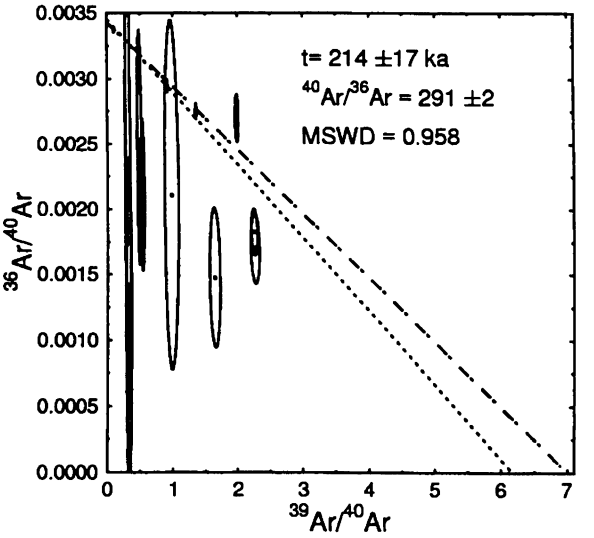

MI79-a38a TEQ-17 Andesite

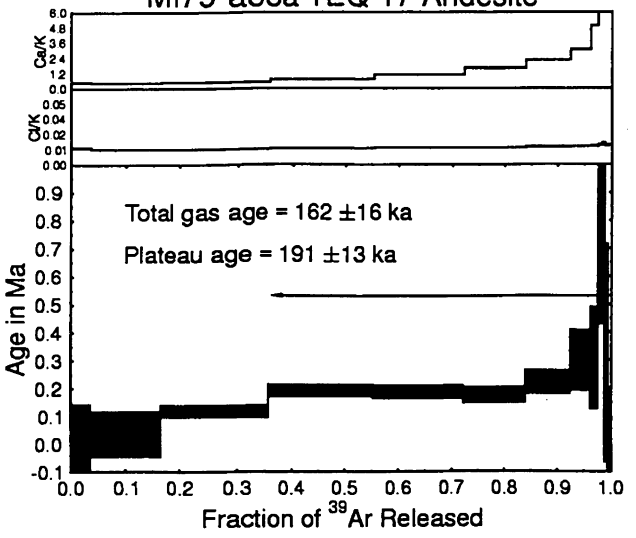

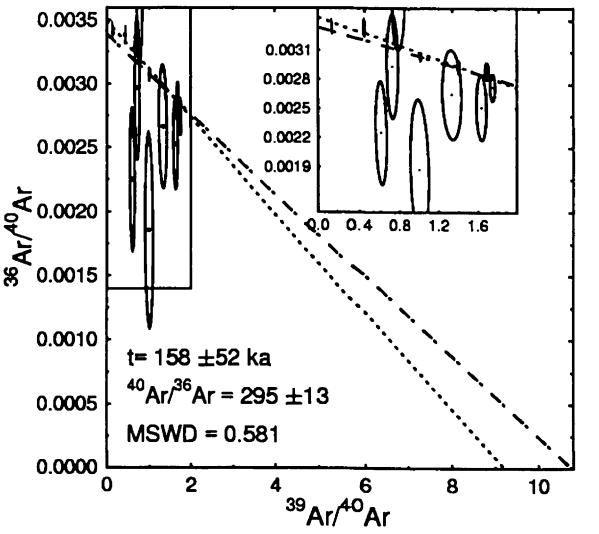

MI79-a36a TEQ-60 Andesite

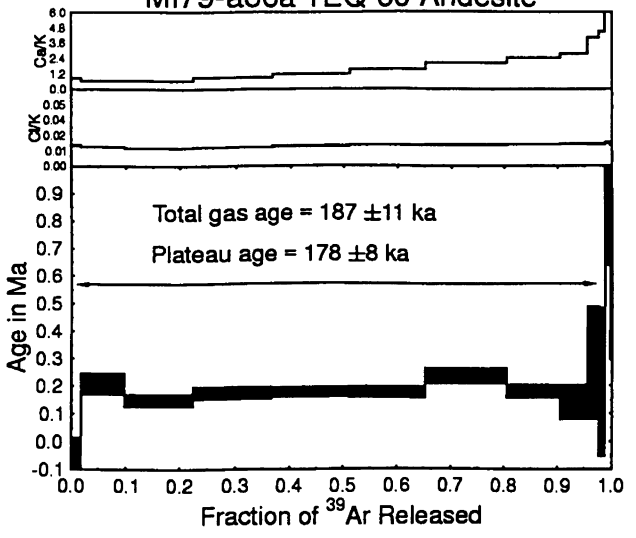

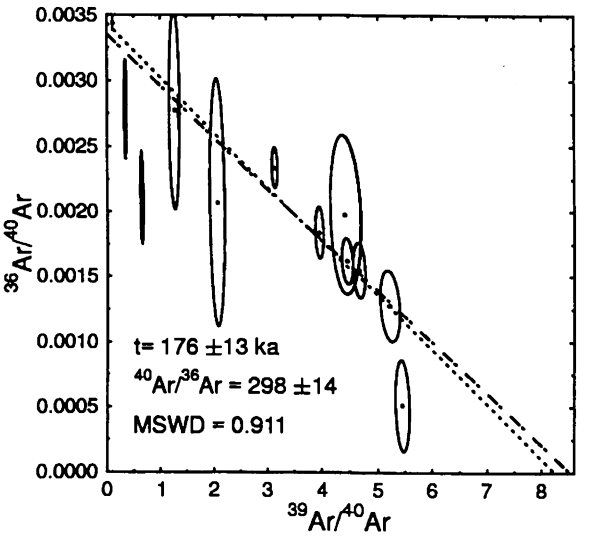

MI79-q8b TEQ-25 Andesite

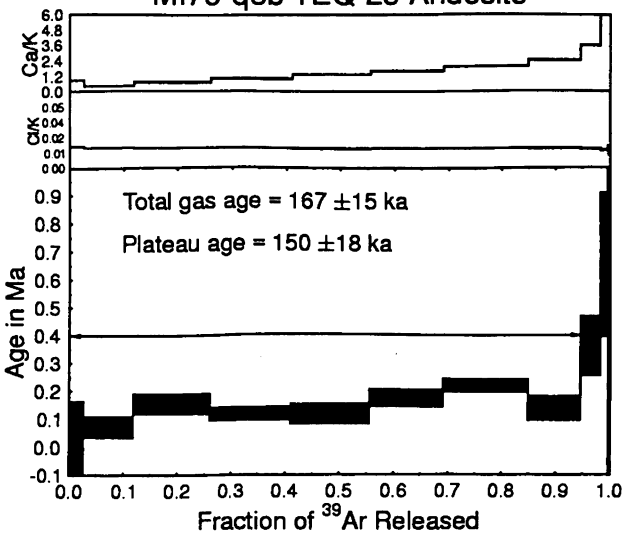

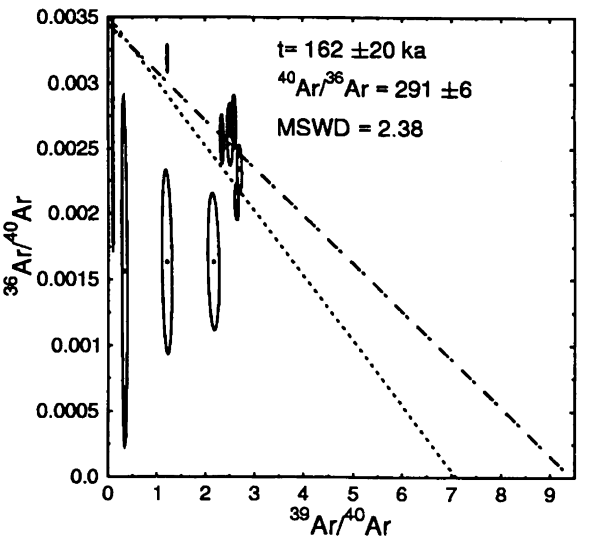

MI79-r4a ETZ-1 Basalt

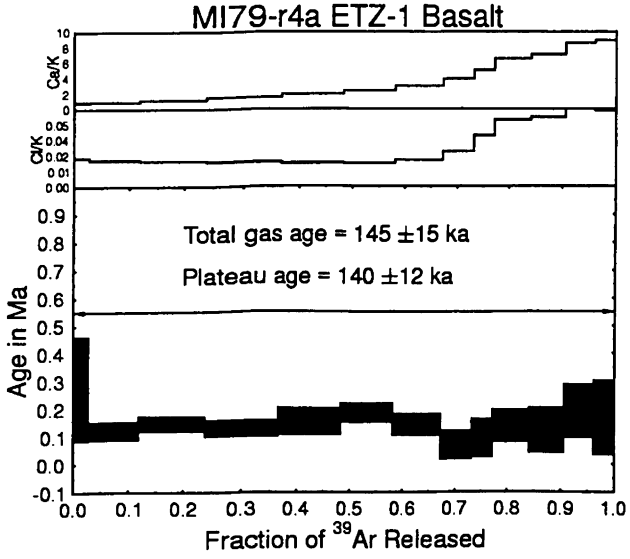

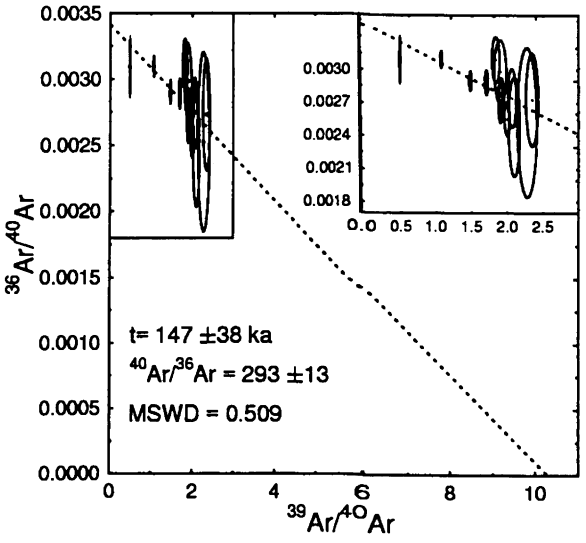

MI79-a32a TEQ-48 Andesite

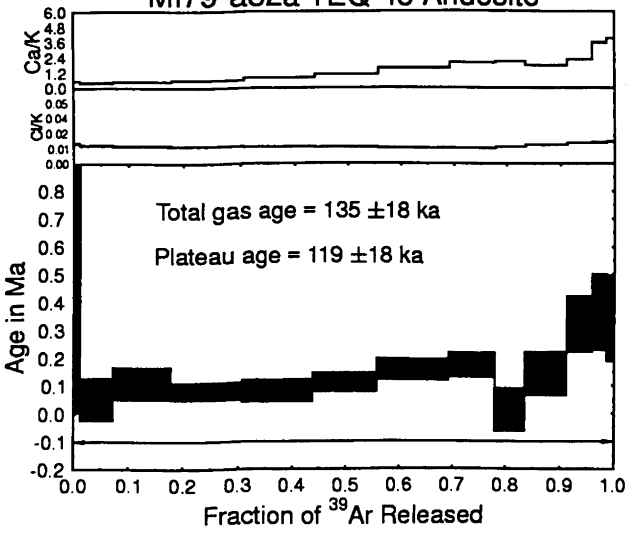

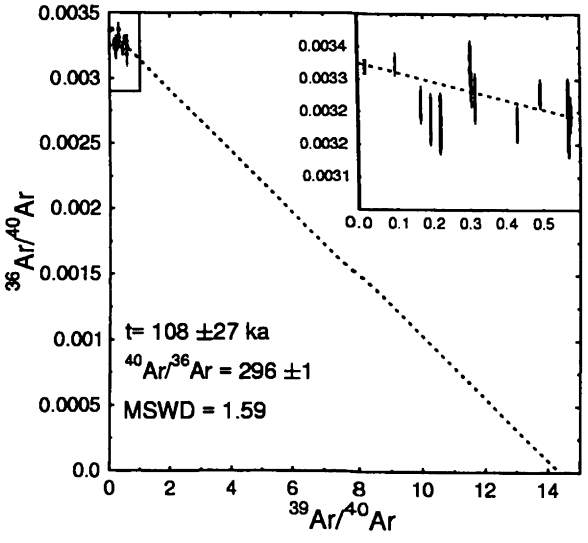

MI79-a27a TEQ-46 Andesite

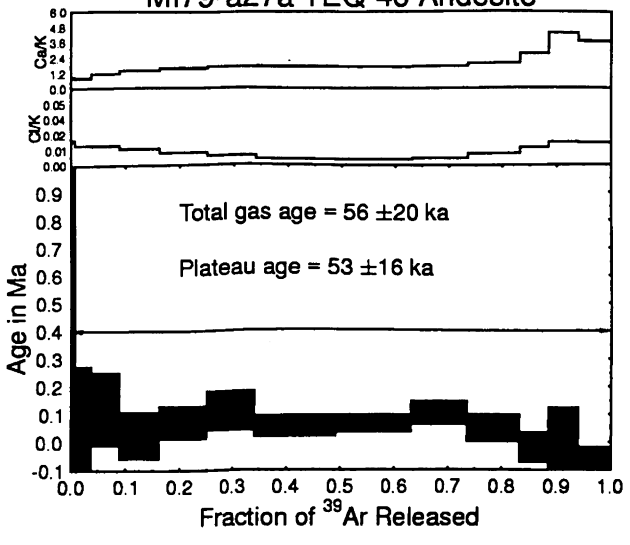

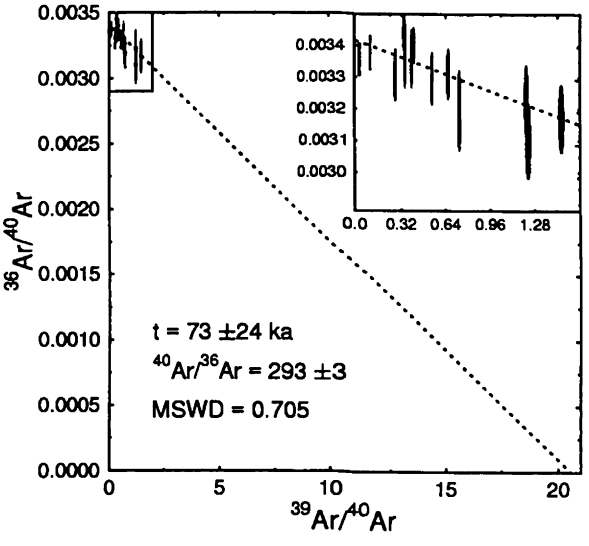

MI87-a25a TAL-1 Andesite

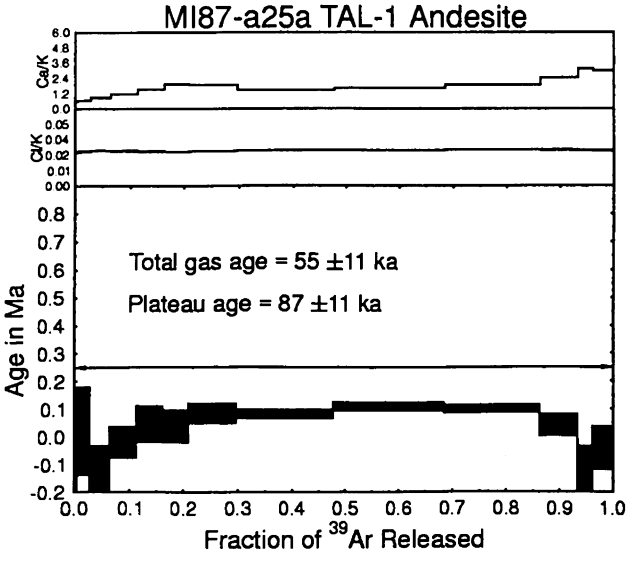

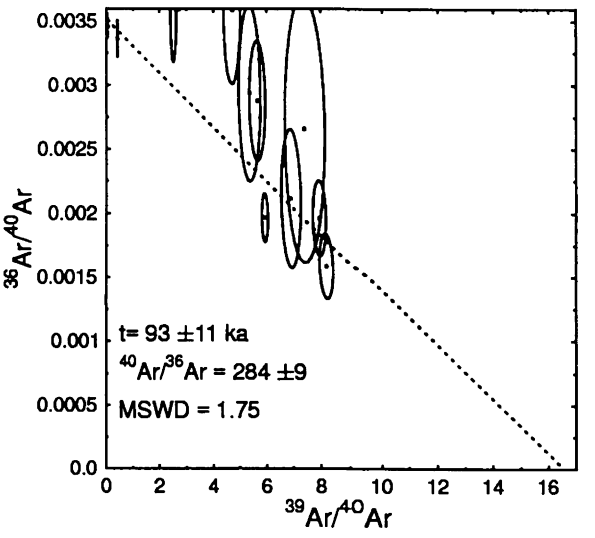

MI79-34ba PW-123 Andesite

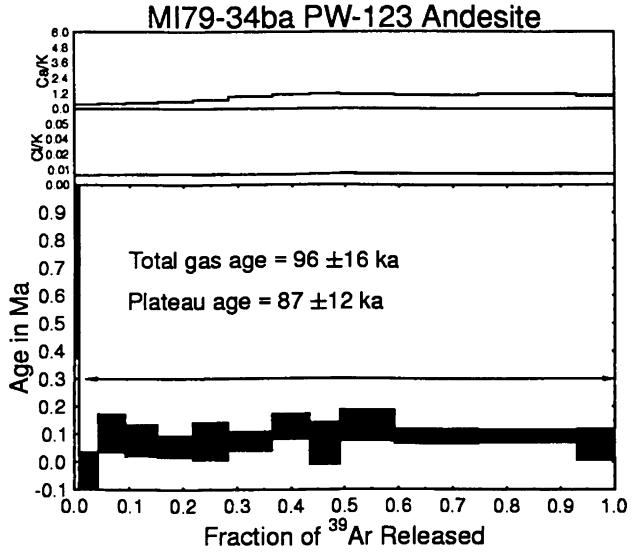

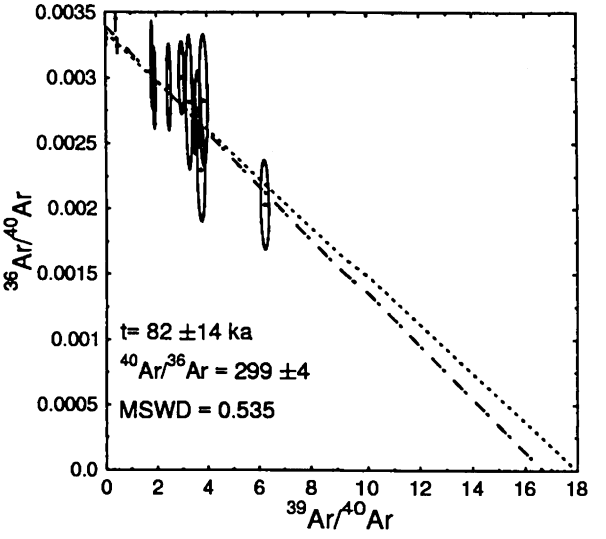

MI79-38ba PW-391 Andesite

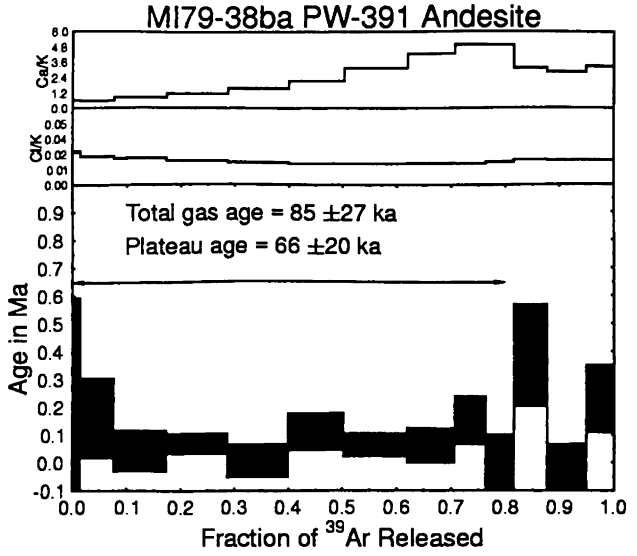

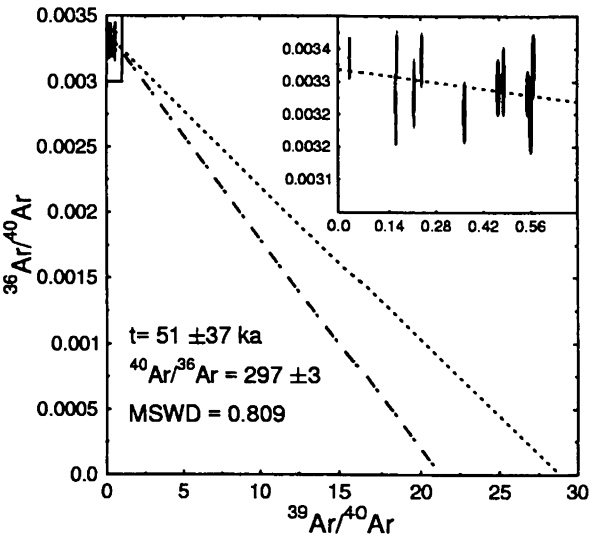

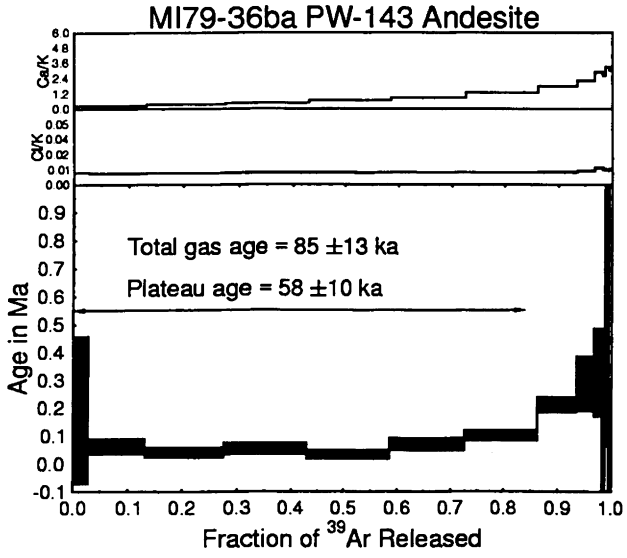
MI79-36ba PW-143 Andesite
Ca/K
Cl/K
Total gas age = 85 ±13 ka
Plateau age = 58 ±10 ka
Age in Ma
Fraction of ^{39}Ar Released

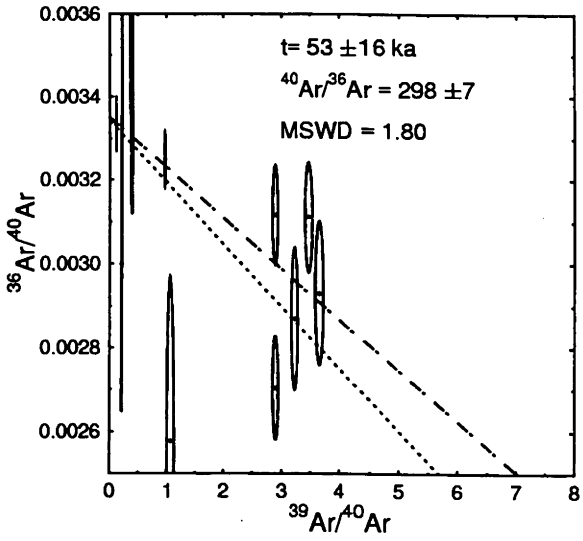
t= 53 ±16 ka
^{40}Ar/^{36}Ar = 298 ±7
MSWD = 1.80
^{36}Ar/^{40}Ar
^{39}Ar/^{40}Ar

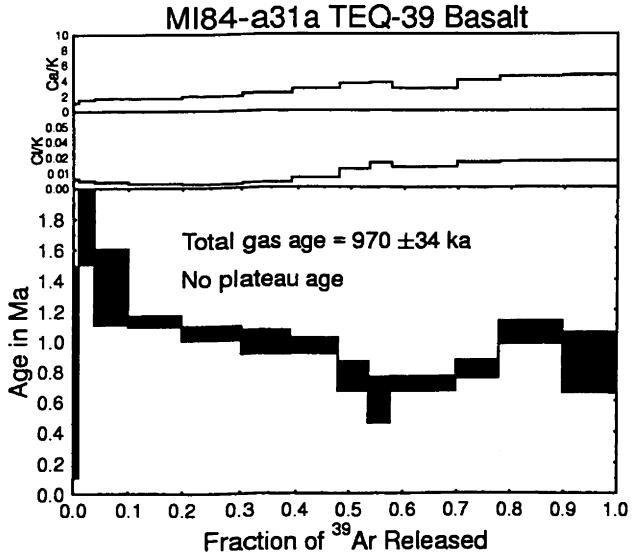
MI84-a31a TEQ-39 Basalt
Ca/K
Cl/K
Total gas age = 970 ±34 ka
No plateau age
Age in Ma
Fraction of ^{39}Ar Released

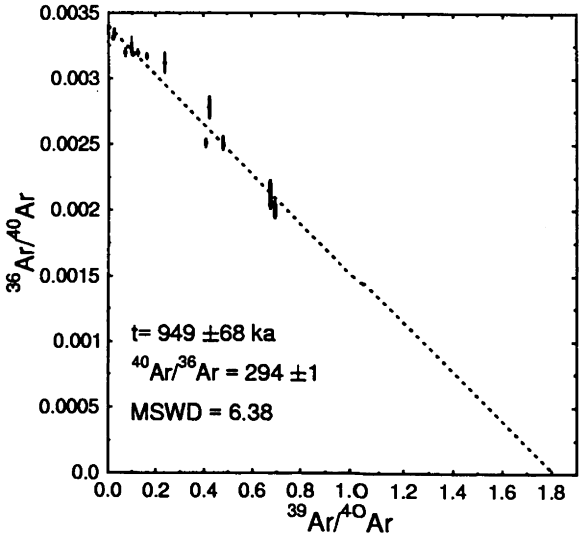
t= 949 ±68 ka
^{40}Ar/^{36}Ar = 294 ±1
MSWD = 6.38
^{36}Ar/^{40}Ar
^{39}Ar/^{40}Ar

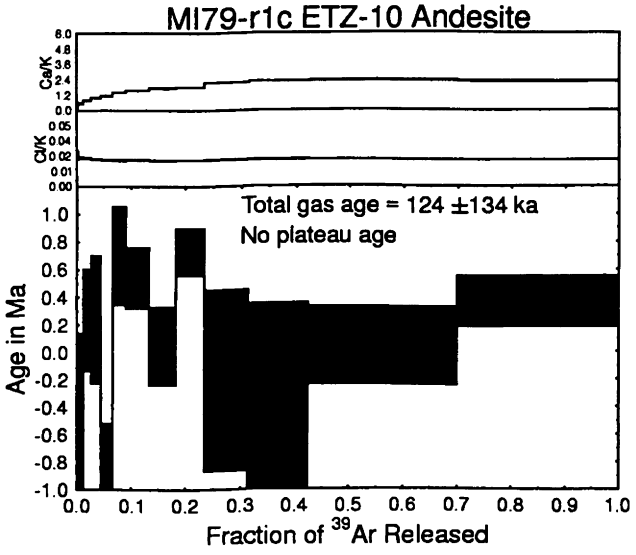
MI79-r1c ETZ-10 Andesite
Ca/K
Cl/K
Total gas age = 124 ±134 ka
No plateau age
Age in Ma
Fraction of ^{39}Ar Released

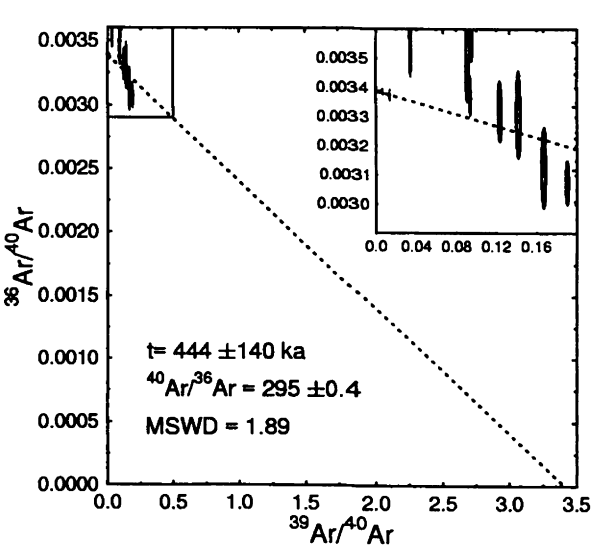
t= 444 ±140 ka
^{40}Ar/^{36}Ar = 295 ±0.4
MSWD = 1.89
^{36}Ar/^{40}Ar
^{39}Ar/^{40}Ar

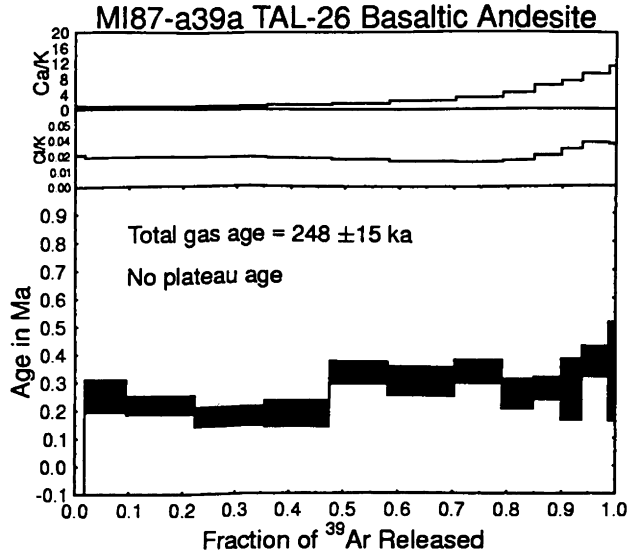
MI87-a39a TAL-26 Basaltic Andesite
Ca/K
Cl/K
Total gas age = 248 ±15 ka
No plateau age
Age in Ma
Fraction of ^{39}Ar Released

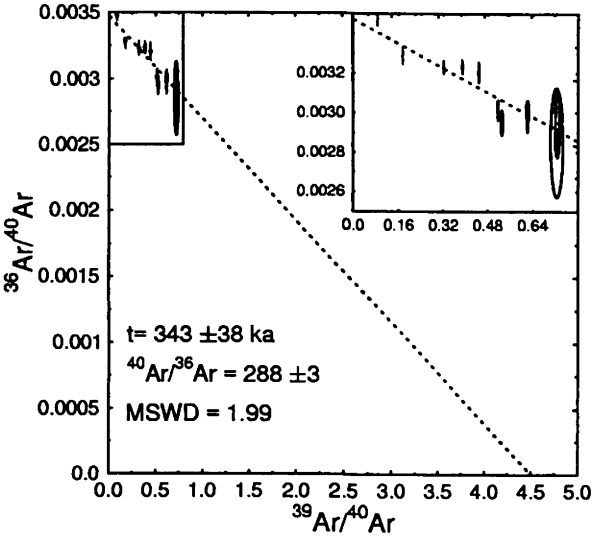
t= 343 ±38 ka
^{40}Ar/^{36}Ar = 288 ±3
MSWD = 1.99
^{36}Ar/^{40}Ar
^{39}Ar/^{40}Ar

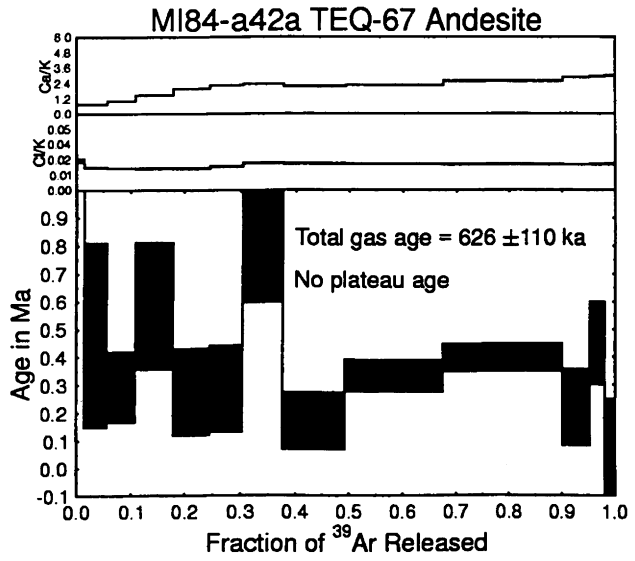
MI84-a42a TEQ-67 Andesite
Ca/K
Cl/K
Total gas age = 626 ±110 ka
No plateau age
Age in Ma
Fraction of ^{39}Ar Released

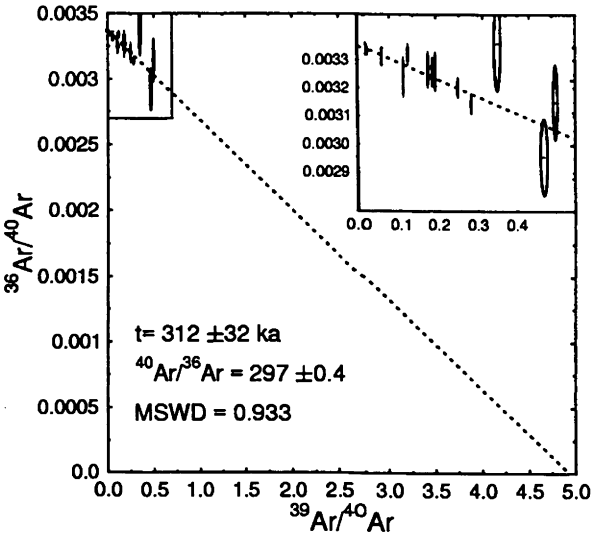
t= 312 ±32 ka
^{40}Ar/^{36}Ar = 297 ±0.4
MSWD = 0.933
^{36}Ar/^{40}Ar
^{39}Ar/^{40}Ar

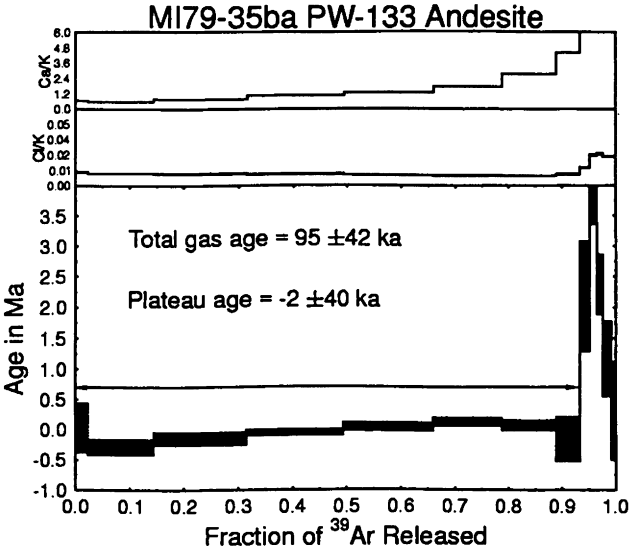
MI79-35ba PW-133 Andesite
Ca/K
Cl/K
Total gas age = 95 ±42 ka
Plateau age = -2 ±40 ka
Age in Ma
Fraction of ^{39}Ar Released

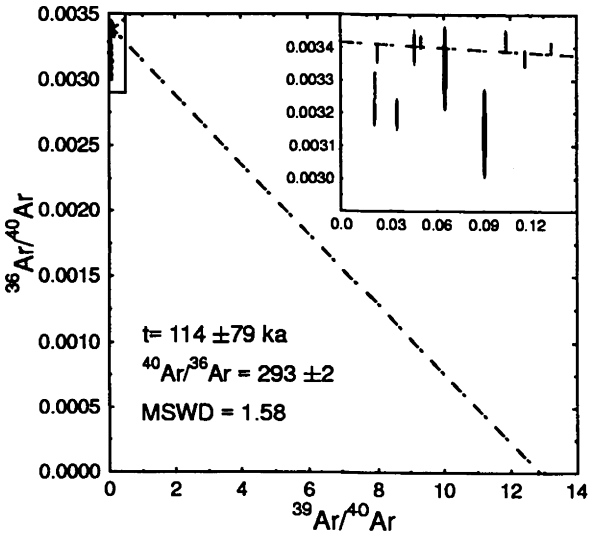
t= 114 ±79 ka
^{40}Ar/^{36}Ar = 293 ±2
MSWD = 1.58
^{36}Ar/^{40}Ar
^{39}Ar/^{40}Ar

MI79-q5b TEQ-9 Andesite (hornblende)

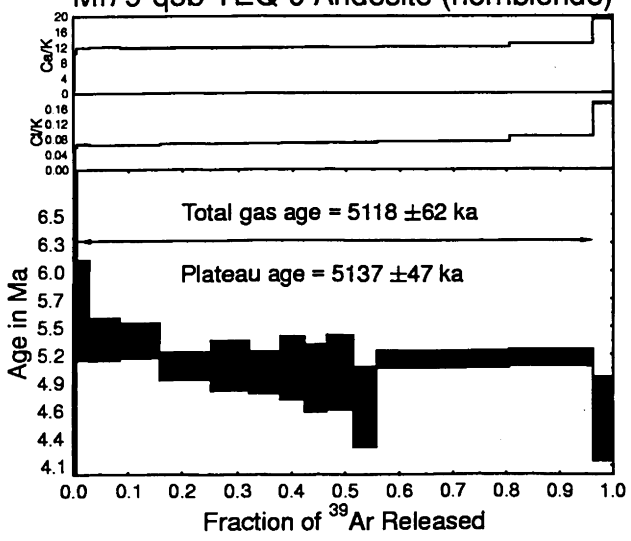

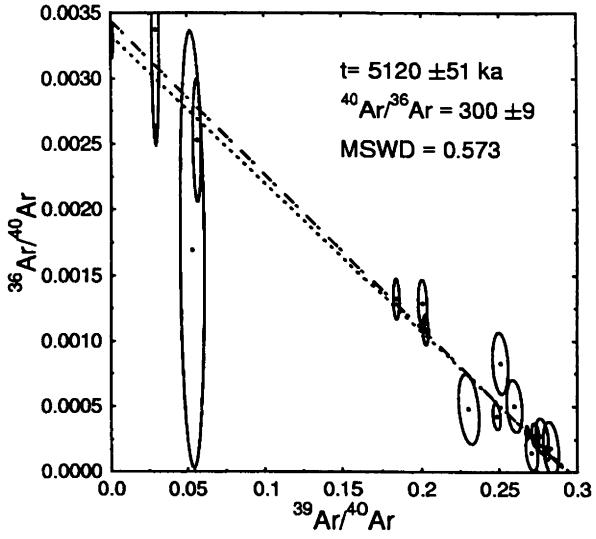

MI84-a46a ETZ-5 Basaltic Andesite

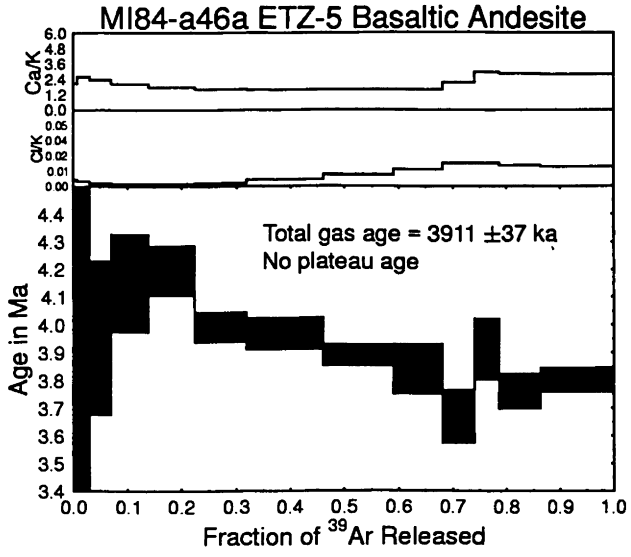

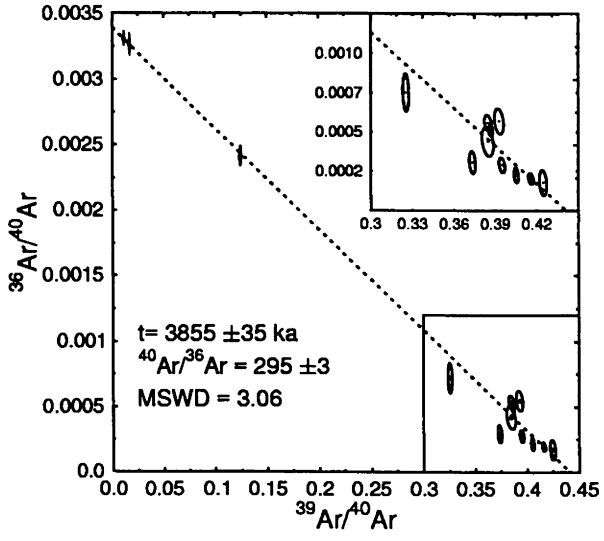

MI84-a29a ETZ-7 Rhyolite

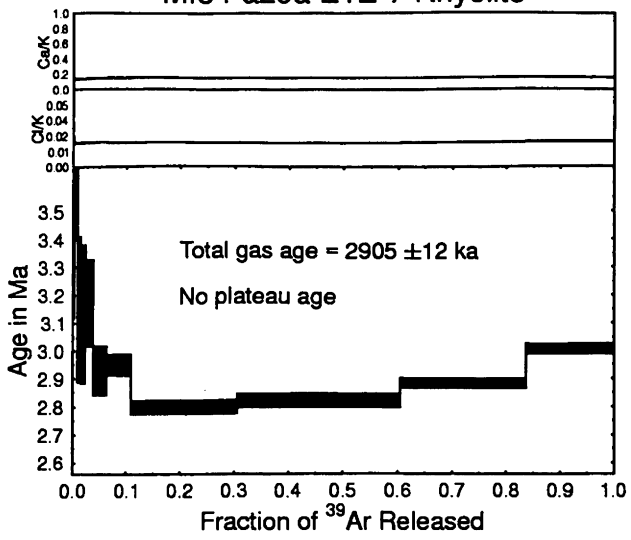

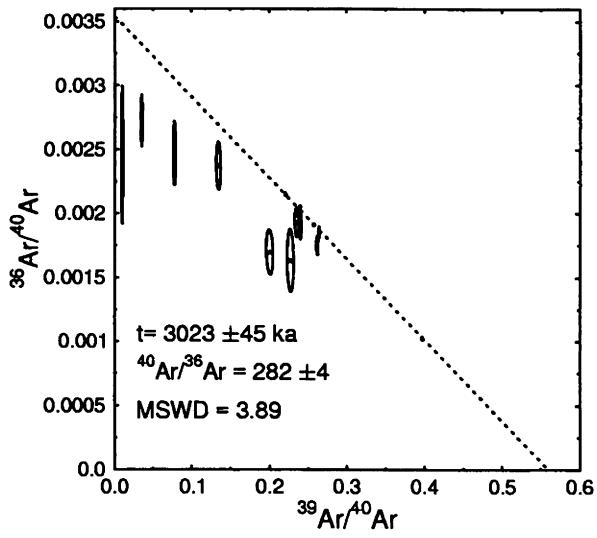

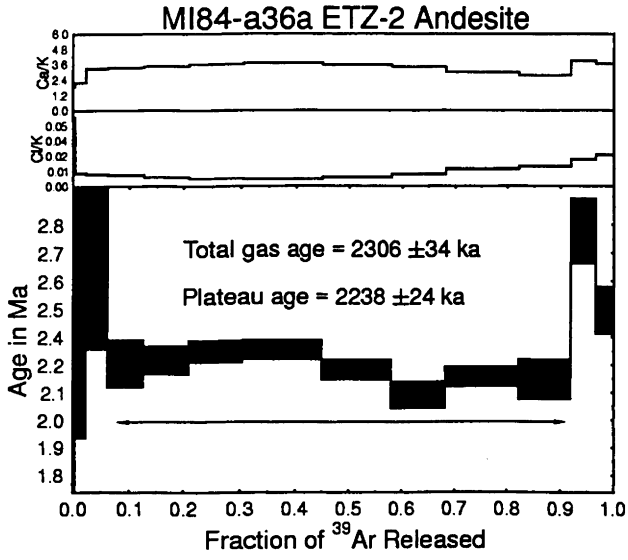
MI84-a36a ETZ-2 Andesite
Ca/K
Cl/K
Total gas age = 2306 ±34 ka
Plateau age = 2238 ±24 ka
Age in Ma
Fraction of ^{39}Ar Released

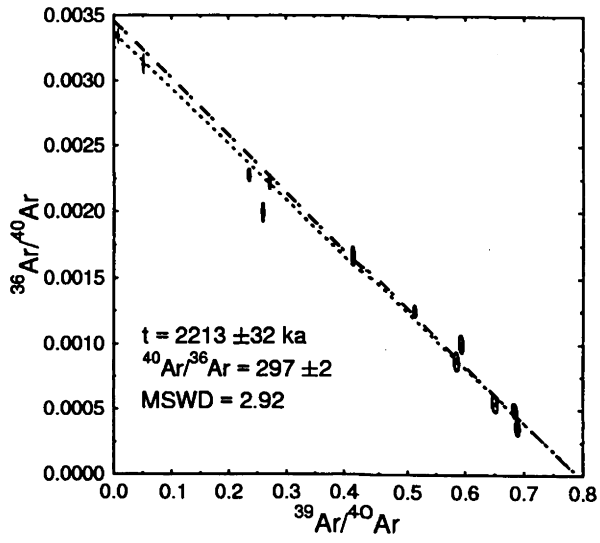
t = 2213 ±32 ka
^{40}Ar/^{36}Ar = 297 ±2
MSWD = 2.92
^{36}Ar/^{40}Ar
^{39}Ar/^{40}Ar

Table DR1. Argon gas fractions released by laser-step heating

mi84-o8a	mass=	0.0023	J=		0.000837154	+/-	1.81004E-06				tot.gas.age=	0.978	+/-	0.283
MI79 O8a TEQ-29	F39	LP(mW)	Vol36	Err36	Vol37	Err37	Vol38	Err38	Vol39	Err39	Vol40	Err40	Age(Ma)	AgeErr
Hornblende	0.0192386	200	22.580	0.142	2.716	0.528	6.154	0.111	12.797	0.200	6667.328	1.162	-0.606	4.962
	0.0350568	400	2.069	0.090	1.401	0.482	2.135	0.049	10.522	0.176	607.617	0.887	-0.547	3.811
	0.0467209	600	1.667	0.079	17.475	0.469	4.935	0.151	7.759	0.158	510.196	1.393	3.405	4.566
	0.2341521	800	1.526	0.106	753.001	1.564	148.782	0.505	124.677	0.486	588.337	0.905	1.665	0.379
	0.4752116	900	1.258	0.072	981.775	2.326	192.513	0.459	160.350	0.564	481.027	1.036	1.030	0.200
	0.6700853	1000	1.024	0.107	794.300	1.537	151.553	0.387	129.628	0.429	394.749	0.894	1.072	0.369
	0.8029691	1100	1.341	0.106	539.621	2.024	100.174	0.283	88.393	0.186	466.322	1.143	1.197	0.534
	0.8749275	1200	0.919	0.081	288.927	1.473	53.287	0.235	47.866	0.240	290.178	1.189	0.586	0.756
	0.9009806	1250	0.845	0.104	105.460	1.175	19.697	0.154	17.330	0.219	249.348	0.864	-0.021	2.667
	0.9230766	1300	0.588	0.120	91.310	0.812	17.336	0.222	14.698	0.270	146.589	0.732	-2.795	3.635
	0.9377899	1350	0.625	0.097	61.725	0.557	11.654	0.139	9.787	0.171	173.554	0.859	-1.729	4.415
	0.9490845	1400	0.504	0.088	48.023	0.461	8.987	0.084	7.513	0.178	169.769	0.952	4.189	5.226
	0.9575614	1450	0.684	0.109	36.404	0.687	6.824	0.140	5.639	0.142	188.880	0.758	-3.568	8.656
	0.961956	1500	0.619	0.103	18.019	0.447	3.447	0.091	2.923	0.123	204.059	0.990	10.966	15.592
	0.9746065	2000	0.380	0.100	51.927	0.749	9.689	0.134	8.415	0.173	122.707	0.749	1.865	5.319
	0.9949	3000	0.997	0.088	82.905	0.844	15.478	0.180	13.499	0.184	314.576	0.823	2.230	2.905
	1	4000	5.947	0.126	18.933	0.386	4.556	0.129	3.392	0.121	1731.456	1.386	-11.544	16.632
mi79-r3a	mass=	0.0116	J=		0.000837593	+/-	1.76662E-06				tot.gas.age=	0.956	+/-	0.048
MI79 R3a ETZ-6	F39	LP(mW)	Vol36	Err36	Vol37	Err37	Vol38	Err38	Vol39	Err39	Vol40	Err40	Age(Ma)	AgeErr
Basalt	0.0140404	100	25.305	0.127	43.100	0.555	28.494	0.114	86.917	0.437	7477.308	2.915	-0.004	0.652
	0.0774814	200	57.946	0.253	221.645	0.497	92.596	0.428	392.729	0.769	17221.550	5.090	0.379	0.289
	0.1774392	300	43.977	0.287	524.438	1.727	125.168	0.370	618.784	1.186	13403.766	5.667	0.998	0.207
	0.2927165	400	38.595	0.232	833.019	2.597	123.663	0.591	713.619	0.872	11772.811	4.942	0.779	0.146
	0.4034912	500	30.639	0.229	1016.939	1.571	95.356	0.390	685.746	0.676	9426.166	3.662	0.820	0.149
	0.5067196	600	24.168	0.170	1075.472	1.669	69.395	0.382	639.031	0.848	7590.649	2.501	1.062	0.119
	0.6437532	800	25.396	0.166	1476.916	2.786	66.535	0.460	848.300	0.818	8107.757	4.304	1.074	0.088
	0.7633795	1000	19.652	0.173	1294.567	2.521	48.715	0.294	740.542	0.826	6272.093	2.760	0.948	0.105
	0.8569173	1200	13.959	0.106	1167.942	2.207	39.256	0.237	579.042	1.386	4589.851	2.417	1.213	0.082
	0.9256528	1600	11.555	0.157	1179.609	1.360	36.179	0.231	425.504	0.832	3809.049	2.181	1.400	0.165
	0.9422088	2000	5.388	0.100	704.220	1.943	16.347	0.128	102.489	0.575	1655.552	0.794	0.935	0.437
	0.9579683	3000	3.532	0.102	802.692	2.239	14.964	0.118	97.559	0.424	1099.770	2.076	0.866	0.466
	1	4000	5.560	0.178	1426.015	2.771	36.874	0.308	260.195	0.363	1816.326	0.852	1.007	0.305
mi84-a48a	mass=	0.015	J=		0.0009979	+/-	1.67966E-06				tot.gas.age=	0.960	+/-	0.042
MI84 A48a TEQ-32	F39	LP(mW)	Vol36	Err36	Vol37	Err37	Vol38	Err38	Vol39	Err39	Vol40	Err40	Age(Ma)	AgeErr
Andesite	0.0033384	100	46.209	0.229	28.092	0.215	14.708	0.238	52.877	0.362	13934.080	7.818	9.483	2.312
	0.0207321	200	42.158	0.131	121.019	0.638	34.769	0.246	275.495	0.616	12602.730	4.568	0.947	0.255
	0.0459074	300	34.191	0.261	201.229	1.162	40.987	0.185	398.747	0.758	10534.827	7.029	1.947	0.349
	0.0779782	400	27.126	0.208	333.500	0.843	46.445	0.270	507.963	0.595	8195.425	2.747	0.637	0.218
	0.1208587	500	65.471	0.214	532.558	1.221	65.599	0.453	679.177	1.371	19723.220	1.056	0.998	0.168
	0.1694682	600	103.682	0.378	690.498	1.925	79.714	0.451	769.917	1.063	31241.652	11.960	1.411	0.262
	0.2532826	800	248.805	0.617	1350.333	2.600	158.633	0.321	1327.519	0.993	74383.582	10.750	1.168	0.248
	0.346744	1000	216.446	0.476	1685.236	2.004	179.531	0.373	1480.318	1.195	64922.916	10.293	1.171	0.171

	0.4363171	1200	126.826	0.473	1741.441	2.409	169.009	0.235	1418.731	0.730	38200.551	7.006	0.918	0.177
	0.6013002	1600	202.201	0.345	3419.326	3.799	304.194	1.057	2613.137	2.396	60980.249	15.239	0.847	0.071
	0.7967386	2000	95.718	0.369	4267.955	3.000	313.501	0.716	3095.511	1.845	29640.560	6.176	0.788	0.063
	0.9491466	3000	32.646	0.272	3551.500	2.942	220.516	0.759	2413.962	2.491	10617.637	3.466	0.724	0.060
	1	4000	10.138	0.123	1250.728	2.146	72.017	0.317	805.457	1.364	3325.044	1.456	0.736	0.081
mi84-a51a	mass=	0.0174	J=		0.0009925	+/-	2.18481E-06				tot.gas.age=	0.617	+/-	0.020
MI84 A51a TEQ-31	F39	LP(mW)	Vol36	Err36	Vol37	Err37	Vol38	Err38	Vol39	Err39	Vol40	Err40	Age(Ma)	AgeErr
Basalt	0.0013096	100	4.844	0.081	1.826	0.556	6.632	0.199	23.964	0.403	1387.933	1.620	-3.260	1.799
	0.0156671	200	15.813	0.175	82.216	0.772	46.009	0.374	262.717	0.669	4669.198	3.359	-0.024	0.353
	0.0480416	300	11.937	0.101	337.286	1.284	89.082	0.195	592.394	0.667	3601.469	2.938	0.224	0.090
	0.0940061	400	8.071	0.125	700.702	1.149	113.894	0.459	841.068	1.282	2588.479	2.014	0.433	0.079
	0.1522236	500	7.022	0.156	1087.546	0.990	124.039	0.485	1065.275	1.874	2396.853	2.868	0.541	0.077
	0.2142983	600	5.692	0.149	1327.963	3.504	112.590	0.288	1135.856	0.745	2129.579	1.504	0.705	0.070
	0.3207307	800	7.160	0.216	2707.739	2.333	141.676	0.418	1947.522	1.265	2968.186	3.242	0.784	0.059
	0.440228	1000	7.552	0.207	3092.855	3.108	129.825	0.527	2186.585	1.854	3093.080	2.121	0.705	0.050
	0.5477137	1200	7.578	0.137	2788.309	3.023	107.936	0.421	1966.796	2.581	3048.304	2.431	0.736	0.037
	0.6650692	1600	12.717	0.162	3181.239	4.822	120.031	0.352	2147.394	1.865	4580.168	2.540	0.686	0.040
	0.7378715	2000	13.411	0.193	1959.836	2.245	83.068	0.299	1332.153	1.339	4420.779	3.940	0.615	0.077
	0.7888613	3000	13.914	0.206	1567.315	2.590	72.514	0.324	933.021	1.390	4335.025	3.086	0.429	0.117
	0.8322344	4000	15.373	0.160	1350.516	1.807	88.383	0.277	793.651	0.825	4755.286	2.957	0.479	0.107
	1	4010	59.795	0.386	4710.236	3.525	362.456	1.073	3069.808	2.753	18739.787	5.661	0.624	0.067
mi87-a35a	mass=	0.0103	J=		0.000857262	+/-	2.50221E-06				tot.gas.age=	0.616	+/-	0.029
MI87 a35a TEQ-38	F39	LP(mW)	Vol36	Err36	Vol37	Err37	Vol38	Err38	Vol39	Err39	Vol40	Err40	Age(Ma)	AgeErr
Andesite	0.0161917	100	39.535	0.289	305.982	1.302	46.335	0.278	222.939	0.429	11927.073	6.384	1.695	0.593
	0.0774638	200	36.805	0.145	493.360	1.638	125.948	0.455	843.641	0.751	11117.092	3.445	0.442	0.079
	0.1749589	300	34.066	0.325	693.540	1.916	173.368	0.486	1342.384	1.466	10383.780	4.933	0.366	0.111
	0.2922338	400	33.730	0.277	938.597	1.527	186.852	0.569	1614.728	1.736	10325.361	2.864	0.343	0.078
	0.4220862	500	31.560	0.189	1215.965	2.344	191.357	0.846	1787.905	1.401	10092.837	2.167	0.663	0.048
	0.5510925	600	28.903	0.280	1399.266	2.643	169.048	0.490	1776.255	1.678	9302.400	3.359	0.663	0.072
	0.7015847	800	31.466	0.312	2087.832	2.784	163.706	0.687	2072.089	1.184	10094.830	2.470	0.595	0.069
	0.7912139	1000	19.965	0.183	1570.164	2.909	83.621	0.269	1234.081	0.717	6469.377	3.469	0.714	0.068
	0.8362524	1200	13.649	0.141	922.033	1.935	43.264	0.397	620.124	0.957	4287.845	2.844	0.635	0.104
	0.8925624	1600	24.594	0.341	1274.845	2.676	76.041	0.377	775.318	1.069	7580.810	2.739	0.625	0.201
	0.939913	2000	25.858	0.147	1422.736	1.256	67.853	0.329	651.958	1.297	8034.360	3.155	0.933	0.103
	0.9808782	3000	25.897	0.244	1819.925	1.605	59.828	0.314	564.040	0.798	8007.024	4.779	0.972	0.198
	1	4000	14.656	0.148	986.781	1.847	26.347	0.145	263.283	0.865	4440.524	3.173	0.644	0.257
mi87-a34a	mass=	0.0124	J=		0.000836676	+/-	1.62662E-06				tot.gas.age=	0.700	+/-	0.021
MI87 a34a TEQ-10	F39	LP(mW)	Vol36	Err36	Vol37	Err37	Vol38	Err38	Vol39	Err39	Vol40	Err40	Age(Ma)	AgeErr
Basalt	0.0014607	100	10.558	0.196	26.142	0.289	3.730	0.126	11.217	0.194	3166.458	1.618	6.248	7.761
	0.0087443	200	14.200	0.121	140.892	0.965	4.258	0.139	55.932	0.188	4262.128	2.995	1.780	0.970
	0.0390192	300	1.357	0.104	571.942	1.836	2.096	0.114	232.484	0.387	524.756	1.080	0.803	0.199
	0.1020997	400	1.209	0.107	1027.878	1.902	2.319	0.152	484.402	0.780	586.350	1.210	0.714	0.099
	0.1941262	500	1.061	0.074	1353.235	2.678	2.804	0.225	706.683	1.079	591.280	1.195	0.593	0.047
	0.3093029	600	0.609	0.074	1467.243	2.220	3.315	0.184	884.455	0.526	594.906	1.267	0.708	0.037
	0.5081206	800	0.883	0.077	2075.619	1.389	8.652	0.311	1526.745	1.358	941.523	1.248	0.673	0.022
	0.6927808	1000	0.843	0.037	1717.993	2.117	14.620	0.194	1418.027	1.068	894.526	0.902	0.687	0.012

	0.8164317	1200	1.038	0.054	1218.887	2.048	19.694	0.286	949.530	0.785	700.457	1.027	0.626	0.025
	0.9024076	1600	2.514	0.067	1497.276	1.630	44.115	0.285	660.219	1.092	991.246	1.603	0.568	0.045
	0.9343301	2000	2.740	0.075	2062.722	2.213	57.142	0.395	245.137	0.949	966.583	1.349	0.967	0.137
	0.969572	3000	5.445	0.118	4307.627	5.088	93.589	0.518	270.627	0.384	1756.606	1.488	0.823	0.194
	1	4000	3.475	0.118	3002.823	4.007	77.627	0.359	233.660	0.650	1156.095	2.082	0.835	0.226
mi84-a35a	mass=	0.011	J=		0.000939816	+/-	1.75102E-06				tot.gas.age=	0.634	+/-	0.008
MI84 A35a TEQ-18	F39	LP(mW)	Vol36	Err36	Vol37	Err37	Vol38	Err38	Vol39	Err39	Vol40	Err40	Age(Ma)	AgeErr
Rhyolite	0.0001246	100	2.271	0.111	0.367	0.208	1.010	0.088	2.806	0.150	640.878	1.422	-18.305	20.124
	0.0010339	200	0.950	0.065	1.092	0.287	3.784	0.140	20.476	0.164	277.992	0.734	-0.237	1.587
	0.0037053	300	0.992	0.078	2.416	0.142	9.228	0.140	60.150	0.477	286.531	1.111	-0.184	0.651
	0.0081928	400	0.316	0.069	3.795	0.234	14.324	0.200	101.043	0.311	139.490	1.043	0.772	0.344
	0.014416	500	0.098	0.071	5.063	0.210	20.657	0.253	140.127	0.468	94.174	0.836	0.791	0.252
	0.0225755	600	-0.090	0.063	6.344	0.180	26.557	0.126	183.727	0.548	99.632	0.678	1.164	0.171
	0.039361	800	0.373	0.085	12.955	0.253	54.138	0.304	377.953	0.422	188.820	1.128	0.353	0.113
	0.0629881	1000	0.069	0.069	18.157	0.357	75.481	0.215	532.007	1.266	233.749	1.084	0.680	0.065
	0.0847918	1200	0.140	0.075	17.374	0.282	70.126	0.365	490.948	0.892	208.287	1.140	0.577	0.076
	0.1163122	1600	0.111	0.087	24.910	0.194	100.433	0.302	709.737	0.945	304.642	0.867	0.649	0.062
	0.1601318	2000	0.232	0.150	34.681	0.378	139.338	0.609	986.675	1.490	403.076	1.252	0.575	0.076
	0.5259336	3000	0.328	0.150	290.156	0.872	1161.095	1.514	8236.666	1.986	3216.525	1.850	0.642	0.009
	1	4000	1.049	0.156	370.782	1.014	1511.493	0.829	10674.430	4.908	4351.374	3.897	0.642	0.007
mi84-a40a	mass=	0.0149	J=		0.000983664	+/-	2.2425E-06				tot.gas.age=	0.612	+/-	0.012
MI84 A40a TEQ-35	F39	LP(mW)	Vol36	Err36	Vol37	Err37	Vol38	Err38	Vol39	Err39	Vol40	Err40	Age(Ma)	AgeErr
Rhyolite	0.0001113	100	0.436	0.082	-0.165	0.099	0.338	0.092	1.866	0.109	140.510	0.546	11.083	22.988
	0.0014425	200	0.786	0.061	0.620	0.179	3.792	0.115	22.328	0.185	268.178	0.546	2.858	1.442
	0.004849	300	0.887	0.077	2.086	0.155	8.018	0.122	57.136	0.351	218.577	0.733	-1.349	0.709
	0.0109053	400	0.369	0.087	3.600	0.165	13.914	0.140	101.581	0.277	144.026	0.933	0.613	0.447
	0.0195119	500	0.332	0.170	4.371	0.286	18.947	0.167	144.357	0.341	99.598	0.772	0.019	0.619
	0.0305928	600	0.310	0.098	6.018	0.217	24.417	0.173	185.856	0.540	90.295	0.560	-0.011	0.276
	0.0533635	800	0.191	0.082	13.073	0.318	50.949	0.337	381.927	0.636	159.115	0.753	0.477	0.113
	0.0886436	1000	0.127	0.083	20.375	0.210	78.342	0.207	591.745	0.677	228.280	0.979	0.572	0.073
	0.1341521	1200	0.156	0.097	26.494	0.338	103.704	0.369	763.303	1.849	293.002	1.081	0.574	0.067
	0.2140663	1600	0.062	0.089	46.141	0.462	178.814	0.545	1340.383	1.643	500.650	0.706	0.639	0.035
	0.3293037	2000	-0.016	0.106	67.295	0.603	258.268	0.723	1932.848	1.886	713.934	1.632	0.660	0.029
	0.7066397	3000	0.859	0.108	219.537	1.122	835.579	1.003	6328.967	1.843	2505.330	1.954	0.631	0.009
	1	4000	3.057	0.174	171.026	0.878	650.717	1.145	4920.461	3.207	2659.394	3.125	0.633	0.019
mi84-a41a	mass=	0.0141	J=		0.000939816	+/-	1.75102E-06				tot.gas.age=	0.642	+/-	0.006
MI84 A41a ETZ-4	F39	LP(mW)	Vol36	Err36	Vol37	Err37	Vol38	Err38	Vol39	Err39	Vol40	Err40	Age(Ma)	AgeErr
Dacite	0.0001932	100	1.330	0.063	0.560	0.155	1.095	0.056	7.354	0.144	391.271	0.804	-0.396	4.279
	0.0030766	200	2.525	0.109	10.763	0.212	11.557	0.151	109.783	0.530	820.979	1.458	1.156	0.495
	0.0113052	300	8.377	0.122	31.527	0.347	23.013	0.205	313.289	0.475	2655.846	1.682	0.977	0.196
	0.0263248	400	1.408	0.064	55.160	0.502	33.307	0.208	571.842	1.124	677.443	1.355	0.775	0.056
	0.0470353	500	2.750	0.081	83.831	0.488	54.179	0.343	788.513	0.894	1136.876	1.788	0.697	0.051
	0.0752274	600	6.319	0.165	130.035	0.525	88.271	0.420	1073.362	0.859	2221.684	1.767	0.560	0.077
	0.1718942	800	5.699	0.152	467.533	0.527	325.085	0.587	3680.411	2.689	3082.076	1.369	0.644	0.021
	0.319228	1000	3.603	0.154	722.756	1.330	500.131	0.853	5609.459	2.620	3159.296	2.241	0.633	0.014
	0.4899799	1200	3.064	0.085	866.436	2.101	580.161	0.903	6501.062	2.282	3348.909	2.882	0.637	0.007

	0.7070199	1600	4.181	0.077	1142.848	2.145	736.490	1.361	8263.397	4.076	4314.699	2.207	0.632	0.005
	0.8726051	2000	24.984	0.133	779.820	1.801	547.871	0.622	6304.347	4.300	9706.759	2.805	0.625	0.011
	0.9699597	3000	1.749	0.100	505.729	0.591	328.484	0.639	3706.597	2.464	1959.019	1.956	0.660	0.014
	1	4000	0.711	0.107	172.443	0.695	99.815	0.406	1143.729	1.927	653.779	1.863	0.658	0.047
mi79-a54a	mass=	0.0108	J=		0.000968366	+/-	3.13304E-06				tot.gas.age=	0.615	+/-	0.005
MI84 A54a TEQ-21A	F39	LP(mW)	Vol36	Err36	Vol37	Err37	Vol38	Err38	Vol39	Err39	Vol40	Err40	Age(Ma)	AgeErr
Rhyolite	0.0005461	100	0.773	0.078	0.487	0.223	2.204	0.119	18.587	0.277	247.305	0.652	1.785	2.167
	0.0032383	200	0.868	0.095	3.344	0.194	11.443	0.187	91.634	0.565	305.145	0.892	0.930	0.534
	0.0082347	300	0.403	0.072	5.764	0.203	20.401	0.146	170.059	0.486	185.648	0.625	0.685	0.218
	0.0153334	400	0.207	0.092	9.104	0.271	29.162	0.264	241.613	0.527	124.575	0.692	0.459	0.197
	0.0247344	500	0.011	0.070	12.006	0.258	38.751	0.352	319.976	0.507	132.035	0.528	0.703	0.114
	0.0378537	600	0.217	0.095	16.041	0.298	54.229	0.354	446.532	0.767	174.321	1.008	0.431	0.110
	0.0617758	800	0.062	0.082	30.281	0.218	97.191	0.369	814.224	1.840	308.479	0.496	0.623	0.052
	0.0896273	1000	0.174	0.061	37.002	0.395	113.040	0.582	947.961	1.347	354.855	0.803	0.559	0.033
	0.1197296	1200	0.189	0.097	41.734	0.275	121.263	0.341	1024.574	1.079	379.841	0.597	0.552	0.049
	0.1631742	1600	0.262	0.049	74.566	0.477	175.376	0.573	1478.695	1.701	549.087	0.848	0.557	0.017
	0.3331653	2000	0.066	0.100	261.744	0.972	689.732	1.024	5785.877	2.700	2082.940	2.269	0.623	0.009
	0.9267588	3000	0.151	0.105	881.750	1.048	2399.527	2.318	20203.762	7.243	7242.384	1.422	0.622	0.003
	1	4000	0.070	0.123	108.447	0.446	294.498	0.798	2492.863	2.743	922.131	0.985	0.632	0.025
mi79-a56a	mass=	0.0128	J=		0.000968366	+/-	3.13304E-06				tot.gas.age=	0.624	+/-	0.010
MI84 A56a ETZ-11	F39	LP(mW)	Vol36	Err36	Vol37	Err37	Vol38	Err38	Vol39	Err39	Vol40	Err40	Age(Ma)	AgeErr
Dacite	0.0008331	100	1.086	0.099	1.999	0.237	2.397	0.092	16.658	0.272	316.905	0.819	-0.426	3.060
	0.0048023	200	1.399	0.072	10.243	0.474	10.413	0.131	79.367	0.437	443.761	1.070	0.667	0.468
	0.0119609	300	1.331	0.065	23.345	0.268	17.081	0.162	143.139	0.262	434.671	1.057	0.504	0.234
	0.0221969	400	1.177	0.098	37.791	0.317	22.288	0.173	204.676	0.403	415.044	0.953	0.573	0.247
	0.0355329	500	1.027	0.079	54.979	0.409	26.580	0.269	266.659	0.874	405.927	0.984	0.671	0.152
	0.0535729	600	1.124	0.102	83.134	0.473	32.978	0.198	360.722	0.676	468.458	0.696	0.660	0.146
	0.0849358	800	1.675	0.093	174.668	0.509	54.999	0.244	627.118	1.061	731.750	1.439	0.660	0.077
	0.1209284	1000	1.714	0.099	219.304	0.568	64.248	0.344	719.694	0.969	794.051	0.933	0.698	0.071
	0.1592147	1200	1.814	0.086	246.941	0.624	68.120	0.405	765.556	0.584	833.489	1.318	0.678	0.058
	0.2444891	1600	5.243	0.142	585.180	1.472	154.084	0.383	1705.110	2.277	2141.810	1.760	0.607	0.043
	0.5628492	2000	15.816	0.136	2104.812	2.341	585.126	0.909	6365.794	3.886	6893.545	4.894	0.609	0.011
	0.8531395	3000	9.632	0.170	1910.611	2.386	531.191	0.565	5804.520	3.616	4963.482	2.074	0.637	0.015
	1	4000	5.906	0.104	958.212	1.889	268.476	0.897	2936.560	1.444	2768.530	1.435	0.609	0.018
mi87-a26a	mass=	0.0122	J=		0.000830131	+/-	2.50866E-06				tot.gas.age=	0.603	+/-	0.006
MI87 a26a TEQ-45b	F39	LP(mW)	Vol36	Err36	Vol37	Err37	Vol38	Err38	Vol39	Err39	Vol40	Err40	Age(Ma)	AgeErr
Rhyolite	0.000194	100	0.518	0.068	0.289	0.160	1.133	0.082	5.613	0.135	142.312	0.989	-2.847	5.377
	0.0015613	200	0.801	0.070	1.217	0.218	6.494	0.067	39.551	0.286	248.585	0.993	0.450	0.779
	0.0046632	300	0.761	0.079	4.063	0.250	13.595	0.184	89.730	0.341	234.524	1.009	0.160	0.388
	0.0095631	400	0.458	0.077	4.354	0.209	20.851	0.242	141.742	0.622	191.291	1.158	0.591	0.241
	0.0161359	500	0.347	0.078	7.292	0.271	28.412	0.289	190.134	0.664	158.914	1.031	0.444	0.183
	0.0241112	600	0.126	0.067	7.849	0.169	33.592	0.350	230.704	0.522	154.559	0.700	0.761	0.129
	0.0415419	800	0.241	0.081	17.487	0.241	74.965	0.375	504.223	0.987	253.674	1.055	0.542	0.071
	0.0688748	1000	0.098	0.081	34.891	0.244	117.697	0.423	790.667	1.407	349.153	1.422	0.607	0.045
	0.1007605	1200	0.054	0.080	31.957	0.374	137.489	0.693	922.369	1.076	395.879	1.347	0.617	0.038
	0.1488839	1600	0.151	0.063	50.515	0.411	206.516	0.584	1392.084	0.717	588.069	0.979	0.584	0.020

	0.2410459	2000	0.079	0.101	98.243	0.728	397.847	0.568	2666.003	1.095	1102.746	1.619	0.606	0.017
	0.6971469	3000	70.695	0.292	481.481	1.222	1973.894	2.043	13193.790	2.512	26257.536	4.411	0.609	0.010
	1	4000	0.568	0.072	316.389	0.970	1289.227	1.655	8760.737	4.061	3700.580	2.767	0.604	0.004
mi79-r0a	mass=	0.0107	J=		0.000839751	+/-	1.68865E-06				tot.gas.age=	0.631	+/-	0.027
MI79 R0a TEQ-12	F39	LP(mW)	Vol36	Err36	Vol37	Err37	Vol38	Err38	Vol39	Err39	Vol40	Err40	Age(Ma)	AgeErr
Basalt	0.0044103	100	5.248	0.136	54.823	0.497	6.178	0.087	25.667	0.230	1584.051	2.449	1.961	2.370
	0.0364064	200	1.898	0.110	498.629	0.911	2.953	0.105	186.212	0.698	661.033	0.827	0.815	0.265
	0.1326473	300	1.887	0.101	1241.607	1.471	2.378	0.172	560.105	1.243	752.042	1.423	0.526	0.081
	0.264999	400	1.415	0.098	1457.117	1.472	2.553	0.150	770.263	0.581	717.608	1.302	0.589	0.057
	0.4092266	500	0.916	0.078	1363.788	2.454	3.358	0.243	839.379	1.450	609.104	1.288	0.611	0.041
	0.5532601	600	0.706	0.076	1151.573	1.715	4.748	0.218	838.249	1.429	536.059	1.164	0.592	0.041
	0.7215182	800	0.982	0.092	1250.987	1.957	12.019	0.160	979.232	1.091	683.942	1.227	0.609	0.042
	0.8313186	1000	1.317	0.086	941.017	1.458	18.937	0.238	639.018	0.787	621.841	0.803	0.551	0.060
	0.8895238	1200	1.678	0.104	837.317	1.687	23.320	0.207	338.744	0.805	623.774	1.465	0.573	0.137
	0.9158993	1600	3.167	0.084	1783.436	1.843	30.890	0.285	153.501	0.552	992.860	1.300	0.563	0.244
	0.9352668	2000	2.272	0.087	1535.396	1.547	25.435	0.192	112.715	0.202	747.638	1.339	1.024	0.345
	0.9694429	3000	3.418	0.097	2504.643	2.318	42.024	0.219	198.899	0.335	1158.969	1.474	1.134	0.218
	1	4000	2.594	0.102	2159.412	2.319	37.048	0.264	177.837	0.604	861.354	1.053	0.807	0.256
mi79-y0a	mass=	0.0085	J=		0.000838121	+/-	1.58795E-06				tot.gas.age=	0.458	+/-	0.036
MI79 Y0a TAL-12	F39	LP(mW)	Vol36	Err36	Vol37	Err37	Vol38	Err38	Vol39	Err39	Vol40	Err40	Age(Ma)	AgeErr
Andesite	0.0022118	100	0.742	0.108	3.031	0.162	2.992	0.075	9.449	0.122	211.222	0.913	-1.282	5.117
	0.0110203	200	0.620	0.085	14.101	0.377	5.152	0.135	37.632	0.205	164.594	0.848	-0.742	1.015
	0.0259894	300	0.327	0.115	27.926	0.482	5.901	0.137	63.952	0.332	127.216	0.986	0.727	0.800
	0.0460691	400	0.152	0.102	47.671	0.474	7.313	0.109	85.786	0.368	80.407	0.749	0.625	0.530
	0.0721045	500	0.137	0.057	73.241	0.955	9.198	0.127	111.230	0.414	103.804	0.441	0.859	0.228
	0.1044335	600	0.142	0.087	101.408	1.082	11.535	0.144	138.118	0.523	96.320	0.716	0.595	0.280
	0.156746	800	0.181	0.066	177.638	1.396	18.372	0.092	223.493	0.284	124.107	0.883	0.477	0.131
	0.2172897	1000	0.251	0.072	213.666	1.146	21.558	0.136	258.658	0.473	122.058	1.925	0.279	0.124
	0.2801379	1200	0.182	0.101	223.406	1.118	22.118	0.182	268.504	0.345	127.057	0.565	0.412	0.167
	0.4130333	1600	4.754	0.078	510.086	1.121	47.058	0.324	567.764	1.144	1526.656	1.423	0.324	0.061
	0.5651183	2000	0.813	0.110	612.253	2.572	52.972	0.280	649.747	1.434	442.183	1.008	0.470	0.075
	0.8195265	3000	0.548	0.129	1409.318	2.672	158.324	0.714	1086.899	1.478	510.214	0.871	0.485	0.053
	1	4000	0.139	0.090	739.440	2.626	64.084	0.215	771.030	0.964	314.833	1.154	0.537	0.052
mi79-r5b	mass=	0.0087	J=		0.000836499	+/-	1.71734E-06				tot.gas.age=	0.429	+/-	0.025
MI79 R5b TEQ-37	F39	LP(mW)	Vol36	Err36	Vol37	Err37	Vol38	Err38	Vol39	Err39	Vol40	Err40	Age(Ma)	AgeErr
Basaltic Andesite	0.026637	100	21.377	0.170	85.726	1.909	24.877	0.207	212.282	0.658	6414.348	3.101	0.693	0.357
	0.1018907	200	13.416	0.077	221.674	1.972	56.787	0.242	599.731	0.220	4141.957	3.061	0.447	0.058
	0.1960685	300	9.041	0.115	365.858	3.718	64.779	0.247	750.545	1.432	2909.051	2.452	0.477	0.068
	0.2930997	400	8.020	0.137	515.695	2.507	62.661	0.320	773.286	1.096	2494.499	2.586	0.243	0.079
	0.3942452	500	6.525	0.120	688.009	2.306	61.980	0.359	806.074	0.890	2153.529	2.345	0.422	0.067
	0.4936182	600	5.850	0.135	817.770	1.943	61.424	0.417	791.948	1.291	1969.430	1.655	0.459	0.076
	0.6135214	800	6.631	0.137	1284.386	4.521	79.483	0.295	955.563	0.810	2201.125	1.149	0.381	0.064
	0.7025346	1000	4.982	0.076	1161.652	4.520	69.547	0.169	709.386	1.198	1663.224	0.762	0.406	0.048
	0.7580392	1200	3.602	0.072	778.485	2.119	47.599	0.289	442.341	0.796	1172.556	2.145	0.369	0.073
	0.8205644	1600	10.391	0.068	875.668	3.438	51.061	0.226	498.291	0.426	3245.138	2.618	0.528	0.061
	0.8704536	2000	8.144	0.138	780.409	3.702	39.912	0.299	397.590	0.422	2559.474	2.446	0.580	0.155

	0.950914	3000	8.307	0.189	1501.243	6.217	63.912	0.350	641.226	0.770	2624.910	2.777	0.401	0.131
	1	4000	8.107	0.094	1025.419	2.103	37.281	0.322	391.188	0.345	2518.878	1.412	0.476	0.107
mi84-a47a	mass=	0.0096	J=		0.000941998	+/-	1.39749E-06				tot.gas.age=	0.420	+/-	0.007
MI84 A47a TEQ-22	F39	LP(mW)	Vol36	Err36	Vol37	Err37	Vol38	Err38	Vol39	Err39	Vol40	Err40	Age(Ma)	AgeErr
Rhyolite	0.0002862	100	0.083	0.082	0.206	0.147	1.108	0.132	6.868	0.187	34.609	0.613	2.519	5.978
	0.0021479	200	0.148	0.087	2.167	0.145	5.060	0.147	44.678	0.367	51.818	0.555	0.313	0.974
	0.0061488	300	0.160	0.140	4.360	0.215	9.869	0.174	96.015	0.315	44.394	0.512	-0.051	0.731
	0.0118473	400	0.105	0.094	6.517	0.198	14.647	0.212	136.754	0.561	45.549	0.402	0.179	0.345
	0.0195362	500	-0.052	0.073	9.125	0.207	19.256	0.161	184.522	0.693	52.801	0.415	0.628	0.198
	0.0292705	600	0.024	0.100	11.698	0.264	24.455	0.345	233.608	0.763	72.087	0.513	0.472	0.215
	0.0487795	800	0.042	0.117	23.839	0.275	48.510	0.305	468.184	0.851	131.358	0.401	0.431	0.125
	0.0762979	1000	0.008	0.095	34.002	0.357	68.430	0.316	660.396	1.021	179.560	0.852	0.456	0.072
	0.1062456	1200	-0.215	0.118	37.470	0.397	74.722	0.174	718.698	0.885	192.750	0.894	0.606	0.083
	0.1515385	1600	0.214	0.099	64.388	0.386	111.025	0.440	1086.956	1.022	322.357	0.979	0.405	0.046
	0.3347902	2000	0.167	0.074	260.363	1.129	453.344	0.897	4397.743	3.714	1087.739	1.169	0.401	0.009
	0.8582857	3000	0.127	0.070	734.236	1.182	1287.666	1.830	12563.042	4.652	3121.625	2.204	0.417	0.003
	1	4000	0.224	0.084	196.747	0.810	347.738	0.644	3400.914	2.589	906.185	1.487	0.420	0.012
mi84-q4a	mass=	0.0079	J=		0.000839038	+/-	1.49528E-06				tot.gas.age=	0.375	+/-	0.024
MI79 Q4a TAL-9	F39	LP(mW)	Vol36	Err36	Vol37	Err37	Vol38	Err38	Vol39	Err39	Vol40	Err40	Age(Ma)	AgeErr
Dacite	0.0042574	100	31.761	0.211	6.192	0.134	43.222	0.250	34.215	0.257	9518.549	3.238	5.879	2.757
	0.0167725	200	3.475	0.173	21.058	0.355	35.248	0.145	100.578	0.365	1006.655	1.201	-0.306	0.770
	0.0347921	300	0.430	0.066	35.587	0.279	15.573	0.158	144.815	0.494	130.781	0.832	0.038	0.206
	0.0589357	400	0.170	0.082	56.319	0.494	13.601	0.203	194.031	0.486	98.661	0.905	0.378	0.190
	0.0896917	500	0.439	0.078	86.704	0.675	17.015	0.167	247.171	0.513	102.491	0.868	-0.167	0.141
	0.1254665	600	0.280	0.125	113.528	0.513	19.160	0.209	287.505	0.812	96.938	0.763	0.075	0.195
	0.1747558	800	0.086	0.108	176.112	0.848	27.197	0.211	396.115	0.694	129.251	0.591	0.397	0.121
	0.2288146	1000	0.135	0.130	200.322	0.757	29.492	0.336	434.445	0.551	170.838	0.734	0.456	0.134
	0.2969258	1200	0.649	0.108	286.753	0.628	38.099	0.220	547.377	0.390	288.260	0.777	0.267	0.088
	0.5317201	1600	0.488	0.123	1004.664	1.779	130.222	0.511	1886.930	1.887	604.909	1.262	0.370	0.029
	0.7354918	2000	-0.127	0.095	791.955	1.478	111.613	0.408	1637.616	0.559	432.732	0.523	0.434	0.026
	0.9080867	3000	-0.020	0.091	649.192	1.287	92.967	0.446	1387.063	1.144	370.249	1.000	0.410	0.029
	1	4000	0.056	0.097	306.339	1.101	48.979	0.410	738.663	1.179	218.217	1.046	0.413	0.059
mi87-a44a	mass=	0.0108	J=		0.000828743	+/-	2.57006E-06				tot.gas.age=	0.378	+/-	0.007
MI87 a44a TEQ-66	F39	LP(mW)	Vol36	Err36	Vol37	Err37	Vol38	Err38	Vol39	Err39	Vol40	Err40	Age(Ma)	AgeErr
Dacite	0.00097	100	0.952	0.103	2.209	0.253	3.369	0.114	20.146	0.222	258.488	0.444	-1.692	2.251
	0.0052956	200	0.604	0.098	8.410	0.306	6.737	0.124	89.833	0.548	189.616	0.595	0.185	0.483
	0.0128424	300	0.456	0.085	17.120	0.314	9.990	0.116	156.733	0.618	144.269	0.712	0.091	0.240
	0.0231417	400	0.308	0.092	27.231	0.417	12.907	0.076	213.899	0.699	115.162	0.825	0.169	0.190
	0.035797	500	0.124	0.091	39.544	0.457	15.587	0.180	262.825	0.664	101.598	0.530	0.369	0.152
	0.0509338	600	0.176	0.086	54.595	0.416	18.986	0.139	314.364	0.618	110.051	0.515	0.275	0.121
	0.0788738	800	0.139	0.083	110.471	0.591	35.253	0.261	580.260	0.880	181.666	0.493	0.362	0.063
	0.1138613	1000	0.068	0.092	145.171	0.703	42.398	0.460	726.624	1.026	214.124	0.814	0.399	0.056
	0.1492235	1200	0.068	0.076	152.790	0.463	43.285	0.481	734.405	1.054	212.656	0.915	0.392	0.046
	0.2595288	1600	0.024	0.092	536.626	0.917	138.663	0.578	2290.832	1.063	627.087	1.612	0.405	0.018
	0.640472	2000	-0.017	0.106	1882.832	2.601	485.657	0.955	7911.467	3.621	2055.702	1.960	0.389	0.006
	0.9310486	3000	0.152	0.057	1566.053	1.820	371.267	1.041	6034.724	2.127	1575.108	1.808	0.379	0.004

	1	4000	0.151	0.078	385.089	1.324	87.749	0.596	1431.989	1.988	413.668	0.925	0.385	0.024
mi87-a45a	mass=	0.0105	J=		0.000856157	+/-	3.33724E-06				tot.gas.age=	0.339	+/-	0.014
MI87 a45a TAL-8	F39	LP(mW)	Vol36	Err36	Vol37	Err37	Vol38	Err38	Vol39	Err39	Vol40	Err40	Age(Ma)	AgeErr
Dacite	0.001493	100	0.409	0.090	2.324	0.409	1.293	0.130	14.972	0.206	100.797	0.365	-2.060	2.741
	0.0081156	200	0.445	0.079	10.476	0.275	5.806	0.134	66.411	0.329	133.998	0.403	0.056	0.541
	0.0198492	300	0.359	0.096	22.690	0.440	9.917	0.131	117.664	0.538	124.982	0.590	0.248	0.373
	0.0358073	400	0.316	0.087	37.144	0.383	13.094	0.215	160.026	0.435	113.373	0.461	0.194	0.247
	0.0559006	500	0.124	0.083	56.168	0.444	16.127	0.183	201.494	0.772	106.051	0.632	0.531	0.188
	0.0807342	600	0.345	0.102	81.804	0.335	18.854	0.187	249.029	0.627	106.492	0.712	0.028	0.187
	0.1233868	800	0.377	0.083	175.746	1.139	32.229	0.159	427.716	0.685	165.636	0.504	0.196	0.088
	0.1752874	1000	0.310	0.107	244.439	1.018	38.665	0.252	520.455	1.440	180.144	0.816	0.263	0.093
	0.2039314	1200	0.214	0.090	137.774	0.987	21.314	0.186	287.239	0.927	89.373	0.630	0.141	0.144
	0.2967433	1600	0.313	0.075	492.486	1.331	70.285	0.269	930.710	0.912	290.636	0.566	0.329	0.037
	0.5225483	2000	0.090	0.081	1114.594	1.694	175.242	0.304	2264.354	1.411	589.713	0.576	0.384	0.016
	0.9148416	3000	0.132	0.077	1909.204	2.112	298.454	0.629	3933.885	2.320	1001.321	1.018	0.378	0.009
	1	4000	0.113	0.073	414.044	1.658	65.260	0.223	853.962	0.880	243.609	1.324	0.380	0.039
mi79-q6a	mass=	0.009	J=		0.000839627	+/-	1.55969E-06				tot.gas.age=	0.254	+/-	0.036
MI79 Q6a TAL-13	F39	LP(mW)	Vol36	Err36	Vol37	Err37	Vol38	Err38	Vol39	Err39	Vol40	Err40	Age(Ma)	AgeErr
Andesite	0.0044135	100	107.542	0.300	11.448	0.245	31.904	0.183	25.674	0.153	31298.795	6.256	-28.536	5.324
	0.017222	200	0.436	0.099	38.746	0.532	12.779	0.157	74.509	0.382	174.157	0.973	0.923	0.595
	0.033791	300	0.290	0.085	66.844	0.395	10.643	0.206	96.384	0.311	118.261	0.776	0.510	0.394
	0.0523044	400	0.226	0.109	88.274	0.458	10.553	0.176	107.695	0.435	95.796	0.848	0.407	0.454
	0.0749374	500	0.183	0.096	116.286	0.642	13.186	0.125	131.660	0.408	94.190	0.651	0.461	0.325
	0.1035026	600	0.013	0.113	147.955	0.619	17.676	0.156	166.168	0.353	100.509	0.824	0.880	0.304
	0.1532791	800	0.915	0.126	259.113	0.801	29.785	0.187	289.557	0.659	351.926	0.686	0.426	0.195
	0.2214522	1000	4.350	0.108	367.474	1.069	40.340	0.252	396.573	0.563	1317.590	2.060	0.122	0.122
	0.4033016	1200	4.020	0.147	1013.764	1.184	108.295	0.673	1057.844	1.001	1446.441	0.938	0.370	0.062
	0.6567924	1600	2.039	0.091	1460.944	1.684	147.795	0.314	1474.593	1.100	991.377	1.196	0.399	0.028
	0.7511312	2000	0.130	0.103	566.198	0.759	54.774	0.477	548.782	0.932	159.373	0.605	0.334	0.084
	0.8629752	3000	0.256	0.073	656.838	0.903	65.324	0.373	650.613	0.948	220.147	0.732	0.337	0.050
	1	4000	0.223	0.060	806.639	1.204	80.443	0.437	797.093	1.092	251.200	0.930	0.352	0.034
mi79-q7a	mass=	0.0182	J=		0.000839751	+/-	1.61833E-06				tot.gas.age=	0.371	+/-	0.014
MI79 Q7a TEQ-33	F39	LP(mW)	Vol36	Err36	Vol37	Err37	Vol38	Err38	Vol39	Err39	Vol40	Err40	Age(Ma)	AgeErr
Basalt	0.0123194	100	5.800	0.108	72.116	0.377	27.729	0.218	203.470	0.606	1800.641	1.518	0.645	0.238
	0.0727154	200	10.186	0.153	362.718	0.789	125.408	0.381	997.519	1.466	3242.951	1.755	0.354	0.068
	0.1714053	300	11.400	0.197	747.749	1.421	193.702	0.739	1629.992	1.438	3734.757	2.402	0.340	0.054
	0.2830145	400	11.973	0.131	1112.758	1.663	206.102	0.438	1843.371	2.215	3969.188	2.531	0.354	0.032
	0.3897665	500	11.411	0.160	1426.633	1.217	179.813	0.569	1763.149	1.674	3772.449	2.841	0.344	0.041
	0.4815987	600	8.555	0.154	1659.019	1.718	137.123	0.587	1516.728	2.541	2929.440	2.886	0.401	0.045
	0.5909875	800	10.194	0.182	2481.868	3.149	156.159	0.473	1806.698	1.533	3460.176	2.127	0.375	0.045
	0.6634045	1000	7.054	0.103	1885.957	1.506	107.998	0.307	1196.061	0.851	2319.748	1.618	0.298	0.039
	0.7138882	1200	5.311	0.151	1345.856	2.283	84.114	0.425	833.804	0.955	1782.239	2.166	0.387	0.081
	0.8132749	1600	10.855	0.130	2258.502	2.277	186.095	0.500	1641.501	1.135	3561.676	0.980	0.327	0.036
	0.8941783	2000	7.904	0.144	2197.142	2.937	163.147	0.669	1336.226	1.543	2727.026	1.566	0.444	0.048
	0.9650065	3000	6.698	0.138	2703.070	2.407	153.304	0.305	1169.820	1.809	2290.805	0.928	0.403	0.053
	1	4000	3.392	0.104	1496.507	2.319	79.297	0.345	577.963	0.711	1171.860	2.066	0.444	0.081

mi87-a23a	mass=	0.0112	J=		0.000821397	+/-	3.12402E-06				tot.gas.age=	0.394	+/-	0.013
MI87 a23a TAL-25	F39	LP(mW)	Vol36	Err36	Vol37	Err37	Vol38	Err38	Vol39	Err39	Vol40	Err40	Age(Ma)	AgeErr
Andesite	0.0116684	100	31.960	0.296	45.261	0.330	30.682	0.253	210.158	0.619	9732.429	8.573	2.031	0.619
	0.0692273	200	14.318	0.158	247.772	0.682	114.222	0.678	1036.683	1.050	4567.972	5.889	0.481	0.067
	0.1722712	300	4.052	0.129	573.919	1.825	186.495	0.646	1855.908	2.221	1581.037	4.714	0.306	0.031
	0.3126792	400	3.341	0.142	878.584	1.950	241.623	0.654	2528.865	2.553	1544.014	3.010	0.326	0.025
	0.4693883	500	3.556	0.134	1166.695	1.640	251.275	0.972	2822.461	1.898	1674.452	3.132	0.327	0.021
	0.6313427	600	3.602	0.144	1535.112	2.334	227.301	0.708	2916.936	2.033	1798.617	2.909	0.373	0.022
	0.8018633	800	3.189	0.136	2163.842	3.060	191.861	0.798	3071.219	1.525	1721.223	2.372	0.376	0.019
	0.8802573	1000	1.137	0.107	1380.128	1.594	71.539	0.290	1411.941	1.066	737.009	1.440	0.421	0.033
	0.9083863	1200	0.369	0.102	681.433	1.389	31.930	0.298	506.626	0.850	305.309	1.542	0.574	0.088
	0.9338107	1600	0.627	0.111	909.031	1.094	63.202	0.201	457.915	1.203	340.778	2.063	0.503	0.107
	0.9596103	2000	0.965	0.107	1099.497	1.441	71.220	0.361	464.673	1.037	389.365	1.917	0.332	0.101
	0.9859492	3000	0.874	0.096	1298.026	1.581	74.167	0.572	474.385	0.780	412.153	1.797	0.481	0.089
	1	4000	0.866	0.091	696.040	1.577	38.300	0.297	253.067	0.772	332.686	2.473	0.449	0.158
mi79-s2a	mass=	0.0058	J=		0.000828371	+/-	1.95513E-06				tot.gas.age=	0.351	+/-	0.045
MI79 S2a ETZ-3	F39	LP(mW)	Vol36	Err36	Vol37	Err37	Vol38	Err38	Vol39	Err39	Vol40	Err40	Age(Ma)	AgeErr
Andesite	0.0087563	100	1.750	0.115	16.484	0.339	2.679	0.094	44.230	0.297	577.293	0.875	2.037	1.149
	0.0243918	200	2.569	0.103	41.041	0.429	5.519	0.121	78.979	0.240	772.686	1.226	0.256	0.575
	0.0465539	300	1.358	0.107	84.257	0.654	7.585	0.122	111.947	0.467	426.795	0.708	0.342	0.422
	0.0767917	400	1.740	0.068	141.950	1.076	10.809	0.173	152.740	0.419	536.299	0.876	0.217	0.196
	0.1100395	500	9.898	0.177	176.551	0.919	14.334	0.128	167.944	0.329	2959.803	2.904	0.311	0.466
	0.1445098	600	2.920	0.119	190.290	0.937	13.837	0.139	174.119	0.478	972.327	1.779	0.940	0.301
	0.2127142	800	5.945	0.132	364.984	0.975	29.308	0.181	344.519	1.043	1842.801	1.691	0.374	0.170
	0.3951787	1000	24.289	0.224	1007.622	0.909	82.295	0.207	921.679	0.742	7312.263	3.506	0.218	0.108
	0.6546295	1200	31.244	0.272	1567.125	2.169	118.117	0.376	1310.558	0.824	9510.786	4.257	0.317	0.092
	0.8115396	1600	6.385	0.092	1077.288	1.566	69.402	0.425	792.596	1.201	2085.793	2.440	0.375	0.052
	0.8741459	2000	1.289	0.089	445.685	1.038	27.333	0.232	316.242	0.754	412.959	0.632	0.152	0.124
	0.9407501	3000	1.388	0.077	505.716	1.333	29.221	0.142	336.436	0.250	496.712	0.827	0.385	0.101
	1	4000	1.405	0.117	412.638	1.106	26.423	0.247	299.288	0.822	518.167	4.853	0.515	0.174
mi79-r6a	mass=	0.0173	J=		0.000835775	+/-	1.68553E-06				tot.gas.age=	0.261	+/-	0.011
MI79 R6a TEQ-36	F39	LP(mW)	Vol36	Err36	Vol37	Err37	Vol38	Err38	Vol39	Err39	Vol40	Err40	Age(Ma)	AgeErr
Basalt	0.027309	100	5.899	0.101	197.720	1.046	38.601	0.291	400.202	0.751	1788.517	1.043	0.171	0.112
	0.1062408	200	4.334	0.124	537.612	1.121	103.964	0.388	1156.716	1.530	1490.744	1.283	0.274	0.048
	0.2062413	300	2.302	0.104	900.830	1.751	125.902	0.524	1465.468	1.522	907.729	1.152	0.234	0.032
	0.2961865	400	1.697	0.102	1116.275	1.533	105.304	0.431	1318.112	1.181	691.132	1.507	0.217	0.034
	0.3747508	500	1.469	0.090	1335.895	2.339	86.217	0.364	1151.329	1.342	579.202	1.507	0.190	0.035
	0.4419908	600	1.146	0.102	1413.078	1.497	72.444	0.279	985.376	1.226	522.787	1.346	0.282	0.046
	0.5304582	800	1.705	0.089	2105.628	1.579	107.323	0.487	1296.455	1.289	751.807	1.373	0.288	0.031
	0.6148001	1000	1.506	0.111	2025.504	2.791	122.166	0.302	1235.998	0.854	673.161	1.464	0.278	0.040
	0.6896531	1200	1.117	0.148	1892.107	1.761	119.911	0.600	1096.942	1.046	573.237	1.358	0.334	0.060
	0.7976755	1600	1.565	0.095	3179.789	1.849	183.664	0.515	1583.025	1.088	784.417	1.522	0.307	0.027
	0.8718685	2000	1.520	0.077	2548.893	2.375	134.456	0.433	1087.270	1.178	603.312	1.051	0.214	0.032
	0.9449378	3000	1.642	0.057	2793.897	3.359	135.262	0.592	1070.802	1.267	686.965	0.833	0.284	0.024
	1	4000	1.104	0.077	2407.706	2.260	101.231	0.397	806.915	0.919	463.408	0.611	0.256	0.042
mi87-a41a	mass=	0.0095	J=		0.000813545	+/-	3.83592E-06				tot.gas.age=	0.271	+/-	0.019

MI87 a41a TAL-11	F39	LP(mW)	Vol36	Err36	Vol37	Err37	Vol38	Err38	Vol39	Err39	Vol40	Err40	Age(Ma)	AgeErr
Andesite	0.029164	100	24.832	0.164	132.664	0.395	50.858	0.285	412.689	1.138	7286.500	4.915	-0.183	0.174
	0.1226965	200	26.236	0.226	308.264	0.958	143.317	0.459	1323.547	2.301	7937.264	2.259	0.204	0.074
	0.2612167	300	26.751	0.209	634.446	1.065	207.477	0.570	1960.153	1.468	8225.938	4.527	0.240	0.046
	0.4125212	400	27.088	0.227	886.704	1.574	217.693	0.426	2141.058	2.983	8280.219	4.103	0.189	0.046
	0.5633055	500	24.028	0.147	1102.719	1.144	199.473	0.640	2133.697	2.095	7400.180	3.942	0.206	0.030
	0.7012156	600	18.686	0.218	1244.710	2.284	161.471	0.609	1951.519	1.826	5918.238	3.488	0.298	0.049
	0.8474033	800	15.372	0.237	1775.583	2.317	138.384	0.496	2068.653	2.915	5140.246	1.926	0.424	0.050
	0.9259552	1000	7.354	0.178	1298.912	0.844	67.343	0.361	1111.561	1.057	2473.629	2.512	0.397	0.069
	0.9577451	1200	3.124	0.113	707.130	2.035	33.675	0.376	449.849	0.279	1013.665	1.457	0.295	0.109
	0.9676192	1600	1.241	0.105	507.163	1.304	24.020	0.304	139.724	0.408	415.276	1.082	0.511	0.327
	0.9758233	2000	1.016	0.082	739.896	0.639	31.019	0.290	116.094	0.425	374.609	1.643	0.938	0.306
	0.9901229	3000	2.362	0.116	1269.377	1.595	50.840	0.303	202.348	0.454	709.453	1.314	0.083	0.249
	1	4000	1.860	0.100	730.234	1.563	29.008	0.229	139.767	0.568	612.628	1.403	0.661	0.310
mi79-a32a	mass=	0.0118	J=		0.000969174	+/-	3.53427E-06				tot.gas.age=	0.227	+/-	0.016
MI84 A32a TEQ-6	F39	LP(mW)	Vol36	Err36	Vol37	Err37	Vol38	Err38	Vol39	Err39	Vol40	Err40	Age(Ma)	AgeErr
Andesite	0.0003149	100	-0.033	0.075	1.400	0.100	0.237	0.079	3.004	0.093	28.933	0.637	22.369	12.833
	0.0046135	200	0.878	0.078	18.200	0.254	2.454	0.096	41.000	0.188	260.241	0.931	0.039	0.984
	0.0150283	300	0.549	0.070	46.827	0.533	4.986	0.100	99.339	0.416	201.923	0.534	0.696	0.366
	0.0311395	400	0.329	0.094	78.415	0.417	8.043	0.112	153.670	0.332	113.642	0.720	0.187	0.315
	0.0520587	500	0.172	0.077	112.626	0.621	10.478	0.174	199.531	0.387	101.677	0.664	0.446	0.199
	0.0767537	600	0.360	0.093	147.147	0.595	12.223	0.142	235.544	0.615	91.834	0.662	-0.107	0.204
	0.1176328	800	0.349	0.076	288.053	0.533	19.505	0.095	389.912	0.792	147.959	0.754	0.202	0.100
	0.1681914	1000	0.652	0.089	407.839	1.121	24.870	0.217	482.235	0.797	246.549	0.880	0.195	0.095
	0.2505945	1200	0.372	0.065	660.312	1.506	38.791	0.284	785.973	1.227	201.188	0.898	0.203	0.043
	0.558284	1600	0.406	0.085	2329.869	2.920	146.803	0.455	2934.787	0.956	478.608	0.873	0.214	0.015
	0.77087	2000	0.315	0.081	1920.916	3.439	100.787	0.311	2027.677	2.853	324.593	1.091	0.200	0.021
	0.9116505	3000	0.315	0.086	1510.404	1.874	67.036	0.149	1342.785	0.737	305.131	0.803	0.276	0.033
	1	4000	0.249	0.101	990.092	1.824	41.644	0.159	842.691	1.177	189.978	3.316	0.241	0.062
mi84-a65a	mass=	0.0093	J=		0.000966635	+/-	2.88743E-06				tot.gas.age=	0.211	+/-	0.012
MI84 A65a JH009	F39	LP(mW)	Vol36	Err36	Vol37	Err37	Vol38	Err38	Vol39	Err39	Vol40	Err40	Age(Ma)	AgeErr
(Spine of Tequila)	0.0024046	100	0.816	0.093	17.325	0.259	0.894	0.091	35.907	0.204	247.827	2.155	0.321	1.338
Andesite	0.0223444	200	1.108	0.078	254.038	0.427	4.314	0.105	297.744	0.553	387.050	1.985	0.349	0.135
	0.0635328	300	0.679	0.084	634.260	1.154	4.919	0.155	615.034	0.674	274.487	1.217	0.209	0.070
	0.1412451	400	0.620	0.081	1052.642	0.882	5.458	0.188	1160.418	1.336	323.249	1.159	0.211	0.036
	0.2586533	500	0.461	0.102	1345.713	1.003	4.613	0.149	1753.165	2.485	371.230	0.882	0.234	0.030
	0.4023324	600	0.511	0.105	1456.627	2.115	4.539	0.202	2145.448	2.448	399.526	0.938	0.202	0.025
	0.6347469	800	1.077	0.132	2120.190	2.001	10.526	0.223	3470.465	2.277	654.221	1.388	0.169	0.020
	0.8145668	1000	0.545	0.143	1528.959	1.528	11.997	0.343	2685.111	1.597	471.551	1.717	0.202	0.027
	0.9104376	1200	0.373	0.099	899.388	1.441	14.104	0.144	1431.564	1.298	273.812	1.092	0.199	0.036
	0.9657721	1600	0.361	0.099	1258.784	0.664	28.557	0.247	826.267	1.055	246.781	0.722	0.296	0.062
	0.9807539	2000	0.238	0.099	799.211	1.452	12.080	0.129	223.712	0.633	106.168	0.764	0.279	0.227
	0.9941838	3000	0.407	0.070	1574.130	2.670	16.341	0.131	200.538	0.740	145.498	1.998	0.220	0.182
	1	4000	0.326	0.068	658.698	1.719	7.836	0.119	86.849	0.399	128.459	2.891	0.648	0.407
mi84-a50a	mass=	0.0126	J=		0.000983664	+/-	2.2425E-06				tot.gas.age=	0.211	+/-	0.011
MI84 A50a TEQ-23C	F39	LP(mW)	Vol36	Err36	Vol37	Err37	Vol38	Err38	Vol39	Err39	Vol40	Err40	Age(Ma)	AgeErr

Andesite	0.019957	100	11.036	0.138	88.786	0.294	26.912	0.177	384.265	0.862	3360.712	3.426	0.460	0.188	
	0.1017365	200	8.555	0.189	348.616	0.753	98.212	0.425	1574.636	0.854	2736.882	3.097	0.235	0.063	
	0.2426273	300	2.029	0.095	834.792	1.121	164.857	0.672	2712.805	1.875	818.471	1.172	0.143	0.018	
	0.4151515	400	1.668	0.120	1303.422	1.552	200.263	0.814	3321.894	1.476	826.978	1.838	0.178	0.019	
	0.5731619	500	0.742	0.093	1543.002	2.323	181.067	0.339	3042.435	1.784	512.354	0.887	0.171	0.016	
	0.7093195	600	0.240	0.111	1882.091	3.726	148.079	0.466	2621.669	1.416	445.359	1.289	0.253	0.022	
	0.8309071	800	0.331	0.128	2730.952	1.902	122.937	0.479	2341.127	1.837	404.334	1.387	0.232	0.029	
	0.8882121	1000	-0.047	0.094	2065.337	2.208	55.990	0.406	1103.389	1.496	208.593	0.707	0.358	0.045	
	0.9259012	1200	-0.002	0.114	1432.329	2.072	38.009	0.218	725.691	0.811	165.080	0.533	0.405	0.083	
	0.9600831	1600	0.119	0.104	1288.098	1.308	36.844	0.237	658.159	0.791	173.490	0.893	0.373	0.083	
	0.9818545	2000	0.388	0.066	891.032	1.634	24.344	0.210	419.202	0.836	116.994	1.055	0.010	0.082	
	0.9939947	3000	0.346	0.115	983.961	1.862	12.731	0.232	233.756	0.452	86.740	0.776	-0.117	0.258	
	1	4000	0.530	0.071	591.421	1.039	5.971	0.175	115.629	0.496	99.419	0.747	-0.877	0.324	
mi79-a39a	mass=	0.0142	J=		0.000986754	+/-	2.22451E-06				tot.gas.age=	0.223	+/-	0.009	
MI84 A39a TEQ-15	F39	LP(mW)	Vol36	Err36	Vol37	Err37	Vol38	Err38	Vol39	Err39	Vol40	Err40	Age(Ma)	AgeErr	
Andesite	0.016101	100	2.371	0.125	176.257	0.690	20.629	0.339	364.085	0.854	864.918	13.180	0.803	0.191	
	0.091906	200	11.577	0.120	482.659	1.305	75.626	0.521	1714.146	1.200	3482.075	10.856	0.064	0.039	
	0.2717722	300	3.168	0.113	1449.479	2.356	160.395	0.280	4067.236	3.006	1405.348	5.028	0.205	0.015	
	0.4963838	400	1.147	0.063	2466.873	4.007	208.665	0.558	5079.046	5.584	862.041	2.075	0.183	0.007	
	0.6973986	500	0.764	0.120	3211.719	2.125	194.100	0.743	4545.460	3.066	757.727	0.818	0.208	0.014	
	0.8396914	600	0.522	0.088	3354.075	2.275	138.016	0.420	3217.606	1.622	549.334	2.028	0.219	0.014	
	0.9463949	800	0.597	0.104	4386.789	4.422	100.673	0.454	2412.841	2.038	490.461	1.082	0.232	0.023	
	0.9821736	1000	0.217	0.099	2699.783	3.303	34.609	0.275	809.048	0.959	204.237	0.740	0.308	0.064	
	0.9921432	1200	-0.059	0.098	1519.319	2.527	12.764	0.138	225.439	0.727	74.284	0.967	0.724	0.228	
	0.9982242	1600	-0.048	0.142	1957.927	0.881	20.227	0.287	137.507	0.563	73.354	0.822	1.132	0.545	
	0.9994997	2000	0.201	0.100	905.780	1.320	6.412	0.135	28.842	0.390	70.504	0.608	0.679	1.829	
	0.999801	3000	0.253	0.118	922.953	1.656	1.072	0.102	6.813	0.151	100.391	1.020	6.684	9.111	
	1	4000	0.532	0.127	416.374	0.532	0.864	0.121	4.501	0.200	180.247	1.306	9.101	14.836	
mi79-s0a	mass=	0.0093	J=		0.000830504	+/-	0.000001741				tot.gas.age=	0.233	+/-	0.018	
MI79 s0a TEQ-40	F39	LP(mW)	Vol36	Err36	Vol37	Err37	Vol38	Err38	Vol39	Err39	Vol40	Err40	Age(Ma)	AgeErr	
Basalt	0.0582935	100	16.152	0.138	132.100	0.722	75.964	0.458	516.236	0.867	4783.723	2.509	0.031	0.118	
	0.23285	200	10.593	0.136	443.712	1.009	180.080	0.318	1545.839	0.943	3281.360	2.315	0.147	0.039	
	0.4411769	300	5.907	0.090	847.525	1.769	194.064	0.460	1844.903	1.801	2005.367	2.815	0.211	0.022	
	0.6240465	400	3.274	0.071	1236.155	1.588	142.361	0.415	1619.458	1.998	1191.228	1.330	0.207	0.019	
	0.7699512	500	1.757	0.117	1389.707	2.277	94.407	0.301	1292.104	0.932	651.412	1.143	0.153	0.040	
	0.8706431	600	0.726	0.069	1308.401	2.357	61.632	0.417	891.708	1.185	397.875	1.214	0.308	0.034	
	0.9404374	800	0.467	0.074	1411.776	1.366	57.613	0.275	618.085	1.339	274.173	0.859	0.330	0.053	
	0.9706379	1000	0.241	0.086	936.700	1.690	34.778	0.221	267.450	0.835	163.020	0.843	0.515	0.142	
	0.9787518	1200	0.155	0.098	539.588	1.017	9.807	0.140	71.855	0.308	73.470	0.782	0.576	0.602	
	0.9812953	1600	0.076	0.084	370.130	0.991	2.846	0.102	22.525	0.253	67.705	0.637	3.011	1.643	
	0.9836488	2000	0.147	0.121	299.728	1.045	2.632	0.143	20.841	0.277	66.542	0.989	1.653	2.567	
	0.9903929	3000	0.301	0.108	611.257	0.932	7.675	0.095	59.725	0.414	121.590	0.604	0.820	0.803	
	1	4000	0.333	0.091	796.196	1.288	10.826	0.207	85.079	0.468	157.701	0.623	1.042	0.475	
mi79-a38a	mass=	0.0084	J=		0.000943828	+/-	1.43947E-06				tot.gas.age=	0.162	+/-	0.016	
MI84 A38a TEQ-17	F39	LP(mW)	Vol36	Err36	Vol37	Err37	Vol38	Err38	Vol39	Err39	Vol40	Err40	Age(Ma)	AgeErr	
Andesite	0.0358798	100	11.849	0.152	137.579	0.498	33.759	0.300	492.224	1.080	3497.555	5.842	-0.013	0.157	

	0.1643837	200	13.493	0.285	400.356	1.005	105.301	0.574	1762.904	1.606	4024.475	4.692	0.036	0.081
	0.3552371	300	12.907	0.108	710.357	1.599	153.210	0.514	2618.256	2.213	3992.493	3.830	0.116	0.021
	0.5532764	400	8.263	0.111	1029.723	1.873	162.844	0.477	2716.837	1.961	2746.410	2.847	0.191	0.021
	0.7219297	500	4.897	0.108	1345.617	2.182	143.989	0.455	2313.700	1.940	1701.241	1.845	0.187	0.023
	0.8390467	600	2.777	0.087	1388.572	1.756	102.237	0.399	1606.690	2.740	985.606	1.248	0.175	0.027
	0.9245483	800	1.842	0.097	1427.436	2.335	77.267	0.488	1172.969	1.508	696.539	1.258	0.221	0.042
	0.9615479	1000	0.785	0.109	844.688	1.355	34.547	0.219	507.585	0.449	321.602	0.636	0.300	0.108
	0.9745584	1200	0.357	0.065	477.110	1.080	12.275	0.102	178.488	0.398	137.876	0.735	0.308	0.182
	0.982127	1600	0.192	0.077	441.235	0.575	7.616	0.181	103.831	0.419	105.856	0.568	0.805	0.375
	0.9867231	2000	0.234	0.057	327.437	0.795	5.073	0.155	63.052	0.263	105.164	0.910	0.976	0.452
	0.9932149	3000	0.365	0.069	540.939	0.997	6.476	0.165	89.059	0.415	124.950	1.224	0.326	0.390
	1	4000	0.435	0.063	522.929	1.449	6.951	0.165	93.082	0.449	120.510	0.997	-0.148	0.339
mi79-a36a	mass=	0.0105	J=		0.000834659	+/-	1.75947E-06				tot.gas.age=	0.187	+/-	0.011
MI87 a36a TEQ-60	F39	LP(mW)	Vol36	Err36	Vol37	Err37	Vol38	Err38	Vol39	Err39	Vol40	Err40	Age(Ma)	AgeErr
Andesite	0.0187838	100	8.347	0.133	128.090	0.468	22.950	0.201	273.605	0.720	2429.792	1.733	-0.202	0.216
	0.0985002	200	2.368	0.100	393.183	2.042	83.621	0.338	1161.151	1.671	861.360	1.561	0.210	0.038
	0.2235326	300	1.355	0.089	645.784	2.119	123.275	0.461	1821.225	1.562	579.603	1.762	0.148	0.022
	0.3649708	400	0.958	0.103	995.128	1.974	144.459	0.359	2060.193	2.043	520.826	1.121	0.174	0.022
	0.511138	500	0.773	0.082	1346.739	1.417	155.693	0.593	2129.075	1.381	477.253	0.897	0.176	0.017
	0.6516024	600	0.682	0.091	1667.969	1.757	155.099	0.561	2046.008	1.130	439.701	0.605	0.175	0.020
	0.8049158	800	0.210	0.141	2466.365	3.055	173.469	0.527	2233.166	1.646	410.022	0.958	0.235	0.028
	0.9052302	1000	0.358	0.074	1929.664	3.489	116.455	0.547	1461.182	1.773	280.368	0.998	0.180	0.022
	0.9558244	1200	0.329	0.101	1096.738	1.462	59.864	0.358	736.956	1.610	166.653	0.602	0.142	0.061
	0.9762313	1600	0.297	0.136	645.639	1.048	23.983	0.349	297.247	0.715	143.904	0.836	0.284	0.203
	0.9870517	2000	0.347	0.095	384.135	1.180	12.793	0.160	157.610	0.284	124.786	0.489	0.214	0.268
	0.9964729	3000	0.448	0.074	534.607	1.809	11.657	0.165	137.230	0.461	212.399	0.662	0.878	0.239
	1	4000	0.414	0.055	189.725	0.863	4.131	0.131	51.376	0.439	148.889	0.884	0.774	0.478
mi79-q8b	mass=	0.0078	J=		0.000839689	+/-	1.71966E-06				tot.gas.age=	0.167	+/-	0.015
MI79 Q8b TEQ-25	F39	LP(mW)	Vol36	Err36	Vol37	Err37	Vol38	Err38	Vol39	Err39	Vol40	Err40	Age(Ma)	AgeErr
Andesite	0.0267877	100	7.133	0.093	111.922	1.182	20.254	0.220	233.450	0.596	2105.417	1.326	-0.015	0.179
	0.1181877	200	2.081	0.066	178.102	1.514	61.085	0.215	796.534	0.918	653.273	1.694	0.073	0.037
	0.2601704	300	1.356	0.099	476.502	3.198	92.081	0.297	1237.354	1.125	527.418	0.860	0.155	0.036
	0.4106328	400	1.401	0.065	721.022	3.692	97.590	0.202	1311.252	1.477	517.027	1.441	0.119	0.022
	0.5556225	500	1.314	0.099	923.539	5.876	91.847	0.412	1263.559	0.866	486.110	1.213	0.117	0.035
	0.6910102	600	1.021	0.080	1041.692	4.263	87.039	0.267	1179.879	1.463	436.220	0.599	0.173	0.031
	0.8488763	800	1.087	0.072	1468.155	5.771	102.610	0.336	1375.775	1.532	519.952	0.581	0.219	0.023
	0.9456729	1000	0.874	0.080	1122.409	4.690	61.789	0.338	843.565	1.399	335.603	0.351	0.139	0.042
	0.9824749	1200	0.242	0.076	630.165	3.632	22.382	0.194	320.722	0.684	148.233	0.548	0.362	0.106
	0.9955201	1600	0.154	0.065	419.246	2.522	7.554	0.143	113.686	0.364	94.562	0.706	0.652	0.255
	0.9973628	2000	0.076	0.063	162.605	2.182	1.211	0.090	16.059	0.170	48.222	0.398	2.441	1.744
	0.997987	3000	0.165	0.067	99.543	1.804	0.365	0.072	5.439	0.149	57.333	0.609	2.369	5.527
	1	4000	0.460	0.088	228.740	1.855	1.177	0.065	17.543	0.191	163.406	1.065	2.359	2.251
mi79-r4a	mass=	0.0099	J=		0.000837593	+/-	1.76662E-06				tot.gas.age=	0.145	+/-	0.015
MI79 R4a ETZ-1	F39	LP(mW)	Vol36	Err36	Vol37	Err37	Vol38	Err38	Vol39	Err39	Vol40	Err40	Age(Ma)	AgeErr
Andesite	0.0283836	100	1.527	0.098	110.346	0.599	25.271	0.094	234.798	0.836	493.843	1.169	0.274	0.187
	0.1185614	200	2.172	0.053	354.753	0.816	73.122	0.351	745.979	1.229	701.837	1.877	0.121	0.032

	0.2384179	300	1.957	0.059	609.663	1.558	93.968	0.556	991.490	0.939	674.109	1.566	0.146	0.027
	0.3650278	400	1.781	0.068	837.215	1.477	94.826	0.413	1047.358	1.427	616.684	1.606	0.130	0.029
	0.4830607	500	1.402	0.104	1006.494	1.416	83.358	0.254	976.405	0.440	514.625	0.826	0.155	0.048
	0.5801099	600	1.027	0.061	1029.512	1.694	68.201	0.308	802.821	0.911	402.193	1.121	0.186	0.034
	0.6729435	800	1.112	0.065	1236.429	2.047	74.056	0.260	767.950	0.844	401.816	0.573	0.144	0.038
	0.7315074	1000	0.819	0.055	1012.677	0.933	62.106	0.367	484.459	1.298	264.544	0.811	0.071	0.051
	0.7714421	1200	0.519	0.051	900.744	1.973	62.001	0.132	330.353	0.598	174.147	0.803	0.094	0.068
	0.8413296	1600	0.769	0.075	2050.859	1.721	141.465	0.536	578.132	0.921	279.990	0.756	0.138	0.058
	0.9057218	2000	0.620	0.095	2044.103	2.858	136.145	0.518	532.672	0.594	226.899	2.748	0.124	0.080
	0.9617945	3000	0.550	0.099	2159.491	1.884	132.420	0.322	463.852	0.516	221.292	2.767	0.192	0.096
	1	4000	0.351	0.094	1527.198	2.176	88.619	0.507	316.048	0.540	138.772	2.677	0.168	0.133
mi87-a32a	mass=	0.011	J=		0.000857951	+/-	2.44985E-06				tot.gas.age=	0.135	+/-	0.018
MI87 a32a TEQ-48	F39	LP(mW)	Vol36	Err36	Vol37	Err37	Vol38	Err38	Vol39	Err39	Vol40	Err40	Age(Ma)	AgeErr
Andesite	0.0125916	100	49.317	0.277	59.362	0.669	24.795	0.223	208.954	0.571	14655.804	4.594	0.612	0.607
	0.072184	200	35.515	0.162	220.061	0.912	74.069	0.371	988.921	1.101	10528.139	3.101	0.052	0.075
	0.1782923	300	19.240	0.226	455.295	2.035	119.075	0.360	1760.839	1.454	5809.816	4.150	0.109	0.059
	0.3057552	400	14.173	0.142	678.785	1.978	139.583	0.410	2115.214	1.289	4298.298	2.742	0.081	0.031
	0.4362043	500	12.504	0.191	926.652	2.271	138.364	0.574	2164.769	2.099	3809.835	2.477	0.082	0.040
	0.5568603	600	11.304	0.150	1156.118	2.123	122.964	0.399	2002.255	1.590	3484.513	2.565	0.111	0.034
	0.691405	800	12.474	0.189	1856.073	2.242	130.174	0.406	2232.736	2.739	3914.463	1.692	0.158	0.039
	0.7788671	1000	10.882	0.142	1547.072	1.635	84.688	0.207	1451.411	0.923	3380.353	2.413	0.176	0.045
	0.8347147	1200	10.428	0.155	1032.194	1.985	59.218	0.347	926.776	0.717	3089.735	1.529	0.014	0.076
	0.9119855	1600	13.457	0.220	1225.191	2.256	90.569	0.465	1282.290	1.302	4095.634	3.249	0.144	0.078
	0.9589542	2000	15.461	0.169	934.324	1.845	62.664	0.340	779.433	1.600	4730.764	2.722	0.322	0.099
	0.9852972	3000	7.386	0.130	848.391	2.228	35.452	0.327	437.156	0.862	2285.948	2.901	0.366	0.136
	1	4000	3.610	0.082	517.219	0.808	20.485	0.182	243.988	0.402	1120.988	1.787	0.343	0.153
mi87-a25a	mass=	0.0133	J=		0.000856088	+/-	3.30894E-06				tot.gas.age=	0.055	+/-	0.011
MI87 a25a TAL-1	F39	LP(mW)	Vol36	Err36	Vol37	Err37	Vol38	Err38	Vol39	Err39	Vol40	Err40	Age(Ma)	AgeErr
Andesite	0.0045626	100	4.009	0.116	21.013	0.219	9.062	0.110	67.184	0.303	1157.709	2.065	-0.617	0.788
	0.0278854	200	2.739	0.120	118.545	0.452	44.034	0.255	343.432	0.552	813.940	3.123	0.021	0.160
	0.0647907	300	0.882	0.141	257.290	1.326	70.957	0.294	543.436	1.260	207.175	2.018	-0.152	0.119
	0.1123618	400	0.534	0.086	436.470	1.409	90.408	0.188	700.493	1.454	148.734	1.719	-0.020	0.056
	0.1626118	500	0.266	0.104	611.137	1.560	93.809	0.310	739.939	0.719	99.999	1.558	0.045	0.064
	0.2098603	600	0.381	0.089	731.299	0.827	87.091	0.404	695.740	1.146	129.847	1.046	0.038	0.059
	0.2963992	800	0.390	0.099	1290.306	2.240	162.220	0.477	1274.298	0.810	184.468	1.466	0.084	0.036
	0.4768893	1000	0.657	0.098	2100.451	1.688	345.542	0.773	2657.743	1.538	334.891	1.574	0.082	0.017
	0.6845214	1200	1.014	0.096	2643.242	3.919	396.104	0.866	3057.413	1.167	515.995	1.774	0.109	0.014
	0.8620452	1600	0.506	0.079	2625.090	4.435	344.510	0.995	2614.064	2.494	319.167	1.758	0.100	0.014
	0.9333937	2000	0.535	0.087	1392.437	2.671	137.931	0.517	1050.617	0.963	186.059	1.200	0.041	0.038
	0.9615237	3000	0.636	0.094	703.782	1.098	54.214	0.260	414.218	0.655	151.246	1.077	-0.137	0.104
	1	4000	0.809	0.095	916.099	2.127	73.606	0.408	566.570	0.832	224.455	1.366	-0.040	0.077
mi79-34ba	mass=	0.0091	J=		0.000813756	+/-	1.11431E-06				tot.gas.age=	0.096	+/-	0.016
MI79 34Ba TQ-123	F39	LP(mW)	Vol36	Err36	Vol37	Err37	Vol38	Err38	Vol39	Err39	Vol40	Err40	Age(Ma)	AgeErr
Andesite	0.0091709	100	11.252	0.202	17.154	0.470	5.748	0.119	97.485	0.200	3409.829	2.840	1.276	0.901
	0.0433929	200	3.047	0.090	68.798	0.669	13.720	0.177	363.775	0.556	882.580	1.407	-0.072	0.108
	0.0932484	300	0.807	0.084	111.912	1.271	20.574	0.251	529.956	0.827	276.001	0.921	0.104	0.069

	0.1527254	400	0.744	0.083	145.032	1.035	24.720	0.175	632.232	0.809	253.914	0.896	0.079	0.057
	0.2176496	500	0.693	0.064	195.525	0.907	27.360	0.178	690.135	0.617	230.941	0.776	0.056	0.040
	0.2832287	600	0.598	0.108	253.777	1.357	27.269	0.185	697.096	1.040	212.598	0.857	0.075	0.067
	0.3643766	800	0.656	0.069	434.971	1.709	33.369	0.153	862.591	1.282	237.426	0.886	0.074	0.035
	0.4344981	1000	0.458	0.077	444.301	1.141	28.962	0.198	745.381	0.887	199.715	1.181	0.127	0.045
	0.4909126	1200	1.020	0.105	369.648	1.296	23.958	0.128	599.678	0.774	328.749	0.864	0.067	0.076
	0.5933051	1600	7.454	0.140	637.978	1.727	46.775	0.295	1088.417	1.133	2299.379	1.797	0.130	0.056
	0.7464448	2000	1.232	0.104	905.831	1.859	68.549	0.323	1627.852	1.445	466.152	1.524	0.092	0.028
	0.9300289	3000	0.637	0.106	1214.922	2.947	80.866	0.415	1951.473	1.922	313.325	1.137	0.094	0.024
	1	4000	0.547	0.097	412.329	1.300	30.443	0.203	743.782	1.240	193.368	0.715	0.063	0.057
mi79-38ba	mass=	0.007	J=		0.000812235	+/-	1.1153E-06				tot.gas.age=	0.085	+/-	0.027
MI79 38Ba TQ-391	F39	LP(mW)	Vol36	Err36	Vol37	Err37	Vol38	Err38	Vol39	Err39	Vol40	Err40	Age(Ma)	AgeErr
Andesite	0.0150252	100	11.293	0.174	35.600	0.941	14.963	0.177	102.906	0.398	3327.204	2.395	-0.141	0.733
	0.0763833	200	6.463	0.140	129.541	1.484	46.165	0.288	420.233	0.613	1956.153	2.003	0.162	0.145
	0.1729836	300	4.599	0.112	295.880	2.376	66.386	0.197	661.602	0.575	1378.971	1.379	0.044	0.074
	0.2866081	400	4.592	0.068	487.155	2.334	70.073	0.346	778.199	0.700	1394.209	1.584	0.070	0.038
	0.3997692	500	4.602	0.107	664.988	2.908	64.828	0.461	775.025	1.158	1364.406	1.280	0.008	0.060
	0.5025006	600	4.063	0.108	826.442	3.922	56.638	0.319	703.593	0.846	1254.042	0.557	0.111	0.066
	0.6195566	800	4.798	0.078	1390.251	4.864	63.972	0.334	801.700	0.903	1452.379	0.933	0.063	0.042
	0.7062682	1000	4.249	0.087	1391.445	4.317	48.136	0.219	593.876	1.130	1280.207	1.285	0.060	0.063
	0.7635745	1200	3.501	0.079	1062.387	2.831	31.465	0.209	392.483	0.355	1075.520	1.119	0.153	0.087
	0.8152497	1600	5.058	0.090	955.836	2.961	30.694	0.293	353.916	0.470	1492.600	0.698	-0.009	0.110
	0.8774819	2000	8.588	0.180	728.996	3.557	41.366	0.188	426.219	0.633	2650.360	1.911	0.387	0.183
	0.9500739	3000	10.415	0.137	768.045	4.551	47.317	0.288	497.172	0.709	3060.034	2.206	-0.052	0.120
	1	4000	7.129	0.095	617.760	3.481	32.439	0.353	341.937	0.634	2160.336	3.598	0.230	0.122
mi79-36ba	mass=	0.007	J=		0.000812948	+/-	1.02146E-06				tot.gas.age=	0.085	+/-	0.013
MI79 36Ba TQ-143	F39	LP(mW)	Vol36	Err36	Vol37	Err37	Vol38	Err38	Vol39	Err39	Vol40	Err40	Age(Ma)	AgeErr
Andesite	0.028012	100	8.560	0.175	39.244	1.472	14.685	0.246	286.444	0.501	2567.091	2.347	0.192	0.265
	0.1303223	200	3.530	0.068	131.631	1.088	44.225	0.220	1046.201	1.239	1086.262	1.628	0.061	0.028
	0.2753653	300	1.598	0.061	261.205	2.580	62.888	0.235	1483.175	0.958	512.908	1.505	0.040	0.018
	0.4296407	400	1.265	0.074	394.674	2.126	69.911	0.332	1577.584	1.384	431.844	0.831	0.054	0.020
	0.5853529	500	1.425	0.060	543.919	0.617	71.013	0.428	1592.276	0.858	458.039	0.834	0.034	0.016
	0.7254932	600	1.273	0.075	659.434	3.632	65.131	0.311	1433.041	0.925	443.445	1.082	0.069	0.023
	0.862146	800	1.305	0.059	965.349	3.601	63.439	0.250	1397.379	1.239	482.600	1.019	0.102	0.018
	0.9353071	1000	0.645	0.048	714.026	4.153	34.839	0.243	748.128	1.027	298.235	0.471	0.211	0.028
	0.9678097	1200	0.261	0.076	396.032	1.711	17.052	0.136	332.364	0.673	141.840	0.863	0.286	0.099
	0.9817411	1600	0.343	0.052	220.920	1.674	8.938	0.189	142.458	0.543	133.050	0.538	0.326	0.158
	0.9875775	2000	0.968	0.078	84.283	1.139	3.636	0.111	59.682	0.223	267.973	1.296	-0.441	0.565
	0.9940369	3000	0.949	0.112	117.521	1.200	3.788	0.140	66.052	0.371	316.204	0.789	0.796	0.732
	1	4000	0.558	0.068	100.073	1.180	3.694	0.080	60.978	0.379	157.079	0.619	-0.190	0.486
mi87-a27a	mass=	0.0108	J=		0.000837122	+/-	1.75574E-06				tot.gas.age=	0.056	+/-	0.020
MI87 a27a TEQ-46	F39	LP(mW)	Vol36	Err36	Vol37	Err37	Vol38	Err38	Vol39	Err39	Vol40	Err40	Age(Ma)	AgeErr
Andesite	0.0068088	100	9.018	0.140	37.796	0.409	9.113	0.141	81.272	0.363	2686.734	2.636	0.409	0.768
	0.037791	200	12.562	0.204	162.476	0.926	29.833	0.232	369.812	0.897	3718.219	3.226	0.025	0.247
	0.0895226	300	7.334	0.181	385.206	1.787	46.497	0.282	617.482	1.292	2216.572	2.346	0.121	0.131
	0.1620533	400	7.339	0.163	648.605	1.649	53.780	0.275	865.745	0.854	2183.793	0.623	0.026	0.084

	0.2508476	500	6.433	0.140	906.218	1.917	48.405	0.389	1059.873	2.007	1950.745	1.570	0.071	0.059
	0.3408311	600	4.651	0.170	994.540	1.263	35.176	0.299	1074.067	1.144	1454.880	1.699	0.113	0.071
	0.491227	800	4.756	0.154	1685.193	2.272	39.625	0.239	1795.165	1.180	1472.747	2.054	0.057	0.038
	0.6317604	1000	3.621	0.119	1546.998	2.540	35.187	0.275	1677.444	1.163	1142.244	0.977	0.065	0.032
	0.7350566	1200	3.103	0.116	1187.774	1.755	33.019	0.195	1232.970	1.273	1000.540	1.945	0.103	0.042
	0.8317069	1600	5.795	0.126	1237.896	2.668	50.093	0.213	1153.643	1.207	1750.171	1.669	0.049	0.049
	0.8851941	2000	5.271	0.076	938.248	2.077	42.102	0.118	638.437	0.981	1549.872	1.675	-0.018	0.053
	0.9403393	3000	6.362	0.163	1554.878	1.580	56.427	0.246	658.229	1.047	1885.786	1.547	0.013	0.111
	1	4000	7.250	0.112	1438.522	1.651	59.197	0.379	712.125	1.006	2100.557	1.877	-0.089	0.070
mi84-a31a	mass=	0.0139	J=		0.000953116	+/-	2.9113E-06				tot.gas.age=	0.970	+/-	0.034
MI84 A31a TEQ-39	F39	LP(mW)	Vol36	Err36	Vol37	Err37	Vol38	Err38	Vol39	Err39	Vol40	Err40	Age(Ma)	AgeErr
Basalt	0.0101479	100	15.531	0.160	70.171	0.317	6.893	0.178	117.474	0.373	4644.110	2.834	0.800	0.692
	0.0393974	200	54.352	0.271	272.121	0.675	19.484	0.169	338.597	0.560	16437.426	8.179	1.910	0.408
	0.100727	300	31.437	0.347	648.218	0.498	21.963	0.292	709.961	1.036	9849.351	5.651	1.355	0.248
	0.1989396	400	6.989	0.086	1037.292	1.756	19.287	0.284	1136.925	1.718	2809.833	2.406	1.126	0.039
	0.3008322	500	3.396	0.111	1232.268	1.534	17.761	0.393	1179.526	0.925	1720.762	1.566	1.045	0.048
	0.3879007	600	3.151	0.160	1261.119	2.569	19.885	0.275	1007.919	0.811	1509.537	1.322	0.987	0.081
	0.4774267	800	5.408	0.110	1588.359	1.611	38.467	0.331	1036.368	0.833	2178.716	1.241	0.963	0.054
	0.534782	1000	4.355	0.128	1272.528	1.277	44.953	0.299	663.955	0.660	1582.106	1.755	0.764	0.098
	0.5758798	1200	6.252	0.139	929.997	1.385	43.625	0.442	475.755	1.052	2015.635	2.550	0.608	0.149
	0.6985667	1600	27.762	0.137	2230.475	1.001	111.777	0.459	1420.243	1.538	8794.102	4.207	0.715	0.049
	0.7773518	2000	23.426	0.105	1977.697	2.196	88.817	0.344	912.030	0.790	7351.592	4.007	0.809	0.059
	0.8972543	3000	43.248	0.205	3378.285	3.556	142.184	0.552	1388.010	0.890	13627.644	6.035	1.050	0.076
	1	4000	38.992	0.468	2978.345	3.738	123.084	0.486	1189.401	2.206	12110.713	2.483	0.851	0.200
mi79-r1c	mass=	0.008	J=		0.000839326	+/-	1.77884E-06				tot.gas.age=	0.124	+/-	0.134
MI79 R1c ETZ-10	F39	LP(mW)	Vol36	Err36	Vol37	Err37	Vol38	Err38	Vol39	Err39	Vol40	Err40	Age(Ma)	AgeErr
Andesite	0.0024513	100	1.462	0.079	2.723	1.352	1.967	0.109	13.771	0.139	401.053	1.212	-3.397	2.566
	0.0117696	200	2.006	0.081	14.996	1.287	5.988	0.192	52.348	0.347	573.797	1.014	-0.548	0.690
	0.0267929	300	2.266	0.069	35.492	1.071	9.338	0.103	84.398	0.250	682.714	0.758	0.234	0.368
	0.0454447	400	2.440	0.108	54.464	2.056	11.107	0.177	104.782	0.503	737.505	1.245	0.239	0.463
	0.0670453	500	4.561	0.116	73.795	0.997	12.958	0.190	121.348	0.653	1272.256	1.306	-0.943	0.428
	0.0913639	600	2.555	0.109	104.284	1.782	13.877	0.202	136.617	0.516	818.282	1.158	0.700	0.356
	0.132803	800	4.420	0.114	196.000	2.163	23.760	0.251	232.796	0.624	1389.360	1.630	0.542	0.219
	0.1832106	1000	10.153	0.179	267.102	2.299	29.401	0.206	283.180	0.757	3009.081	2.061	0.047	0.284
	0.2343972	1200	4.638	0.109	284.220	1.579	28.992	0.147	287.556	0.811	1508.445	2.661	0.726	0.171
	0.3122464	1600	225.204	0.643	516.186	4.193	85.583	0.325	437.341	1.075	66488.476	5.544	-0.205	0.658
	0.4229688	2000	551.553	0.926	764.073	4.319	165.328	0.495	622.016	1.559	162852.995	40.359	-0.319	0.673
	0.6994899	3000	929.169	0.976	1931.460	7.249	327.295	0.774	1553.439	1.737	274613.146	31.553	0.043	0.283
	1	4000	418.857	0.689	2061.371	7.270	243.239	0.552	1688.205	1.920	124181.460	23.538	0.367	0.184
mi87-a39a	mass=	0.0146	J=		0.000858207	+/-	2.99117E-06				tot.gas.age=	0.248	+/-	0.015
MI87 a39a TAL-26	F39	LP(mW)	Vol36	Err36	Vol37	Err37	Vol38	Err38	Vol39	Err39	Vol40	Err40	Age(Ma)	AgeErr
Andesite	0.0178221	100	12.921	0.145	155.095	0.838	38.537	0.339	311.213	0.702	3716.705	3.978	-0.505	0.215
	0.0955744	200	25.821	0.175	499.489	1.422	150.092	0.547	1357.723	1.321	7852.748	3.647	0.254	0.059
	0.2229349	300	22.451	0.163	848.881	1.527	244.813	0.756	2223.992	1.644	6949.312	1.435	0.219	0.034
	0.3541231	400	19.132	0.173	1081.727	2.387	250.190	0.684	2290.831	2.192	5916.679	4.959	0.178	0.035
	0.4745978	500	15.104	0.216	1353.837	2.975	223.273	0.421	2103.751	2.252	4713.674	4.610	0.184	0.047

	0.580424	600	10.808	0.168	1620.081	2.475	187.476	0.712	1847.957	1.844	3586.786	2.482	0.329	0.042
	0.7025454	800	10.228	0.243	2711.778	3.907	199.340	0.598	2132.505	1.594	3437.608	1.808	0.301	0.052
	0.7897102	1000	6.004	0.138	2624.999	3.019	139.332	0.641	1522.087	1.706	2105.785	1.474	0.337	0.042
	0.8477338	1200	4.074	0.118	2361.407	3.244	97.206	0.438	1013.217	0.865	1372.529	1.820	0.258	0.053
	0.8982634	1600	4.276	0.078	2981.328	2.911	101.403	0.359	882.357	1.613	1422.355	1.085	0.279	0.041
	0.9374283	2000	2.772	0.162	2765.970	2.956	93.929	0.563	683.905	1.179	940.600	1.111	0.275	0.109
	0.9866294	3000	4.790	0.101	4310.052	4.591	139.307	0.508	859.158	1.391	1623.164	1.727	0.374	0.054
	1	4000	0.918	0.089	1432.519	2.543	36.249	0.275	233.480	0.436	322.247	1.368	0.338	0.175
mi87-a42a	mass=	0.0088	J=		0.000853122	+/-	3.05675E-06				tot.gas.age=	0.626	+/-	0.110
MI87 a42a TEQ-67	F39	LP(mW)	Vol36	Err36	Vol37	Err37	Vol38	Err38	Vol39	Err39	Vol40	Err40	Age(Ma)	AgeErr
Basalt	0.0145544	100	1188.799	1.902	51.221	0.456	235.940	0.686	124.373	0.743	352682.106	45.344	17.145	6.914
	0.056436	200	22.651	0.260	141.760	0.442	34.118	0.156	357.895	1.093	6805.160	2.329	0.480	0.330
	0.1089743	300	8.006	0.125	247.427	1.374	38.156	0.299	448.961	1.177	2451.727	2.099	0.295	0.127
	0.1792904	400	17.964	0.302	479.534	1.774	51.868	0.411	600.879	1.145	5536.743	3.278	0.585	0.228
	0.2453759	500	9.708	0.195	604.026	1.225	47.505	0.272	564.727	1.173	2970.356	1.659	0.277	0.157
	0.3033089	600	9.445	0.169	601.445	1.230	44.814	0.393	495.061	0.709	2883.541	1.709	0.287	0.155
	0.3757879	800	114.487	0.482	777.297	1.213	83.194	0.416	619.362	0.732	34214.143	11.082	0.952	0.355
	0.4919154	1000	27.600	0.223	1158.351	1.545	101.389	0.444	992.356	1.713	8266.088	3.932	0.171	0.103
	0.6745255	1200	20.117	0.197	1886.637	2.661	153.880	0.717	1560.476	1.634	6282.268	2.626	0.333	0.057
	0.9016857	1600	21.569	0.214	2695.457	2.922	188.802	0.659	1941.175	1.262	6874.460	4.006	0.397	0.050
	0.9531255	2000	2.768	0.132	678.735	0.810	41.938	0.170	439.574	0.788	880.608	1.360	0.220	0.136
	0.981596	3000	1.513	0.080	384.654	1.041	23.154	0.267	243.291	0.615	518.222	1.404	0.450	0.149
	1	4000	1.521	0.085	252.450	0.705	15.414	0.245	157.270	0.488	449.976	1.928	0.005	0.246
mi79-35ba	mass=	0.0066	J=		0.000813025	+/-	1.02357E-06				tot.gas.age=	0.095	+/-	0.042
MI79 35Ba TQ-133	F39	LP(mW)	Vol36	Err36	Vol37	Err37	Vol38	Err38	Vol39	Err39	Vol40	Err40	Age(Ma)	AgeErr
Andesite	0.0233255	100	25.715	0.151	55.562	0.847	13.200	0.103	161.816	0.604	7602.351	2.920	0.031	0.405
	0.1445934	200	57.925	0.248	244.236	1.456	48.631	0.310	841.270	1.670	16950.416	4.697	-0.290	0.128
	0.314628	300	38.714	0.282	474.729	2.125	59.096	0.121	1179.579	0.885	11316.305	4.962	-0.154	0.104
	0.4937649	400	31.623	0.143	691.600	1.450	57.785	0.376	1242.724	1.614	9302.050	2.717	-0.050	0.050
	0.6589619	500	24.953	0.180	789.127	1.423	49.118	0.290	1146.019	1.127	7409.569	1.887	0.046	0.068
	0.7872495	600	18.875	0.131	835.659	2.150	36.052	0.301	889.968	1.061	5655.531	2.636	0.128	0.064
	0.8890737	800	20.399	0.138	1043.749	2.677	28.879	0.133	706.384	1.066	6060.045	1.515	0.067	0.084
	0.9337419	1000	23.183	0.260	742.344	2.697	17.387	0.188	309.876	0.561	6816.769	3.708	-0.160	0.365
	0.9518904	1200	20.886	0.259	494.297	2.154	12.238	0.084	125.902	0.434	6359.132	2.829	2.180	0.892
	0.9655326	1600	15.573	0.149	643.773	2.724	13.602	0.237	94.640	0.434	4862.797	3.078	4.039	0.681
	0.9761426	2000	6.891	0.083	622.127	2.195	9.954	0.149	73.605	0.173	2155.525	1.574	2.375	0.488
	0.9922189	3000	3.868	0.157	1220.228	2.538	12.567	0.099	111.526	0.279	1231.922	1.551	1.168	0.609
	1	4000	2.768	0.100	391.337	1.942	6.315	0.088	53.980	0.189	829.440	1.488	0.312	0.807
mi79-q5b	mass=	0.0075	J=		0.000838954	+/-	1.49654E-06				tot.gas.age=	5.118	+/-	0.062
MI79 Q5b TEQ-9	F39	LP(mW)	Vol36	Err36	Vol37	Err37	Vol38	Err38	Vol39	Err39	Vol40	Err40	Age(Ma)	AgeErr
Hornblende	0.0004699	200	3.058	0.098	1.972	0.210	0.744	0.088	1.301	0.121	929.725	1.745	30.133	33.397
	0.0016894	400	0.386	0.100	1.777	0.199	0.202	0.052	3.377	0.130	114.559	0.855	0.222	13.270
	0.0027878	600	0.097	0.094	2.003	0.197	0.188	0.077	3.041	0.159	57.207	0.433	14.163	13.802
	0.0064687	800	0.456	0.084	58.726	0.487	3.014	0.076	10.193	0.174	180.494	0.520	6.763	3.695
	0.0297633	900	0.136	0.071	414.563	0.785	20.393	0.243	64.505	0.367	280.096	0.730	5.623	0.495
	0.0857374	1000	0.086	0.074	1006.910	1.779	46.919	0.186	154.996	0.330	572.313	0.985	5.332	0.214

	0.1588591	1100	0.348	0.078	1296.003	1.693	62.277	0.253	202.479	0.489	815.520	1.097	5.320	0.172
	0.2527903	1200	0.270	0.082	1661.179	1.633	82.846	0.246	260.102	0.805	952.123	1.127	5.069	0.142
	0.3205671	1250	1.007	0.105	1199.968	1.521	60.828	0.101	187.679	0.552	927.070	1.062	5.068	0.249
	0.3784096	1300	0.159	0.075	1018.531	1.682	51.385	0.251	160.170	0.567	577.364	1.243	5.006	0.211
	0.4246916	1350	0.083	0.089	823.361	1.871	42.186	0.196	128.158	0.321	452.678	0.764	5.048	0.309
	0.4662972	1400	0.224	0.086	744.457	0.923	37.684	0.249	115.209	0.581	443.523	1.104	4.949	0.333
	0.5158384	1450	0.986	0.113	883.965	1.576	45.460	0.199	137.183	0.363	745.500	1.121	5.005	0.369
	0.5575549	1500	0.743	0.102	746.014	0.958	38.442	0.171	115.516	0.143	576.396	0.971	4.669	0.395
	0.8052026	2000	0.780	0.128	4487.237	4.465	236.011	0.480	685.754	0.953	2559.997	2.995	5.134	0.084
	0.9634872	3000	0.232	0.082	3045.986	3.189	179.356	0.454	438.301	0.589	1562.226	1.394	5.151	0.084
	1	4000	0.335	0.093	1059.280	1.398	83.055	0.367	101.106	0.408	403.377	0.925	4.549	0.411
mi84-a46a	mass=	0.0088	J=		0.00094467	+/-	1.56527E-06				tot.gas.age=	3.911	+/-	0.037
MI84 A46a ETZ-5	F39	LP(mW)	Vol36	Err36	Vol37	Err37	Vol38	Err38	Vol39	Err39	Vol40	Err40	Age(Ma)	AgeErr
Andesite	0.0078355	100	17.800	0.138	68.183	0.355	4.793	0.121	60.825	0.240	5381.471	3.244	3.404	1.146
	0.0301067	200	33.245	0.385	244.858	0.849	9.411	0.148	172.885	0.417	10200.229	5.493	3.705	1.120
	0.070645	300	6.079	0.174	400.055	0.937	4.216	0.141	314.687	0.668	2527.395	2.521	3.954	0.278
	0.138915	400	1.175	0.185	578.808	1.285	4.536	0.152	529.960	0.967	1639.776	2.170	4.152	0.176
	0.2240836	500	0.522	0.117	630.018	1.361	6.073	0.205	661.139	1.002	1783.816	1.637	4.196	0.089
	0.3184007	600	0.516	0.078	636.762	1.310	8.872	0.208	732.156	0.905	1868.914	2.086	3.991	0.054
	0.4604117	800	0.588	0.123	936.906	1.622	26.404	0.226	1102.390	1.567	2743.124	1.196	3.968	0.056
	0.5909465	1000	0.479	0.077	849.975	0.621	42.212	0.268	1013.303	1.268	2457.440	1.793	3.891	0.038
	0.6808023	1200	0.281	0.123	591.966	1.457	43.876	0.313	697.524	0.977	1657.057	1.656	3.842	0.089
	0.7402386	1600	0.643	0.087	530.789	0.685	39.335	0.240	461.386	0.705	1184.451	1.666	3.670	0.095
	0.7866427	2000	0.394	0.078	571.640	1.122	31.127	0.404	360.221	0.880	944.395	1.936	3.913	0.109
	0.8643096	3000	0.840	0.074	923.035	2.347	46.487	0.367	602.905	1.076	1580.019	1.161	3.761	0.062
	1	4000	1.332	0.089	1599.880	1.247	76.085	0.125	1053.325	1.729	2746.126	1.928	3.802	0.043
mi84-a29a	mass=	0.0159	J=		0.000938414	+/-	2.12142E-06				tot.gas.age=	2.905	+/-	0.012
MI84 A29a ETZ-7	F39	LP(mW)	Vol36	Err36	Vol37	Err37	Vol38	Err38	Vol39	Err39	Vol40	Err40	Age(Ma)	AgeErr
Rhyolite	0.0000366	100	0.360	0.078	0.308	0.138	0.245	0.090	1.416	0.122	146.597	0.916	47.310	27.133
	0.0003477	200	0.934	0.068	0.962	0.157	1.416	0.083	12.047	0.194	342.997	0.952	9.409	2.816
	0.0012286	300	1.082	0.108	2.805	0.154	3.932	0.075	34.112	0.178	438.627	0.867	5.893	1.578
	0.002853	400	1.108	0.086	4.698	0.163	5.789	0.105	62.902	0.272	468.479	0.982	3.792	0.684
	0.0052403	500	0.785	0.079	7.071	0.190	8.328	0.101	92.441	0.353	464.054	0.963	4.247	0.427
	0.0084381	600	0.891	0.132	8.944	0.218	11.385	0.153	123.829	0.446	548.862	1.112	3.899	0.534
	0.0143248	800	1.873	0.109	17.566	0.301	20.840	0.253	227.952	0.660	975.918	1.263	3.136	0.238
	0.023942	1000	2.965	0.168	28.294	0.399	33.843	0.213	372.408	0.502	1563.178	1.777	3.121	0.226
	0.0388117	1200	3.854	0.163	44.845	0.472	52.099	0.448	575.801	1.037	2213.705	1.731	3.157	0.142
	0.0645177	1600	6.998	0.161	79.013	0.580	91.700	0.435	995.419	0.588	3795.842	1.699	2.936	0.081
	0.1104467	2000	12.439	0.122	147.923	0.940	160.120	0.715	1778.510	2.744	6782.796	4.018	2.955	0.035
	0.3056864	3000	64.726	0.337	632.656	1.893	685.088	0.709	7560.289	2.841	31719.495	7.794	2.818	0.022
	0.6049289	4000	113.189	0.517	977.148	1.358	1050.830	0.813	11587.599	5.906	52871.264	6.984	2.836	0.022
	0.8375393	4010	67.153	0.284	759.791	1.839	837.745	1.485	9007.400	3.203	35252.095	7.756	2.894	0.016
	1	4020	16.250	0.209	529.498	0.598	581.917	1.135	6290.982	4.100	15980.969	6.120	3.006	0.017
mi84-a36a	mass=	0.0129	J=		0.000972643	+/-	2.76347E-06				tot.gas.age=	2.306	+/-	0.034
MI84 A36a ETZ-2	F39	LP(mW)	Vol36	Err36	Vol37	Err37	Vol38	Err38	Vol39	Err39	Vol40	Err40	Age(Ma)	AgeErr
Andesite	0.0032125	100	21.814	0.148	31.756	0.412	11.833	0.191	30.468	0.256	6516.336	2.659	4.053	2.517

0.0227927	200	88.597	0.395	220.685	0.759	25.583	0.336	185.702	0.841	26501.783	6.008	3.034	1.103
0.0618037	300	22.561	0.266	657.662	1.463	20.347	0.240	369.987	0.680	7233.067	4.429	2.684	0.372
0.1253335	400	4.932	0.118	1092.177	1.909	26.071	0.407	602.527	1.183	2230.918	1.808	2.252	0.102
0.2096804	500	1.192	0.095	1503.872	2.910	27.200	0.222	799.961	1.415	1385.421	1.338	2.265	0.062
0.3042841	600	0.750	0.082	1758.675	1.880	26.223	0.145	897.238	0.571	1398.564	1.389	2.300	0.048
0.44896	800	0.721	0.112	2775.915	2.768	36.587	0.280	1372.132	0.782	2019.812	1.515	2.309	0.042
0.579813	1000	0.897	0.099	2392.158	2.148	39.821	0.329	1241.033	1.311	1839.449	2.307	2.225	0.041
0.6825427	1200	1.651	0.109	1805.302	2.104	43.349	0.366	974.306	0.935	1664.038	1.486	2.117	0.058
0.8214511	1600	3.211	0.106	2134.453	3.471	84.328	0.341	1317.432	1.921	2598.092	2.673	2.195	0.042
0.919241	2000	3.713	0.152	1384.355	2.159	68.346	0.351	927.456	0.930	2251.287	2.812	2.182	0.085
0.967064	3000	3.479	0.119	958.423	1.849	45.608	0.382	453.562	0.871	1755.338	1.793	2.811	0.136
1	4000	3.013	0.060	621.577	1.237	36.906	0.369	312.371	0.734	1331.282	1.873	2.476	0.099


Oxford
ESSELTE